1   **Palaeosols and their cover sediments of a glacial landscape in northern central Europe:**

2   **spatial distribution, pedostratigraphy and evidence on landscape evolution**

3

4   Knut Kaiser[1*], Thomas Schneider[2], Mathias Küster[3], Elisabeth Dietze[1,4], Alexander Fülling[5],

5   Susann Heinrich[6], Christoph Kappler[1], Oliver Nelle[7], Manuela Schult[8], Martin Theuerkauf[8],

6   Sebastian Vogel[9], Anna Maartje de Boer[10], Andreas Börner[11], Frank Preusser[5], Matthias

7   Schwabe[12], Jens Ulrich[13], Michael Wirner[14], Oliver Bens[1]

8

9   [1]GFZ German Research Centre for Geosciences, Telegrafenberg, D-14473 Potsdam,

10   Germany (*Corresponding author)

11   [2]Institute of Earth- and Environmental Science, University of Potsdam, Karl-Liebknecht-

12   Straße 24-25, D-14476 Potsdam

13   [3]Müritzeum, Zur Steinmole 1, D-17192 Waren (Müritz), Germany

14   [4]Helmholtz Centre for Polar and Marine Research (AWI), Telegrafenberg, D-14473 Potsdam,

15   Germany

16   [5]Institute of Earth and Environmental Sciences, University of Freiburg, Albertstraße 23b, D-

17   79104 Freiburg, Germany

18   [6]Max Planck Institute for Evolutionary Anthropology, Department of Human Evolution,

19   Deutscher Platz 6, D-04103 Leipzig, Germany

20   [7]Dendrochronologisches Labor, Landesamt für Denkmalpflege Baden-Württemberg,

21   Regierungspräsidium Stuttgart, Fischersteig 9, D-78343 Hemmenhofen, Germany

22   [8]Institute of Geography and Geology, University of Greifswald, Friedrich-Ludwig-Jahn-

23   Strasse 16, D-17487Greifswald, Germany

24   [9]Leibniz Institute for Agricultural Engineering and Bioeconomy (ATB), Max-Eyth-Allee

25   100, D-14469 Potsdam, Germany

26   [10]Wageningen University, Soil Geography and Landscape Group, P.O. Box 476700 AA

27   Wageningen, The Netherlands

28   [11]Landesamt für Umwelt, Naturschutz und Geologie (LUNG) Mecklenburg-Vorpommern,

29   Goldberger Straße 12, D-18263 Güstrow, Germany

30   [12]Müritz National Park Authority, Schlossplatz 3, D-17237 Hohenzieritz, Germany

31   [13]State Archaeological Survey of Mecklenburg-Vorpommern, Domhof 4-5, D-19055

32   Schwerin, Germany

33   [14]Landesforst Mecklenburg-Vorpommern, Fachgebiet Standortskartierung, Hauptstraße 11,

34   D-19306 Klein Laasch, Germany

35

36   In memory of Klaus-Dieter Jäger (1936-2019)

37

38   **Abstract**

39   Knowledge of the distribution, types and properties of buried soils, i.e. palaeosols, is essential

40   in understanding how lowlands in northern central Europe have changed over past millennia.

41   This is an indispensable requirement for evaluating long-term human impact including soil

42   erosion and land-cover dynamics. In the Serrahn area (62 km^2), a young glacial landscape

43   representative for northeastern Germany and part of the Müritz National Park, 26

44   pedosedimentary sections were documented and analysed. To this end, a multiproxy-

45   approach was applied using pedology, micromorphology, geochronology, and palaeoecology.

46   Statistical and spatial analyses of c. 5200 soil profiles, of which 10% contain palaeosols,

47   show that buried soils cover an area of 5.7 km^2, i.e. 9% of the area studied. Most palaeosols

48   are Cambisols, Arenosols and Gleysols. Palaeosols are mainly covered by aeolian and

49   colluvial sands, as well as by lacustrine sands and peat. Radiocarbon and luminescence dating

50   together with palynological and anthracological data reveal that former land surfaces were

51   dominantly buried through erosion triggered by human activity in the late Holocene. In

addition, but to a clearly smaller extent, Lateglacial/early Holocene palaeosols and cover

sediments occur. Following medieval clear-cutting and intensive land use, the study area is

today again widely forested. The high share of buried land surfaces detected here is expected

to be representative for the hilly glacial landscapes even in the wider region, i.e. in northern

central Europe, and should be considered in soil mapping, soil carbon budgeting and

assessments of past human impact.

1. Introduction

Buried soils, i.e. palaeosols (Johnson, 1998; Muhs et al., 2013), are highly useful to study

landscape evolution and the role of natural and anthropogenic drivers, triggering, for

instance, changes in climate, erosion/sedimentation and land cover (e.g. Gilbertson et al.,

1999; Mauz and Felix-Henningsen, 2005; Chendev et al., 2018). Palaeosol research is mostly

performed on aeolian sediments with main focus on loesses with their rather thick and

complexly structured pedosedimentary sequences that cover partly several hundreds of

millennia (e.g. Zeeden et al., 2018). By contrast, geologically younger landscapes, such as

recently deglaciated lowland regions, are less represented in literature (e.g. Hirsch et al.,

2015; Jonczak et al., 2019; Kappler et al., 2019).

The loess-free northern parts of Europe represent an example, where the potential of

palaeosol research has only been rudimentarily used so far. This area was occupied by the

Scandinavian Ice Sheet during the late Pleistocene (Hughes et al., 2016), that formed 'young

glacial' (glacial drift) landscapes. Research detecting Quaternary palaeosols here has mainly

focused on late Pleistocene and Holocene sandy aeolian (Kaiser et al., 2009; Jankowski,

2012; Küster et al., 2014; Kruczkowska et al., 2020) and colluvial sequences (Helbig et al.,

78   2002; Dreibrodt et al., 2010; Smolska, 2011; Kappler et al., 2018; Kołodyńska-Gawrysiak,

79   2019; van der Meij et al., 2019), which often formed due to anthropogenic soil erosion.

80   Palaeosols have also been used to study glacial history (Olsen, 1998; Pitkäranta, 2009) and

81   the formation of late Holocene archaeological sites (Hannon et al., 2008; Kittel, 2014;

82   Lungershausen et al., 2017; Khamnueva-Wendt et al., 2019).

83   Only recently research on the spatial distribution and physical-chemical properties of

84   palaeosols has also contributed to the field of carbon budgeting. As a net-sink of soil organic

85   carbon (SOC), subsoil horizons including buried palaeosols play an important role for

86   modelling carbon stocks and dynamics at different spatial and temporal scales (Quinton et al.,

87   2010; Hoffmann et al., 2013; Chaopricha and Marin-Spiotta, 2014; Marin-Spiotta et al.,

88   2014; Wang et al., 2014).

89   Thus, the spatial distribution and characteristics of palaeosols can be useful to explore

90   landscape evolution and estimate SOC distribution. So far, however, studies on palaeosols

91   normally rely on a small number of profiles (several tens in maximum) only. Soil and

92   geologic surveys usually do not map the areas, depths and types of buried soil horizons

93   (Costantini et al., 2007; Layzell and Mandel, 2019). Existing palaeosol maps are restricted to

94   very local archaeological and palaeoecological sites (e.g. Chapman et al., 2009; van Mourik

95   et al., 2012; Sevink et al., 2013; Schneider et al., 2017; van der Kroef et al., 2019). Thus,

96   information about landscape-scale distribution of palaeosols and their spatially variable

97   properties is rare.

98   We here present, to our knowledge, the largest record of palaeosols from a clearly delineated

99   larger landscape in northern central Europe. The dataset has been compiled during various

100 research projects on landscape evolution and geoecology in the Müritz National Park,

101 northeastern Germany (Kaiser et al., 2014a; Küster, 2014; Heinrich et al., 2018). Here now c.

102 5200 soil profiles have been documented across an area of 62 km^2 with a subset of 520

103 palaeosol-bearing profiles. Together with substantial sedimentological, geochronological and

104   palaeobotanical data this dataset offers the rare opportunity to explore the spatial distribution,

105   stratigraphy and evidence of palaeosols on landscape evolution at a larger scale. The present

106   study aims to (1) assess the spatial distribution, types and ages of palaeosols as well as their

107   stratigraphic integration depending on local landforms and geology, (2) characterise the

108   sedimentological and geochemical properties of palaeosols, related cover sediments and

109   topsoils, and (3) explore the potential of palaeosols and cover sediments as geoarchives for

110   reconstructing geomorphical and environmental changes of a geologically young landscape,

111   which was modified by humans for several millennia.

112

113   **2. Study area**

114   The Serrahn study area is located within the reach of the last Scandinavian glaciation

115   (Weichselian glacial period; Fig. 1A). It is part of the Müritz National Park (total area 322

116   km^2; Fig. 1B) of northeastern Germany, which represents a typical young glacial landscape of

117   the northern mid-latitudes, which is characterised by lakes, peatlands and widespread forests

118   on sandy ground (Fig. 1C).

119   The altitude ranges from 58 to 144 m a.s.l. with flat (southern area) to strongly undulating

120   parts (northern area; Fig. 1D). Several mostly NE-SW-stretching lake channels structure this

121   area, which represent former subglacial channels (Börner, 2015; Figs. 2A, 2B). In addition, a

122   multitude of closed basins (kettle-holes) occupied by mires are present (Fig. 2C). The depth

123   of these rather small basins, formed by Lateglacial to early Holocene dead-ice melting

124   (Kaiser et al., 2012), locally reaches up to 35 m.

125   The thickness of the Quaternary sediments varies from c. 50 to 250 m, covering Cretaceous

126   and Tertiary sediments. Directly below prominent hills at Serrahn ('Serrahner Berge' in

127   German, 124 m a.s.l.), a stacked sequence of six glaciofluvial layers and six till layers of

128   Elsterian to Weichselian age reach a total thickness of 230 m (Börner and Schütze, 2005; Fig.

129   3). The late Weichselian Pomeranian terminal moraine (c. 20 ka; Lüthgens et al., 2011; Hardt

and Böse, 2018) forms a prominent arc-shaped structure with a related till plain and an outwash plain to the north and south, respectively (Fig. 1E). This terminal moraine represents the main watershed between the catchments of the Baltic Sea and the North Sea. Aeolian sand sheets and dunes (linear, parabolic and hummocky forms) occur locally (Fig. 2D), particularly in the outwash plain but in some cases even reaching the terminal moraine. Peatlands occupy several depressions, hydrologically representing lake, kettle-hole, swamp and percolation mires (Fig. 2E). Several lacustrine landforms occur along the lake shorelines, such as terraces, fossil cliffs, beach ridges, and mire plains (Kaiser et al., 2014a; Fig. 2F). Although several sediment textures occur in the near subsurface of terrestrial sites (e.g. boulder, gravel, sand, till/loam), the surface is dominated by sands of different grain size, originating from intensive periglacial reworking and subsequent soil formation as well as erosion and related deposition processes. Lacustrine sediments and peats are spread in lakes and wet depressions, respectively. Depending on the texture, Luvisols (till plain) and Cambisols (terminal moraine and outwash plain) developed at terrestrial sites (BGR, 2011; Fig. 1F). By contrast, Regosols indicate immature soil formation, following rather young soil erosion. Correspondingly, Colluvic Regosols ('Kolluvisole' in German) are common on footslopes and depressions. Only very locally, (Gleyic) Podzols occur. Wet sites are occupied by Gleysols and Histosols.

The present climate of the study area is documented by data from the nearby German Weather Service (DWD) climate station at Neustrelitz, showing a mean annual temperature of 8.0 °C and a mean annual precipitation of 584 mm (range 428-814 mm) with dominating summer rainfalls for the reference period between 1961-90 (Kaiser et al., 2014b). For the last decades, distinct changes of climatic parameters were observed (e.g. increasing temperatures and winter precipitation, increase of extreme weather events; Stüve, 2015).

Forests (86%) dominate the present-day land cover, complemented by lakes (7%), pastures and some arable land (4%), peatlands (2%), and settlements (<1%; Schneider, 2017; Fig. 1G).

156 In the wider Lake Müritz region, agricultural land use started some 6000 years ago. Human

157 activity since then can be characterised by repeated changes between higher and lower land

158 use intensities (Kaiser et al., 2002; Küster, 2014; Müller et al., 2016). Human occupation of

159 the Serrahn area is proven since the Neolithic (Supplement 1). After widespread agricultural

160 land use during the Medieval, local human impact has decreased since the 18th century AD.

161 Sustainable forestry, manorial hunting and the establishment of a nature reserve has resulted

162 in the reestablishment of near-natural beech (*Fagus sylvatica*) forests at parts of the terminal

163 moraine, representing the UNESCO World Natural Heritage Serrahn site (Schwabe et al.,

164 2015; Müller et al., 2016; Fig. 2C). Further forest sites consisting of glaciofluvial and aeolian

165 sands are widely covered with (formerly intensively managed) forests dominated by Scots

166 pine (*Pinus sylvestris*; Figs. 2B, 2D). Generally, stronger human impact by forestry,

167 agriculture, fishing, and intensive hunting widely ceased during the 1990s when the Müritz

168 National Park was established in that area, leaving extensive tourism as the only remaining

169 important local economy (Jeschke, 2014).

170

171 **3. Material and methods**

172 **3.1. Soil profile data, soil classification, pedogenic features, and palaeosol mapping**

173 Soil profile data from the Serrahn area are available from two soil mapping campaigns in

174 1958/1959 and 1997/1998 as part of forest management plans (StaO, 1962; LFoA M-V,

175 1999). These campaigns resulted in a total of 5080 soil profiles, which are available for this

176 study. Moreover, within the framework of recent studies on Holocene landscape evolution

177 and geoecology (Kaiser et al., 2014a; Küster, 2014; Müller, 2014), a dataset of additional 134

178 soil profiles was retrieved, contributing to a total of 5214 soil profiles for the Serrahn area

179 (Table 1; Fig. 4A). The soil profiles are rather densely distributed, i.e. c. 1 profile per ha,

180 except in a c. 2.3 km^2-large agriculturally used area around Goldenbaum village, where no

181 profile data exist. The profile datasets were digitised, evaluated and attributed as well as

182 finally mapped and certain parameters were calculated using the ArcGIS software. As proper

183 profile descriptions are not available for all profiles, highly aggregated information from

184 archived working maps were extracted in such cases (Schneider, 2017). Consequently, the

185 statistics for the parameters 'thickness of sediment covering' and 'number of palaeosols per

186 profile' is based on a much lower population number (n = 95).

187 Soil survey and research in this area is originally based on the German classification

188 standards 'KA5' and 'SEA95' (Ad-hoc-AG Boden, 2005; Landesforst Mecklenburg-

189 Vorpommern, 2009). In this study, the naming of diagnostic horizons follows both 'KA5' (in

190 text, figures, tables, supplements) and the international FAO standard (FAO, 2006; in

191 Supplement 2) to allow for comparison, whereas the classification of surface soil and

192 palaeosol types follows the international IUSS Working Group WRB (2015) standard.

193 Furthermore, to allow for quick comparison a concordance list is given in Supplement 3,

194 where all German 'KA5' soil horizons used in the text, figures and tables were translated into

195 their FAO pendants (approximations).

196 Only buried palaeosols were identified; relict and exhumed palaeosols (Nettleton et al., 2000)

197 do not play a role in the Serrahn area. Generally, the term 'palaeosol' (syn. fossil soil, buried

198 soil, palaeo-surface) is not consistently used in the literature. Whereas some scholars restrict

199 this term to (even buried) soils older than the Holocene (e.g. Schirmer, 1999; Felix-

200 Henningsen and Bleich, 2014), others plead for a much wider application including the latter

201 (e.g. Johnson, 1998; Muhs et al., 2013), as is used in this study. Consequently, a 'palaeosol'

202 (Table 1) is to be understood here as a former soil of Holocene or late Pleistocene age,

203 including remnants of a palaeosol, which is buried by sediment. It can consist of one (e.g. fH

204 horizon, i.e. buried Histosol) to several buried soil horizons (e.g. fAeh-fAhe-fBsh sequence,

205 i.e. buried Podzol).

206 Some basic pedogenic and sedimentary features will be used in the following to identify, map

207 and interpret palaeosols and related geomorphical processes. The feature 'thin sand covering'

208　(Table 1) describes a sandy layer of 20 cm thickness in maximum (Landesforst Mecklenburg-

209　Vorpommern, 2009), which covers the surface soil, i.e. normally the Ah horizon. Even under

210　present-day forest vegetation a (relic) 'plough horizon' (rAp; Table 1) may occur, which

211　indicates former agricultural land-use. Finally, an 'erosion profile' (Fig. 5) shows traces of

212　truncation of soil horizons indicating soil erosion, whereas a 'deposition profile' (Fig. 5)

213　marks slight colluvial sedimentation, which is not necessarily connected with the formation

214　of a buried soil horizon.

215　The sediment facies was determined by means of both local field properties and evidence

216　from geological mapping (LUNG, 2005). Correspondingly, generalised terms of the

217　sedimentary facies will be used (e.g. colluvial, aeolian, lacustrine, telmatic).

218　The topographic relationships and spatial dimensions (area size and shape) of palaeosols were

219　estimated using a geo-statistical approach developed by Vogel et al. (2016). It is based on the

220　empirically calculated spatial relationship between the find locations of palaeosols as a

221　dependent variable and the digital elevation model (DEM)-based relief attributes as

222　independent variables. At first, digital terrain analysis was carried out using SAGA GIS

223　(Conrad et al., 2015) with a horizontal DEM resolution of 10 m. After preprocessing by sink

224　drainage route detection and sink removal, several primary and secondary relief attributes

225　were deduced (Supplement 4). The palaeosol sites were then mapped with the raster-based

226　relief attributes to derive the relief characteristics for each palaeosol. These characteristics

227　were statistically evaluated by box-and-whisker plots (Supplement 5). The statistical

228　importance of the relief attributes was determined by calculating the median absolute

229　deviation. To estimate their area sizes and forms, the palaeosol data points were interpolated

230　using Voronoi-Thiessen diagrams. Contiguous palaeosol areas were finally combined to one

231　area. The intensity of soil relocation (Fig. 12) was calculated using the tool 'Point density' in

232　ArcGIS. With this statistical method, the points of relocation were spatially interpolated with

233 equal value using nearest neighborhood (Silverman, 1986). The sum of points are divided by

234 the area of the specific neighborhood. The cell size of each neighborhood is around 1260 m^2.

235

236 **3.2. Soil analyses and micromorphology**

237 From 34 profiles and a total of 253 samples, sedimentological laboratory analyses were

238 performed on the sample matter <2 mm (Table 2, Supplement 2) in order to assist the

239 designation of sedimentary facies and soil horizons (data sources: AFSV, 1995; Graventein,

240 2013; Kaiser et al., 2014a; Küster, 2014; Müller, 2014; Landesforst Mecklenburg-

241 Vorpommern, unpublished data).

242 After air drying, hand-crushing and, where applicable, soil organic carbon and carbonate

243 removal (by 30% H_2O_2 and 10% HCl, respectively), different methods were used to

244 determine the grain-size distribution, i.e. laser diffraction (even measuring sand grain sizes)

245 with Fritsch Analysette 22 (Monella et al., 2000), combined pipette sieving and

246 sedimentation ('Köhn') test and a wet-sieving test (Schlichting et al., 1995). We are aware

247 that these different techniques lead to a somewhat biased grain-size dataset. Generally,

248 comparative analyses using laser diffraction and 'Köhn' test reveal differences, particularly

249 with respect to the quantities of silt and clay (e.g. Beuselinck et al., 1998; Spörlein et al.,

250 2004). However, as the majority of our samples is extremely dominated by sand, having only

251 very low silt (<5%) and clay contents (<10%), our mixed dataset is able to estimate the local

252 grain-size conditions. The specific methods used to determine the grain-size distributions are

253 given per profile in Supplement 2. For samples where no clay content was measured, the

254 value of silt represents the sum of clay and silt. The classification of sand grain-size (ranging

255 from fine to medium and coarse) is generally defined by the class sizes <0.2 mm, <0.63 mm

256 and <2.0 mm respectively (Ad-hoc-AG Boden, 2005; FAO, 2006). The content of organic

257 matter was estimated by combustion at 550 °C (loss-on-ignition/LOI; Heiri et al., 2001). The

258 $CaCO_3$ content was determined volumetrically by a Scheibler-apparatus (Schlichting et al.,

259   1995). Soil pH was analysed potentiometrically in 0.01 M $CaCl_2$ or KCl (soil : solution ratio

260   = 1 : 2.5; Schlichting et al., 1995). The statistical analysis of the soil data aggregated the

261   analytical results for designated soil horizons und sediments by providing respective means

262   and standard deviations (Table 2).

263   Two thin sections for micromorphological analysis were prepared from oriented and

264   undisturbed soil samples in profiles S-1 (thin section size: 8 cm x 6 cm) and KFS8 (thin

265   section size 9 cm x 7 cm) in order to clarify hardly visible details of buried soil horizons. The

266   samples were impregnated with polyester resin. The thin sections were analysed using a

267   petrographic microscope under plane (ppl), crossed polarised (xpl) and oblique incident (oil)

268   light. The microscopic description mainly followed the terminology after Bullock et al.

269   (1985) and Stoops (2003).

270

271   **3.3. Geochronology**

272   Geochronological data are available from 73 samples of 26 soil profiles (Fig. 4B).

273   Radiocarbon (^{14}C) dating was performed on 18 profiles on a total of 40 samples in the

274   Poznan, Erlangen and Beta Analytic ^{14}C laboratories by accelerator mass spectroscopy (Table

275   3). Materials used for dating are charcoal (n = 16 samples), peat (n = 15), wood (n = 4), and

276   bulk soil matter (n = 3) as well as small plant remains (n = 2). Pretreatment of the samples

277   was performed using the ABA/AAA (acid-base-acid/acid-alkali-acid) procedure. This three-

278   step treatment removes humic and fulvic acids, and secondary carbonates deposited in

279   organic fractions of sediments (Brock et al., 2010). The radiocarbon ages were calibrated (2σ)

280   with software OxCal version 4.2 (Bronk Ramsey, 2009) using the calibration curve IntCal 13

281   (Reimer et al., 2013).

282   Optically stimulated luminescence (OSL) ages were determined on 12 profiles on a total of

283   33 samples at the luminescence dating laboratory at Humboldt University, Berlin, using sand

284   samples of colluvial (n = 23), aeolian (n = 6) and lacustrine origin (n = 4; Table 4). The OSL

285   analytical procedures followed standard routines as given by Kappler et al. (2018) for the

286   Berlin laboratory, using the sand-size sediment (quartz) fraction of 90 to 250 µm (coarse

287   grain technique). Small aliquots (2 mm) were prepared containing approx. 200 grains each.

288   Equivalent doses were calculated using the Central Age Model (CAM). The pre-heat

289   temperature was set at 180°C (10 s) and the test dose cut-heat temperature at 160°C. The

290   sediment dose rates were estimated by measuring the contents of uranium, thorium and

291   potassium applying high resolution gamma ray spectrometry. The cosmic ray dose rates were

292   estimated from site position, elevation and burial depths. The gamma ray spectrometry did

293   not reveal any radioactive disequilibrium.

294   In the following, all radiocarbon ages are stated as calibrated years/kiloyears before present

295   (a/ka cal BP) with the year AD 1950 as reference. Luminescence ages in this study are

296   reported as years (a) or kiloyears (ka) with the year of measurement as individual reference

297   year, as the term BP is reserved to radiocarbon ages (Brauer et al., 2014). To clearly

298   differentiate radiocarbon and OSL data in the text and figures, they are indicated by different

299   terms (e.g. ^{14}C age = 3210-2967 a cal BP, OSL age = 2090 ± 240 a). There is a systematic

300   offset of up to 66 years in the comparison between luminescence and radiocarbon age data.

301   Regarding the timescales of interest this offset is considered negligible for this study. Partly,

302   when referring to historical or archaeological data the ages are given even as a AD and a BC.

303   For the statistical analysis, i.e. cumulative distribution of radiocarbon and OSL ages, relative

304   probability estimates and kernel density estimates, respectively, were computed using

305   algorithms in the statistical programming environment R (Kappler et al., 2019).

306

307   **3.4. Palaeoecology**

308   Palaeoecological analyses, i.e. pollen and/or charcoal analysis, have been conducted on 10

309   palaeosol-bearing profiles. These pedon-scale analyses primarily aim to reconstruct the very

310   local vegetation and land-use history.

311 Pollen analysis was carried out on six profiles (FUER3, FUER6, FUER14, FUER15, KFS8,

312 Mü-1) and included a range from 3 to 15 samples per profile (48 samples in total).

313 Preparation (cf. Fægri and Iversen, 1989) of the pollen samples (0.25 ml volume) included

314 addition of one *Lycopodium* tablet, treatment with 10% HCl, 20% KOH, sieving (120 µm),

315 acetolysis (7 min), and HF digestion (three days in a shaker). Samples were mounted in

316 silicone oil. Counting was carried out at 400-x magnification. Samples were counted up to a

317 minimum pollen sum of 100, with some exceptions. Pollen identification and nomenclature

318 follows Moore et al. (1991). To clearly distinguish between the original pollen data and the

319 inferred presence of plant taxa, pollen types are written in small capitals and plant taxa in

320 italics (cf. Joosten and de Klerk, 2002).

321 Soil-anthracological analyses (Robin et al., 2013) were performed on 18 samples from 4

322 profiles (S-1, S-3, S-5, S-6), comprising 673 charcoal particles determined. The sampling (10

323 l soil matter per sample) and determination of charcoal follows the procedure described in

324 Robin and Nelle (2014) with wet and dry sieving (mesh size of 1 mm) and taxonomical

325 analysis under a reflected-light microscope at 100-, 200- and 500-x magnifications, using the

326 microscopic anatomical criteria for wood identification from the determination literature

327 (Schweingruber, 1990) and from recent wood.

328

329 **4. Results**

330 **4.1. Spatial occurrence, types and general stratigraphy of palaeosols**

331 With c. 50% the majority of soil profile data from the Serrahn area represents sites with

332 glaciofluvial sand, followed by terminal moraine, till, mire, and lake shoreline sites (Table 1).

333 As surface soils from the total of 5214 soil profiles, Cambisols with well-developed Bv

334 horizons dominate (n = 1842, 36%), followed by Colluvic Regosols (n = 510, 10%), Luvisols

335 (n = 491, 9%), eroded Arenosols ('Rumpfrosterde') (n = 429, 8%), Histosols (n = 360, 7%),

336 and other soil types such as Podzols, Gleysols and Arenosols ('Ranker') (n = 1582, 30%). A

337   subset of 520 profiles (10%) has buried soil horizons (Table 1), which represent palaeosols of

338   different types. Palaeosol-bearing profiles dominantly occur in areas with glaciofluvial sand

339   (62%; Table 1).

340   While the total soil profile data are spread rather uniformly (Fig. 4A), palaeosol-bearing

341   profiles are distributed non-uniformly (Fig. 4B), concentrating in areas with terminal moraine

342   and aeolian sand in the northwest (around Serrahn village), with glaciofluvial and aeolian

343   sand in the southeast (around Waldsee village), and along the shoreline of Lake Fürstenseer

344   See in the southwest (around Fürstensee village). These areas are characterised by sandy

345   sediments and, partly, by a strongly undulating relief (Fig. 1D, E). In contrast, palaeosols

346   nearly lack in the till and terminal moraine area in the northeast (near Goldenbaum village),

347   which is characterised by loamy sediments and moist to wet soils (Fig. 1D, E, F). However,

348   when looking at the 'erosion / deposition profile' feature a more uniform distribution of

349   respective profiles is evident except in the outwash plain east of Lake Fürstenseer See (Fig.

350   5A). Thus, clear signs of soil erosion and deposition becomes visible even for areas, where

351   palaeosols are rare or absent. Moreover, 209 profiles (4% of all profiles) had a thin sand

352   cover ($\leq$ 20 cm), dominantly occurring in areas with glaciofluvial sand (Table 1, Fig. 5A).

353   The occurrences of 543 profiles (10% of all profiles) with relic plough horizons indicate

354   widespread agricultural activities in the past before becoming forested (Table 1, Fig. 5B).

355   Most palaeosols recorded (Fig. 6) belong to the soil types Cambisol (n = 310, 60%), eroded

356   Arenosol ('Rumpfrosterde') (n = 60, 12%) and Gleysol (n = 52, 10%), followed by Arenosol

357   ('Ranker') (n = 34, 7%), Histosol (n = 32, 6%), Podzol (n = 14, 3%), Colluvic Regosol (n =

358   11, 2%), and Luvisol (n = 5, 1%).

359   The thickness of sediments covering palaeosols varies between 10 and 320 cm with a mean

360   of 64 cm (n = 95). These sediments were identified to be of colluvial, aeolian, lacustrine,

361   telmatic (peat), and anthropogenic (overburden) origin. Sands dominate except when peat or

362   gyttja covers palaeosols in mires and lakes, respectively.

363   With respect to the number of palaeosols (layers) per profile, i.e. the record of superimposed

364   palaeosol storeys, from the total of 95 analysed profiles the majority (n = 66) have only one

365   palaeosol layer, followed by profiles having two (n = 19), three (n = 8) as well as four and

366   five palaeosols (n = 1). The most complexly formed palaeosol-bearing profiles, characterised

367   by a multitude of buried horizons reflecting repeatedly changing site conditions, are

368   developed at kettle-holes and lake terraces.

369   The descriptive statistics of the location characteristics of palaeosols by means of box-and-

370   whisker plots are displayed in Supplement 5, whereas Supplement 6 shows the ranking of the

371   relative statistical importance of their relief characteristics. It is remarkable that the digital

372   terrain analysis shows a clustering of palaeosols within flat topography that is prone to

373   sedimentation processes favoring their burial and conservation. Very small values for 'flow

374   accumulation' show that the palaeosols are preferably located in situations of low

375   concentrated fluvial erosion with a small contributing upslope area. That means, that the

376   sediments burying the palaeosols were redistributed rather locally by sheet erosion along

377   micro-topographies. This is an indication for prevailing colluvial processes. A 'plan

378   curvature' and 'profile curvature' near zero and low values in further attributes ('relative

379   slope position', 'vertical distance to channel network', 'LS factor', 'slope') point to locations

380   within the plain or at lower slopes.

381   The spatial interpolation of the palaeosol datapoints and subsequent combination of

382   contiguous areas leads to 349 palaeosol areas with a total area of 5.7 km^2, which is equivalent

383   to 9% of the study area. The areas have an average size of 0.01630 km^2, ranging from

384   0.00006 to 0.18804 km^2 (Fig. 7). Buried Cambisols have with 3.7 km^2 (66%) the highest

385   share, followed by eroded Arenosols and Gleysols with 0.6 km^2 (10%) each, Arenosols with

386   0.35 km^2 (6%), Podzols with 0.14 km^2 (3%) as well as Histosols with 0.09 km^2 (2%) and

387   Colluvic Regosols with 0.08 km^2 (1%). Luvisols, eroded Luvisols and Gyttjas have the

388   smallest shares, totalling 0.07 km^2 (2%).

389

4.2. Soil analytical properties

In general, the number of samples representing various top-/subsoil horizons, buried horizons as well as sediments is highly different, ranging between 1 to 92 samples per category (Table 2). This is due to different research agendas of the underlying studies providing the analyses. The thickness of the recorded sediment types is rather small with a mean ranging between 17 and 105 cm. The minimum represents peat, whereas the maximum represents aeolian sand. Buried A and B horizons have a similar mean thickness (e.g. fAh = 16 cm, fBv = 37 cm) like topsoil A and B horizons (e.g. Ah = 11 cm, Bv = 36 cm).

All sediments and soil horizons are dominated by sand grain sizes, except lacustrine gyttja, were silt and sand occur in nearly equal shares (Table 2). Even the minerogenic residuum from peat horizons, whether buried or not, mainly consists of sand supplemented by a distinct portion of silt. In general, clay has only a share up to 5% (Table 2). The reason for this sand dominance is the texture of glacial parent sediments in that area, widespread comprising glaciofluvial sand and gravel as well as sandy till (Figs. 1, 3). Coarser (e.g. boulder packing) and finer (e.g. glaciolacustrine silt) glacial sediment types only occur very locally. All further sediments originate or received matter from this parent materials by fluvial, lacustrine, colluvial or anthropogenic transport, causing enrichment of sand at the expense of fines.

Compared to their C horizons, both topsoil and buried A and B horizons show an enrichment of silt, which might originate from cryoclastics on Pleistocene surfaces and aeolian as well as partly colluvial input on Pleistocene and Holocene surfaces. There are differences within the sand fraction of the sediments (Table 2). Glaciofluvial and lacustrine sands are dominated by the medium sand class, whereas aeolian sands have their maximum in the fine sand class. Moreover, lacustrine sands are enriched by coarse sand.

Corresponding to the prevailing record of topsoil and palaeosol A horizons at (wet) depression sites, their mean soil organic matter content (LOI) is with c. 4% each rather high

16

415 (Table 2). The same applies to colluvial and lacustrine sands (c. 4-5%). All surface

416 sediments, topsoils and palaeosols lack $CaCO_3$ due to complete decalcification of the

417 uppermost glacial sediments over the millennia. Deeper subsoil sections at sites with till and

418 glaciofluvial sands, however, have $CaCO_3$, being the geochemical source for the enrichment

419 of $CaCO_3$ in lacustrine gyttjas. Due to the low base supply, the mean pH of topsoil and

420 palaeosol A horizons is with 3.5 and 4.6 very strongly and strongly acidic.

421

422 **4.3. Micromorphology**

423 The micromorphological analysis of a buried brownish horizon in profile S-1/site ID 20

424 (IIfBv) aimed at confirmation of its character as an in-situ weathered soil horizon (Figs. 4B,

425 6). The texture is dominated by sandy quartz grains. Finer material (fine silt and clay) can be

426 found between the sand grains and partly covering them (Fig. 8A). The grains are closely

427 packed showing a chitonic and partly enaulic c/f-related distribution pattern with complex

428 packing voids. Mostly, the fine mass is brownish colored and shows a very low birefringence.

429 There are no signs of clay illuviation such as bridges of well oriented clay between the sand

430 grains or the formation of clay bands in the sediment. Moreover the material shows

431 characteristic features supporting the in-situ formation of a weathered (cambic) soil horizon

432 like weathered sand grains and ferruginous punctuation of the fine mass (Figs. 8B-D).

433 In profile KFS8/site ID 13 (Figs. 4B, 6, 9A) the micromorphological analysis closely

434 characterises the contact zone of a palaeosol (Gleyic Podzol) buried by a very thin (0.5-2 cm

435 thickness) sand layer and followed by 48 cm-thick peat. The thin section reveals three units.

436 The uppermost horizon (Hr3) dominantly consists of organic material (plant tissue residues

437 and decomposed material forming peat) and contains only very few mineral grains (Fig. 8E).

438 Also remnants of roots and charcoal pieces can be identified within the material (Fig. 8F).

439 The intermediate horizon (IIGr-fM) is made of loosely packed, mostly blank sand grains

440 (some grains are partly coated; Fig. 8G). Organic material is mixed in by bioturbation

441   documented by faunal infillings that are rich in organic matter (Fig. 8G). The lowermost

442   horizon (IIIfAeh) is in its upper part made of more or less decomposed organic material with

443   only a few sand grains. This composition is continuously changing with depth to sandy

444   material with lower amount of organic matter (Fig. 8H). These findings suggest that a humic

445   soil surface (lowermost horizon) was covered by a thin layer of sand (intermediate horizon)

446   due to local colluvial sedimentation followed by a period of peat formation (uppermost

447   horizon).

448

449   **4.4. Geochronology**

450   Among the dating results (n = 73, 100%), Holocene ages (<11.7 ka) prevail (n = 66, 90%).

451   One radiocarbon and three OSL ages, marked in Tables 3 and 4, are omitted from further

452   analyses, as these appear as implausible. The radiocarbon age in profile Mü-1 (sample Beta-

453   291881) is regarded as being too old, when compared to the palynological data from that

454   profile. The three OSL ages have to be interpreted even as too old because of the equivalent

455   dose distribution characteristics, suggesting partial bleaching (FUER2/HUB-0324,

456   FUER5/HUB-0190) and no bleaching (Mü-1/Beta-291881), respectively.

457   The majority of the radiocarbon subset clusters in the last 3000 a, i.e. during late Holocene.

458   Only few ages cover the mid- and early Holocene as well as the Lateglacial (Fig. 10A1). The

459   distribution of OSL data is even more clustered, peaking in the last 1000 a (Fig. 10A2). We

460   are aware that the data have been obtained for specific study purposes particularly aiming at

461   the late Holocene landscape history and are, thus, based on highly intentional sampling

462   strategies. This could lead to a somewhat overrepresentation of younger ages. However,

463   already this general age distribution indicates intensified soil surface burying, i.e. enhanced

464   geomorphical activity in the late Holocene.

465   Nearly the same distribution pattern applies for radiocarbon and OSL ages from buried humic

466   and peaty surface soil horizons (fAh, fAa, fHv, fHa, fHr; Figs. 10B1, 10B2), accentuating a

467   late Holocene age. For this period the oldest buried surface horizon dates at 2950-2781 a cal

468   BP (Poz-98723, fAeh horizon in profile KFS8/site ID 13; Figs. 4A, 6, 9A), whereas the

469   youngest dates at 452-155 a cal BP (Poz-38927, fO horizon in profile FUER12/site ID 7;

470   Figs. 4A, 6). However, even some Lateglacial palaeosols occur. In profile FUER10-4

471   KM3/site ID 6 at the base of a c. 3 m-thick telmatic infill of a kettle-hole, which is attached to

472   the southeastern shoreline of Lake Fürstenseer See (Figs. 4A, 6), a fAh horizon developed

473   from glaciofluvial sand was dated using charcoal at 13475-13250 a cal BP (Poz-46611),

474   which corresponds to the Older Dryas-Allerød period (c. 13500-12600; Giesecke et al., 2012)

475   period. Further, buried brownish weathering horizons (fBv), occurring in two profiles in the

476   terminal moraine area west and east of Serrahn village, were dated by minimum ages (*termini*

477   *ante quem*) using OSL. In profile S-1/site ID 20 an age of 13440 ± 610 a (HUB-0045) on

478   overlying aeolian sand confirms the Lateglacial dating of a fBv horizon (120-140 cm)

479   immediately below (Figs. 4A, 6, Supplement 1). In profile S-6/site ID 24 a fBv horizon (205-

480   212 cm) is overlain by aeolian sand dating at 10550 ± 510 a (HUB-0061; Figs. 4A, 6), which

481   corresponds to the early Holocene.

482   Colluvial horizons/sediments (n = 21) strongly cluster in the period 1000 to 500 a, peaking at

483   c. 800 a (Fig. 10C). This peak corresponds with a calendar age of c. AD 1200, marking the

484   high Medieval colonisation of that area (Schich, 2003). Thus, in most cases colluvial

485   sediments were formed in the early (Slavic) to late (German) Medieval period in the Serrahn

486   area, referring to widespread soil erosion in historic times. The youngest age on colluvial

487   sand dates at 580 ± 30 a (HUB-114, Wa-3c/site ID 25; Figs. 4A, 6), which refers to very late

488   Medieval erosional processes at nowadays forested sites east of Serrahn village. Only a few

489   colluvial OSL ages date from the prehistoric time at 3350 ± 150 a (HUB-117, Wa-3/site ID

490   25), 2190 ± 160 a (HUB-0052, S-5/site ID 23) and 1460 ± 60 a (HUB-0054, S-4/site ID 22),

491   which all origin from the area west and east of Serrahn village. When including three

492   radiocarbon ages obtained from colluvial soil horizons in profiles Mü-1/site ID 17 (4825-

493   4535 a cal BP, Beta-291882, Gr-M; Figs. 4A, 9B), Ku1ND1/site ID 14 (3228-2959 a cal BP,

494   Erl-16603, M-fAh; Figs. 4A, 6), and KFS8/site ID 13 (3210-2967 a cal BP, Poz-98722, Gr-

495   M; Figs. 4A, 6) local formation of colluvial sediments during the Bronze Age to older Iron

496   Age can further be corroborated.

497   Six OSL data were obtained from aeolian sands in four profiles, showing a dichotomous age

498   distribution into the Lateglacial/early Holocene (S1/site ID 20, S-6/site ID 24) and late

499   Holocene (FUER3/site ID 3, S-2/site ID 21). The youngest age of 320 ± 20 a (HUB-0187,

500   FUER3/site ID 3) from an aeolian-lacustrine sequence next to the southwestern shoreline of

501   Lake Fürstenseer See shows that still in the 17th/18th century AD local aeolian dynamics

502   occurred.

503   A total of 17 ages obtained from charcoal (n = 15) and partly charred wood (n = 2) attests fire

504   dynamics (Fig. 10D). Most ages belong to the late Holocene (n = 13) peaking at c. 800 a cal

505   BP, whereas only few data derive from the Lateglacial (n = 2), early Holocene (n = 1) and

506   mid-Holocene (n = 1).

507

508   **4.5. Palaeoecological evidence**

509   **4.5.1. Palynology**

510   **Pollen diagram Mü-1**

511   Located in a glacial kettle-hole in the terminal moraine area west of Serrahn, profile Mü-1

512   (site ID 17) comprises a 110 cm-thick sequence of colluvial sand, peat and gyttja as well as

513   half-bog (German 'Anmoor') overlying glaciofluvial sand (Figs. 4B, 9B). Local pollen zone

514   Mü-A (110-98 cm) is dominated by PINUS, BETULA and CORYLUS pollen, indicating early

515   Holocene (Boreal period, c. 10500-9500 a cal BP; Giesecke et al., 2012) forest vegetation

516   dominated by the respective tree taxa. The radiocarbon age of that zone correspondingly is

517   9525-9305 a cal BP (Beta-291883; Supplement 7). In zone Mü-B (98-75 cm) also pollen of

518   warm-loving tree taxa is present, i.e. QUERCUS, TILIA, ULMUS and ALNUS. Furthermore, the

continuous presence of PLANTAGO LANCEOLATA TYPE and first findings of FAGUS pollen indicate a much younger age (Subboreal period, c. 5800-2750 a cal BP; Giesecke et al., 2012) of this zone, which is correspondingly dated to 4825-4535 a cal BP (Beta-291882). Consequently, the transition between zone Mü-A and Mü-B is marked by a hiatus for thousands of years, comprising the Atlantic period (c. 9500-5800; Giesecke et al., 2012). Again higher values of BETULA in the following zone Mü-C (75-65 cm) possibly reflect single stands of birch close to the coring site. In zone Mü-D (65-55 cm) a distinctive increase of NAP (non-arboreal pollen) including CHENOPODIACEAE, CALLUNA VULGARIS and PTERIDIUM AQUILINUM indicates increased human activity. The synchronous increase in charred particles may point at land-use by slash-and-burn activities. The closed curve of SECALE CEREALE starts. The radiocarbon age at 59 cm depth (4331-3995 a cal BP, Beta-291881) is regarded as being too old, when compared to the palynological data. Palynologically, the zone is dated to the early Subatlantic period (whole Subatlantic: 2750-0 a cal BP; Giesecke et al., 2012). Zone Mü-E (55-49 cm) shows increased amounts of tree and shrub pollen. The closing of forest is characterised by *Fagus*, *Quercus*, *Alnus* and *Carpinus*. Zone Mü-F (49-35 cm), dated by a radiocarbon age at 50 cm at 1517-1300 a cal BP (Beta-291880), shows a strong rise of NAPs comprising CEREALIA INDIFF. and SECALE CEREALE. It reflects an open, deforested landscape, while several charred particles and high values of PTERIDIUM AQUILINUM give evidence of slash-and-burn practice. In zone Mü-G (35-26 cm) low NAP values suggest moderate to low human impact. The closing forest is reflected by increasing values of FAGUS and QUERCUS. In zone Mü-H (26-15 cm), however, land use activities are recorded again, indicated by increasing values of CEREALIA INDIFF., SECALE CEREALE and RUMEX ACETOSA TYPE. The zones Mü-F to Mü-H archaeologically comprise the Slavic settlement period, c. AD 700-1180. The topping zone Mü-I (15-10 cm) reflects a closed forest with *Quercus* and a distinct increase of *Fagus*. It is dated to the high Medieval German settlement period, c. AD 1180-1300.

Pollen diagram KFS8

Profile KFS8 (site ID 13) is located in a glacial kettle-hole in the outwash plain east of Lake

Fürstenseer See. It comprises a 48 cm-thick peat cover overlying a very thin colluvial

layer/band (48-48.5 cm, IIGr-M) and a buried Gleyic Podzol (48.5-80 cm, IIIfAeh/Go-

fAhe/Go-fBsh/Gor-sequence) developed from glaciofluvial sand (Figs. 4B, 6, 9A). The pollen

diagram KFS8 shows clear changes in tree and herb pollen composition, so three pollen

assemblage zones have been separated (Supplement 8). The lowest zone KFS8-A (47.5-60

cm) is characterised by a dominance of tree pollen, with very high values of PINUS (>50%).

Also BETULA (>15%), ALNUS (10%) and CORYLUS (10%) are well represented. FAGUS,

CARPINUS and further tree pollen occur in low values. Herb pollen amount to only ~5% of all

terrestrial pollen. The most common herb pollen types are WILD GRASS GROUP, ARTEMISIA and

CALLUNA. The latter two, and very high values of charcoal particles (550%) point at some

openness of the forest, probably in relation to fire. Two radiocarbon ages from the colluvial

layer (IIGr-fM) and the buried humic topsoil horizon (IIIfAeh) of the buried Gleyic Podzol

yielded 3210-2967 a cal BP (Poz-98722, IIGr-M) and 2950-2781 a cal BP (Poz-98723,

IIIfAeh), respectively (Fig. 9A). The following zone KFS8-B (22.5-47.5 cm) is characterised

by even lower values of herb taxa, with ARTEMISIA and CALLUNA now being very rare. Also

charcoal particles are now rarer or absent. Tree pollen composition clearly changes at about

40 cm. The proportion of PINUS declines from well above 50% to only about 10%, while

BETULA, QUERCUS, FAGUS and CARPINUS increase to their maxima at 25 cm depth. CORYLUS

is overall rarer than in zone KFS8-A. In the upper zone KFS8-C (0-22.5 cm), the proportion

of herb taxa is clearly elevated to 10-20%. The values of WILD GRASS GROUP are continuously

high (~10%), while ARTEMISIA and CYPERACEAE show high values in single samples only.

Above 20 cm, the settlement indicators SECALE and CENTAUREA CYANUS are well present.

Both pollen types are commonly observed in Medieval or younger settlement periods, but

571 may also be present in records from earlier Slavic periods. Overall, the radiocarbon data and

572 the pollen diagram suggests that the buried land surface dates at ~3000 a cal BP (late Bronze

573 Age) and the lower part of the peat section formed during a period with low land use intensity

574 after ~2500 cal BP (older Iron Age). The upper part instead formed with high land use

575 intensity in the surroundings of the site, probably during the Slavic or German Medieval

576 period.

577

578 **Further pollen diagrams and single samples from profiles at Lake Fürstenseer See**

579 The underwater profile **FUER14** (site ID 8), obtained from a sediment core at a shallow in the

580 southern part of Lake Fürstenseer See (Fig. 4B), includes a thin peat layer (0-13 cm, fHv) on

581 top of calcareous gyttja (13-60 cm, IIfF). The peat layer is radiocarbon dated to the early

582 Holocene (9580-9417 a cal BP, Poz-38929; 8456-8212 a cal BP, Poz-38928). The pollen

583 record (Supplement 9) shows the immigration of *Corylus*, *Alnus*, *Quercus*, and *Tilia* taxa and

584 hence supports this dating. The record is first dominated by PINUS and BETULA pollen alone.

585 CORYLUS pollen slowly increases above 45 cm and is finally well present in zone FUER14-B.

586 Finally ALNUS, QUERCUS and TILIA pollen appear in the upper zone FUER14-C. Herb pollen

587 are very rare in the lower zones FUER14-A and B, indicating an overall dense forest cover.

588 Instead, zone FUER14-C shows clearly elevated values of several herb pollen and spore

589 types, e.g. WILD GRASS GROUP, fern spores and SPARGANIUM EMERSUM type. They probably

590 show local expansion of herbs during drying upof the site.

591 Located at a lake terrace, pollen diagram **FUER15** (site ID 9) was retrieved from a 34 cm-

592 thick sequence of palaeosol horizons (Fig. 4B, Supplement 10), which is overlain by

593 lacustrine sand (lake terrace sediment). Zone I (156-174 cm) includes the IIIGr, IIIfAh and

594 the lower part of the IIfHv2 horizon. Pollen samples from this zone are dominated by PINUS

595 DIPLOXYLON and ALNUS. The presence of deciduous tree pollen still indicates that the sand

596 was deposited during the Holocene. In Zone II (149-156 cm) PINUS DIPLOXYLON is rarer,

597 ALNUS more abundant than before. Also the WILD GRASS GROUP reaches higher values. The

598 presence of MOUGEOTIA spores can be interpreted as episodic flooding. In Zone III (144-149

599 cm) PINUS DIPLOXYLON is again the predominant pollen type, ALNUS rarer than before.

600 QUERCUS occurs regularly. Pollen grains of FAGUS and of cultural indicators (including

601 SECALE CEREALE) indicate that this zone was deposited not earlier than approx. BC 800 (cf.

602 Jahns, 2007). Increased values of some taxa (e.g. CYPERACEAE) point at wet conditions;

603 furthermore MOUGEOTIA might indicate episodic flooding. In zone IV (140-144 cm) PINUS

604 DIPLOXYLON is rarer than before, ALNUS more abundant, BETULA and QUERCUS occur.

605 Cultural indicators are well present and suggest that this zone was not deposited before the

606 Medieval (cf. Jahns, 2007), which is corroborated by the radiocarbon age 908-729 a cal BP

607 (Poz-47654) of the uppermost centimeter of the peat. The presence of some taxa (e.g. TYPHA

608 LATIFOLIA TYPE) points to the existence of reed vegetation, whereas water plants (e.g. CHARA

609 OOSPORES) indicate that the site was occasionally flooded.

610 Three pollen samples from palaeosol horizons (IVfAi, VrGr+fAh, VIfAh) in profile **FUER3**

611 (site ID 3; Figs. 4B, 6, Supplement 11) consist largely of (numerous) charred particles and are

612 characterised by poor pollen preservation. All samples are dominated by PINUS DIOLOXYLON,

613 suggesting that pine did occur at or near the site. Pollen of deciduous tree taxa is

614 correspondingly rare but could indicate at least for the uppermost sample rather diverse tree

615 composition (alder, birch, oak, hazel, beech). The presence of SECALE CEREALE (representing

616 rye) in the uppermost sample reveals that the initial humic soil horizon in lacustrine sands

617 (IVfAi) developed not before the Medieval period (cf. Jahns, 2007).

618 Pollen spectra from palaeosol horizons (IIfHa, IIIfAa, IIIfAh) in profile **FUER6** (site ID 4;

619 Figs. 4B, 6, Supplement 11) are dominated by PINUS DIPLOXYLON, which may primarily

620 result from the poor pollen preservation. This pollen type is rather robust and distinguishable

621 also in highly decomposed material. The occurrence of PEDIASTRUM in the uppermost sample

622   points at wetter conditions with (episodic?) flooding. All samples are rich in charred

623   particles, indicating that fire played an important role during local soil/peat formation.

624

625   **4.5.2. Anthracology**

626   Overall 677 charcoal particles from 18 samples with a total weight of 18 g were

627   taxonomically analysed primarily from colluvial horizons of soil profiles east and west of

628   Serrahn village (Supplement 12). The majority is pine (*Pinus*, n = 371 = 55%), followed by

629   oak (*Quercus*, n = 243 = 36%), birch (*Betula*, n = 39 = 6%), poplar/willow (*Populus/Salix*, n

630   = 10 = 1.5%), and beech (*Fagus*, n = 7 = 1%). Single occurrences (n = 1 = 0.1% each) were

631   identified for alder (*Alnus*) and ash (*Fraxinus*), as well as for stone fruit wood (*Prunus*). In

632   addition, four fragments (0.6%) were identified as deciduous wood only. A total of 84

633   charred non-wood particles (thus not included in the share calculation) shows no wood

634   anatomical features, potentially being bark fragments and impeding further determination.

635   Looking on the different profiles, 10 out of 18 charcoal assemblages are dominated by pine

636   (Supplement 12). Additional three assemblages have pine as a co-dominant taxon (co-

637   dominance defined by a share of at least 33%). Three samples are dominated by oak. There is

638   only one sample (S-5/site ID 23, lowest layer; Fig. 4B) with no pine. In profile S-1/site ID 20,

639   the amount of pine relative to oak is higher in the upper part than in the lower. This can also

640   be observed in profile S-5, where an increase of pine is clearly visible from the Pre-Roman

641   Iron Age to the (Slavic) Medieval. By contrast, in S-6/site ID 24 there is no clear tendency.

642   Generally in this region, an increase of pine towards the Medieval might reflect a land-use

643   effect. Pine is a pioneering species after, for instance, a period of land use and spreading

644   during re-forestation of abandoned fields. The charcoal spectra in S-3/site ID 18 is dominated

645   by pine and oak since the Pre-Roman Iron Age, and at least since the (Slavic) Medieval in S-

646   5 and S-6. Beech and oak dominate together the actual vegetation around the profiles, where

647   beech was only found with small quantities in the lower part of S-5 and in the upper part of

648 S-6. If there were beeches growing before their contemporary occurrence, they left no

649 charcoal signal in the soil profiles investigated.

650

651 **5. Discussion**

652 **5.1. Properties and formation of buried land surfaces**

653 As the modeling of the palaeosol areas shows (Fig. 7), a share of 9% (5.7 km^2) from the total

654 Serrahn study area (62 km^2) has buried land surfaces. Dominant cover sediments are aeolian

655 and colluvial sands supplemented by local lacustrine sands and peat. Further, rarely occurring

656 anthropogenic sediments exist in the form of sandy overburden, which particularly originates

657 from the construction of water ditches and ramparts (Fig. 6). Both the geochronological data

658 (Fig. 10) and the available knowledge on local to regional landscape history (e.g. Kaiser et

659 al., 2002, 2014a; Küster, 2014; Küster et al., 2014) show that human impact dominantly was

660 responsible for stimulating terrestrial erosion processes burying former land surfaces in the

661 late Holocene (see also chapter 5.2.). Despite the fact that this area is widely covered by

662 forest, being the effect of modern natural and anthropogenic afforestation after Medieval

663 clear cutting and land use (Schwabe et al., 2015; Müller et al., 2016), this high share of buried

664 land surfaces could generally be typical for the hilly morainic landscapes in northeastern

665 Germany. The land use history in northeastern Germany and the natural configuration

666 including relief and dominating sandy surface soils are comparable (Zerbe and Brande, 2003;

667 Böse et al., 2018). However, as the Modern period of agrarian land use intensification (Bayerl

668 et al., 2008) did not develop in the Serrahn area, the amount of 9% for buried land surfaces

669 might be a minimum estimate in comparison to the intensively agriculturally used

670 surroundings.

671 For instance, soil research in the nearby agrarian Quillow river catchment (168 km^2, 70%

672 arable land and pasture), located ca. 30 km to the east, has shown that only 10-15% of the

673 area consists of soils unaffected by soil erosion. The majority of soils comprise both eroded

674 surface soils and colluvial soils, whereby the latter widespread bury former land surfaces at

675 depressions (Sommer et al., 2008). The oldest colluvial deposits in this catchment date back

676 to the late Bronze Age. Most datings, however, cluster within the last 600 years with a peak

677 in the last 200 years, ascribing the main phase of local soil erosion to the recent past (Kappler

678 et al., 2018; van der Meij et al., 2019). However, both for the Quillow catchment and for

679 further central European study areas with well-established soil erosion chronologies (e.g.

680 Dotterweich, 2008; Dreibrodt et al., 2010; Kołodyńska-Gawrysiak, 2019), a spatial

681 estimation of buried land surfaces lacks. Even when expanding the spatial and temporal

682 focus, most studies have focused on single sites (pedon scale), rarely providing numbers on

683 the geometry of the buried soil storey except for a few available data from aeolian and near-

684 coastal fluvial landscapes in Germany, Poland and The Netherlands (Kaiser et al., 2006;

685 Jankowski, 2012; van Mourik et al., 2012; Sevink et al., 2013; Missiaen et al, 2015;

686 Verhegge et al., 2016; Schneider et al., 2017). These studies document contiguous buried soil

687 surfaces in a spatial range from 0.02 to 3.4 km^2.

688 With respect to a comparison of soil subtypes occurring either buried or on top of the current

689 land surface there are striking differences in the Serrahn area. When applying the

690 classification system of 'SEA95' (Landesforst Mecklenburg-Vorpommern, 2009), designed

691 for forest management and representing the most complex level of forest soil classification

692 available in Germany, 12 soil subtypes are identified for surface soils, whereas 21 soil

693 subtypes are identified for palaeosols (Schneider, 2017). This means that the soil variability

694 of the former land surface was obviously higher than that of present-day, which was reduced

695 by relief equalisation and particularly by the loss of wet micro-sites.

696

697 **5.2. Pedostratigraphical settings and implications on geomorphodynamics**

698 **5.2.1. Considerations on geochronology**

699   Backbone for reconstructing geomorphodynamics in the study area is the multitude of

700   geochronological datings obtained, comprising 40 radiocarbon ages and 33 OSL ages. To our

701   knowledge, it is generally the largest geochronological dataset available for a local

702   palaeopedological study in the glacial lowlands of central Europe (Starkel et al., 2013;

703   Kappler et al., 2019). However, there are some obvious (e.g. the number of datings per

704   profile) but even some less apparent constraints (e.g. the potential incorporation of older

705   charcoal in sediments by younger relocation), which should be outlined first to critically

706   appreciate the information given in the subchapters below.

707   Most of our dated profiles (20 from 26) have two or more geochronological datings which

708   helps to reliably draw chronological conclusions. However, there are some remaining ones,

709   where only one radiocarbon or OSL age was obtained due to practical reasons (missing or

710   unsuitable dating material, financial constraints). Those cases include some profiles at Lake

711   Fürstenseer See (FUER1/site ID 1, FUER10-2/site ID 5, FUER12/site ID 7, GFS11-A0/site

712   ID 12, Ku4.1/site ID 16) and a profile west of Serrahn village (S-2, site ID 21; Tables 3, 4).

713   The synoptic discussion of all locally available profile datings from the same sedimentary

714   environment including consideration of potential pitfalls (e.g. effects of bioturbation or

715   repeated relocations) allows for their careful use or rejection (Kaiser et al., 2014a, Küster,

716   2014). Further local dating evidence from palynology, archaeology and history, sometimes

717   available from the same profiles/sites (e.g. Müller et al., 2014), could be integrated in this

718   evaluations and corroborate our age estimations for specific events. Datings with obvious

719   doubt (n = 4) are marked in Tables 3 and 4 as well as in Figure 9, and have already been

720   discussed in chapter 4.4.

721   Besides bulk peat charcoal is the most important material for radiocarbon dating in our study,

722   counting for 16 samples (i.e. 40% of the radiocarbon ages). Charcoals were used to mainly

723   date palaeosol horizons including peat and, in a few cases (n = 5), to also date sediments of

724   colluvial (KFS8 / site ID 13, Ku1ND1 / site ID 14, Ku3BTr1 / site ID 15) and lacustrine

origin (FUER3 / site ID 3, GFS-11 / site ID 12; Table 4). With respect on the local fire

source, we assume after predominant natural fires in the Lateglacial and early Holocene a

widely anthropogenic fire regime in the late Holocene (see chapter 5.3. below and Dietze et

al., 2018). However, it should be kept in mind that due to possible relocations the charcoal

age sometimes could be older (thus dating an anthropogenic fire event) than the age of the

sediment deposition (e.g. Henkner et al., 2018). This risk in question primarily cannot be

ruled out if no OSL age is available from the same profile or sampling level for comparison.

Our OSL dataset (33 samples) is dominated by ages obtained from colluvial (n = 23) and

aeolian sands (n = 4), being materials which are generally uncomplicatedly to date (e.g.

Preusser et al., 2008; Alexanderson and Murray, 2012). Also most of our datings from

lacustrine sands (n = 4) have confirmed the local suitability of this material (Kaiser et al.,

2014a), although generally waterlain sediments can be difficult to date (e.g. Preusser et al.,

2008; Argyilan et al., 2010).

As the discussion above illustrates our geochronological dataset as a whole clearly offers the

potential for a reliable age estimation of geomorphodynamic and palaeoecologic events

including anthropogenic, i.e. past land-use activities in the Serrahn area. For specific profiles,

i.e. focusing on the profile-scale, however, several potential constraints including

bioturbation and 'anthroturbation' (Schaetzl and Anderson, 2005) have to be taken in to

account, which can be resolved only by higher horizontal (profiles) and vertical resolution

(datings) in the future.

5.2.2. Aeolian setting

Prominent palaeopedological feature of aeolian sequences in the study area (e.g. site IDs 19,

20, 21, 24) is a 10 to 40 cm-thick brownish buried soil horizon (fBv), showing properties of

silicate weathering (Figs. 6, 8A-D, 11A). Considering its morphology, pedostratigraphical

position and geochronological dating into the Lateglacial up to the very early Holocene, it

751   was already previously identified as 'Finow soil' (Kaiser et al., 2014a; Küster, 2014;

752   Schwabe et al., 2015), representing a widespread buried marker soil (brunic Arenosol) in

753   northern central Europe and beyond (e.g. Bussemer et al., 2009; Kaiser et al., 2009;

754   Jankowski, 2012; Schlaak, 2015; Hirsch et al., 2017; Kappler et al., 2019, Konstantinov et al.,

755   2019). A potentially related fAh horizon usually lacks. Whether this is caused by erosion

756   during the initial aeolian process finally burying the soil or by complete postdepositional

757   mineralisation of the organic matter remains unclear. For the latter assumption a layer with

758   textural properties similar to the fBv horizon could be expected directly above, which has not

759   been found up to now (Kaiser et al., 2009). Former palaeopedological investigations of this

760   soil have shown that clay illuviation bands can occur within, but predominantly occur below

761   this brownish weathering (cambic) horizon (Kaiser et al., 2009). In contrast to Jankowski

762   (2012), Hirsch et al. (2015) and Hirsch and Raab (2018), who identified bridges of illuviated

763   clay and textural band formation as characteristic features of the Finow soil, no signs of clay

764   illuviation could be found in the thin section of the IIfBv horizon in profile S-1 (site ID 20;

765   Fig. 8A-D). Instead, characteristic features of silicate weathering, such as weathered sand

766   grains and ferruginous punctuation of the fine mass, suggest the formation of a proper cambic

767   horizon representing the Finow soil. While weathering of the sand grains could be inherited

768   from the parent material (at least partly), the ferruginous punctuation of the fine mass is

769   formed *in situ*. Impregnations of the fine material covering the sand grains and bridging

770   those, affect large parts of the material, locally intensifying to a degree of moderate to strong

771   impregnation.

772   Soil horizons within (site ID 3) or below Holocene aeolian sands (site IDs 15, 19, 21) are

773   formed as thin fAi/fAh horizons (Arenosols) and fAh-fBv/fAp-fBv sequences (Cambisols) as

774   well as fHv horizons, respectively.

775   Generally, stratigraphical and geochronological evidence from the Serrahn area widely shows

776   a two-phase aeolian dynamic for that area, comprising a Lateglacial to (very) early Holocene

and a late Holocene period of aeolian sedimentation and dune formation (Fig. 11A). In

comparison to the regional dynamics, showing several prominent peaks at 13.8-11.2, 9.5-7.8,

2.2-1.6, and 1.0-0 ka cal BP (Kappler et al., 2019), this assumed local dynamic is rather

simple and could be related to climatic (older period with mobilisation of drift sands by soil

erosion due to cool-dry climate) and anthropogenic impact (younger period with mobilisation

of drift sands by land-use triggered soil erosion). The local aeolian dynamic during the late

Pleistocene and Holocene at Müritz National Park is especially well documented by

geochronologically and palynologically dated records (Dieckmann and Kaiser, 1998; Kaiser

et al., 2002; de Klerk, P., 2008; Küster and Preusser, 2009; Theuerkauf and Joosten, 2012;

Küster, 2014; Küster et al., 2014), corroborating our simple two-phase model for the Serrahn

area. Other mid- to north European regions show far more Holocene aeolian activity periods

associated with climatic or human impact (e.g. Tolksdorf and Kaiser, 2012; Dobrotin et al.,

2013; Sevink et al., 2018; Pierik et al., 2018; Alexanderson and Bernhardson, 2019; Jonczak

et al., 2019; van Mourik and van der Meer, 2019). Although human settlement is proven for

the Serrahn area since the Neolithic (immediately outside the National Park area) and the

Bronze Age (inside; Supplement 1), a close relationship of potential land use (land

degradation) and aeolian dynamics could not be proven here thus far except for the last c. 800

years.

A specific aeolian feature of the study area is the partly direct neighbourhood of dunes and

aeolian sand sheets with lakes. Such locations are particularly well-developed at the transition

from Lake Fürstenseer See to Lake Hinnensee (western shoreline), at the southwestern

shoreline of Lake Fürstenseer See and of the western shoreline of Lake Lutowsee (Fig. 4B).

At the latter, dune flanks, overlying an older lake terrace, steeply dip into the lake. As profile

FUER3 (site ID 3) shows, still in the 17th/18th century AD aeolian dynamics occurred at

such locations, with a similar dating as in the western part of Müritz National Park, where the

Medieval to Modern period could be resolved into three aeolian activity phases (Küster et al.,

803   2014). In general, these aeolian-lacustrine sequences (Sevink et al., 2013; Kaiser et al.,

804   2014a; Hošek et al., 2017) form a widely untapped regional geoarchive, which due to their

805   palaeopedological, palaeoecological and dating potential could help to resolve the sites

806   history more precisely.

807

808   **5.2.3. Colluvial setting**

809   In the Serrahn area colluvial sediments are found widespread particularly in depressions of

810   the terminal moraine and till plain to the north, but even upon slopes of lake and kettle-hole

811   depressions in the outwash plain to the south. Due to their local occurrence (several tens to

812   thousands of square meters), they have not been mapped in geological and geomorphological

813   maps (e.g. Börner and Schütze, 2005). For the first time they were systematically found and

814   described during a large-scale soil mapping campaign in 1997/1998 (Dieckmann and Kaiser,

815   1998; LFoA M-V, 1999). Although it was already known that even the near-natural and

816   rather large beech-dominated forest stands around Serrahn village underwent a complex late

817   Holocene site history comprising sporadically strong human impact (Müller, 1962), the

818   ubiquitous occurrence of signs of past soil erosion such as young pedosedimentary

819   sequences, eroded soil surfaces, colluvial terraces (lynchets) and specific aeolian landforms,

820   i.e. hummocky dunes, is remarkable (Figs. 11, 12). Similar to other well-protected sites in the

821   central European lowlands, a seemingly natural forest vegetation led first to the impression of

822   rather native site conditions but later, after in-depth palaeoenvironmental studies, to the

823   recognition of partly drastic ecosystem disturbances in the past (e.g. Bradshaw et al., 2005;

824   Lorenz et al., 2015; Jaroszewicz et al., 2019). Our local findings give further evidence of

825   substantial landscape changes (and their partial recovery) in the late Holocene.

826   The sandy colluvial layers with thicknesses between 0.5 and 159 cm have no textural or

827   further pedogenic differentiation, as sometimes reported from other colluvial sequences in

828   northern central Europe, where secondary brunification or clay illuviation were found (e.g.

829 Küster et al., 2015a; Kühn et al., 2017; Kołodyńska-Gawrysiak, 2019). This could indicate

830 with perspective on the sediment delivery the same source area and/or no change of sediment

831 composition, while no pedogenic differentiation (well-developed soil formation) could mean

832 a fast sedimentation process and a rather young event or renewed erosion.

833 As the geochronological data from colluvial horizons in the Serrahn area show, there is a

834 record solely from the late Holocene, spanning a time interval from c. 4700 to 300 a (Fig.

835 10C1, C2). The data cluster in the period 1000 to 500 a, peaking at c. 800 a, which is

836 equivalent to the high Medieval colonisation of that area (Schich, 2003). In addition to this

837 Medieval data maximum, further colluvial episodes can be detected for the Bronze Age, the

838 older Iron Age, the Migration Period and the Modern Period (Fig. 11B). In general, this data

839 distribution fits well to the regional record, where additional data for the Neolithic and

840 Roman Iron Age exist (Kappler et al., 2018, 2019).

841 From a regional point of view the record of late Slavic colluvial layers around Serrahn village

842 in profiles S-1 (site ID 20), S-4 (site ID 22), S-5 (site ID 23), and S-6 (site ID 24), dating in

843 range of 1010 ± 40 to 1180 ± 90 a (n = 11), is particularly remarkable. They prove intensive

844 soil erosion already in the 11th to 12th centuries AD, which is corroborated by the

845 palynological record in pollen diagram Mü-1 indicating agriculture at that time. Normally,

846 the somewhat younger high Medieval German colonisation phase during the late 12th/13th

847 centuries AD is considered to be the most important turning point in landscape development

848 during the late Holocene in northeastern central Europe, where human impact by forest

849 clearing, settlement construction and land use intensification dramatically increased (e.g.

850 Starkel, 2005; Böse and Brande, 2009; Küster and Preusser, 2009; Dreibrodt et al., 2010).

851 However, the area around Serrahn village was obviously subjected to intensive agrarian land

852 use somewhat earlier in the Medieval period (Küster, 2014).

853

854 **5.2.4. Lacustrine and mire setting**

Systematic research of lake shore sites and mires in the Serrahn area have proven a wealth of

wet-site palaeosols on a regionally unprecedented scale. Although known in principle that

these sedimentary environments could contain palaeopedologic features, reflecting phases of

temporally prevailing terrestrial or semiterrestrial ('dry-site') conditions, comparing evidence

from northern central Europe is rare (e.g. Mundel et al., 1983; Petzelberger et al., 1999;

Alaily and Brande, 2002; Tolksdorf et al., 2014; Hirsch et al., 2015; Mendyk et al., 2016;

Karasiewicz, 2019). Our findings support some recent records from lakes in northeastern

Germany (e.g. Küster et al., 2012; Küster, 2014; Klos, 2016; Kaiser et al., 2018; Lorenz et

al., 2019), that showed seemingly 'every' lake terrace of at least Holocene age containing

sub-sites, where buried palaeosols mostly of Gleysol or Histosol type occur.

Corresponding research in the Serrahn area concentrated on terraces and related beach ridges

in the southern part of Lake Fürstenseer See. Its shoreline is widely accompanied by a flat

terrain fringe, ranging from a few decimetres to c. 2 m above the mean water level of 63.4 m

a.s.l. (Fig. 2F). Two terrace levels occur; a lower one a few decimetres above the lake of

relatively recent age and an upper one between c. 1 and 2 m above the lake of late Medieval

age (Kaiser et al., 2014a).

Profiles from the upper terrace show a sequence of basal glacial sand, intermediate palaeosols

and lacustrine sand on top (Fig. 11C). The palaeosols mostly show a lower humic (terrestrial)

horizon (fAa or fAh) covered by a peat horizon (fH), indicating a transition to wetter (semi-

terrestrial) site conditions. In profile FUER15 (site ID 9, Fig. 4B) this transition is clearly

reflected in the reconstructed vegetation shift from tree stands, via occasionally flooded alder

carr to flooded reed swamp (Supplement 10). Peat formation here encompasses an age

interval of c. 600 years, ending in the late Medieval. The presence of highly decomposed

horizons (fHa) with cracks within the peat layers in profiles FUER2 (site ID 4), FUER6 (site

ID 4) and FUER16-4 (site ID 10; Fig. 4B) indicates that the water level fluctuated during or

after peat formation. The palaeosol dates from Lake Fürstenseer See span a wide time

interval with an age of 5891 to 550 a cal BP, whereas the OSL dates of the overlying

lacustrine sands encompasses a narrow time interval with an age of 760 to 560 a, i.e. late

Medieval. Consideration of the upper limit of lacustrine sands in the dated profiles suggests

that the lake level during the late Medieval period reached a maximum level of c. 66 m a.s.l.,

i.e. c. 2.5 m above the present mean water level (Kaiser et al., 2014a; 2014b). Comparable

records from shorelines were also obtained from other lakes in northeastern Germany,

referring to consistent hydrological changes in the late Holocene caused by climatic and

anthropogenic impact (Lorenz, 2007; Kaiser et al., 2012; Küster, 2014; Dietze et al., 2016;

Brauer et al., 2019).

Pedosedimentary sequences in the Serrahn area particularly indicate the development of

mires in glacial kettle-holes, which formed in very local depressions resulting from dead-ice

melting (Couwenberg et al., 2001; Kaiser et al., 2012). As the example for a rather deep

kettle-hole south of Lake Fürstenseer See shows, profile FUER10-4 (site ID 6) has a fAh

horizon at the base, which is buried by a 309 cm-thick sequence of peat and gyttja (Figs. 4B,

6). According to the radiocarbon date (13475-13250 a cal BP; Poz-46611), this humic

horizon has developed in the Lateglacial, most probably when the local dead-ice plomb was

still preserved in the ground. The secondary deep position of the terrestrial topsoil horizon

can be related to local subsidence during ice melting. It has caused down-lift of the covering

sediments including soil with subsequent water-logging and peat formation still in the

Lateglacial (Fig. 11D). Dead-ice melting with similar sedimentary phenomena (i.e. mostly

record of basal peat under lacustrine gyttja) is considered to be mainly responsible for the

formation of lake and mire basins in the Weichselian glacial belt of northern central Europe

and beyond (e.g. Słowinski et al., 2015; Stivrins et al., 2017; Kaiser et al., 2018). The small

round mire at FUER10-4 (40 m in diameter) can be hydrogenetically classified as a kettle-

hole mire (Kaiser et al., 2014a), generally being a typical feature of the Serrahn area, where c.

50 of them were recorded (Rowinsky and Kobel, 2011).

907   By contrast, the shallow kettle-hole with profile KFS8 east of Lake Fürstenseer See (site ID

908   13; Figs. 4B, 6, 9) reflects a strongly different site history. After (Lateglacial?) formation of

909   this c. 80 m-long dead-ice hollow, a Gleyic Podzol (fAeh/Go-fAhe/Go-fBsh/Gor-sequence)

910   developed on its relatively dry bottom in the Holocene. As the overlying only 48 cm-thick

911   peat layer as well as the radiocarbon and pollen data attest, local groundwater rise has

912   initiated peat growth between ~3000-2500 a cal BP (Fig. 11D). Although the pollen analysis

913   of the lower part of the peat (older Iron Age) reveals less land use intensity as compared to

914   the upper part (Medieval), this local paludification could be related to the felling or thinning

915   out of the highly water-consuming tree vegetation in the catchment, as demonstrated in

916   similar contexts for central Europe and beyond (e.g. Woodward et al., 2014; Dietze et al.,

917   2016). Taking the stratigraphy including peat thickness and chronology into account, this

918   mire can be hydrogenetically classified as a swamp (paludification) mire (Couwenberg et al.,

919   2001) located in a glacial kettle-hole.

920

921   **5.3. Vegetation development, land use and fire**

922   Unlike continuous sedimentary sequences from lake and mire sections, the palynological data

923   available from discontinuous pedosedimentary sequences in the Serrahn area normally allows

924   only for temporarily and spatially restricted insights into the local vegetation history. The

925   palynological sections analysed comprise in one case nearly the whole Holocene (Mü-1),

926   whereas all other sections comprise either the early (FUER14) or the late Holocene (KFS8,

927   FUER3, FUER6, FUER; Fig. 4A; Supplements 7-11).

928   Although initially decreasing at the beginning of the late Holocene, a consistent property of

929   all sections is a rather high content of pine. This is supported by the anthracological analyses

930   from 677 fragments of profiles around Serrahn village, showing a late Holocene dominance

931   of pine (55%) complemented by oak (36%) and others (9%), such as birch and few beech

932   (Supplement 12). As pollen diagram Mü-1 together with further data from the Serrahn area

933   shows (Küster, 2014; Theuerkauf, 2015; Müller et al., 2016), beech started to expand only

934   about c. 3000 years ago forming beech-dominated tree stands particularly in the terminal

935   moraine and till plain zone. This is in contrast to anthracological data from Iron Age levels of

936   the investigated profiles, showing a few *Fagus* charcoals only. Serrahn pollen data clearly

937   indicate that beech became locally extinct during the Medieval and afterwards by human

938   impact (forest clearing, grazing, agriculture) but recovered after cessation of land use. Forest

939   recovery started with the spread of pioneer trees such as birch and pine followed by

940   hornbeam and beech. Generally, pine plays a significant role in the Serrahn area throughout

941   the Holocene, but showing, after high pollen share in the early Holocene, a marked decrease

942   in the older Subatlantic followed by an increase in the younger Subatlantic again, i.e. from

943   the Medieval period onwards (Kaiser et al., 2014a; Theuerkauf, 2015; Supplement 7). This

944   long-term occurrence of pine since the early Holocene is typical even for other sandy sites in

945   central Europe (Jamrichová et al., 2019).

946   From an only 15 km x 15 km large area with Serrahn in the centre, a total of c. 30 pollen

947   diagrams mostly from the 1960s is available (Müller, 1962; de Klerk, 2008; Theuerkauf and

948   Joosten, 2012; Kaiser et al., 2014a; Theuerkauf, 2015; this study), representing together with

949   the Berlin-Potsdam area (Brande, 1996; Jahns et al., 2013) and Rügen Island (Lange et al.,

950   1986) a focal point of palynological data in northeast Germany. According to these pollen

951   diagrams first human influence on the vegetation by local agrarian land use becomes apparent

952   from the Neolithic onwards, which intensified during the Bronze Age. The subsequent

953   prehistoric and historic settlement periods are represented by different land use intensities.

954   This general pattern becomes apparent even in the temporal distribution of archaeological

955   sites, showing, however, in comparison to open land a markedly reduced overall record due

956   to the prevailing forest cover (Supplement 1).

957   As cartographic sources show, the whole Serrahn area was widespread re-covered by forests

958   not later than in the 18th century AD (Tempel, 2003), with dominating mixed stands (pine,

beech, oak) in the northern part and dominating coniferous stands in the southern part. Parts

of the UNESCO World Natural Heritage Serrahn site developed within only c. 100 years

from a pine-dominated secondary forest in the late 18th century AD to a beech-dominated

'ancient' forest in the late 19th century AD (Schwabe et al., 2015). Although non-uniformly

distributed, some hundred occurrences of relict plough horizons (rAp), observed in topsoils

of the whole area, are direct evidence of preceding agriculture in the Serrahn area (Table 1,

Fig. 5B).

According to the charcoal content of palaeosols and colluvial layers in several of the profiles

investigated, fire has played a significant role in the past. Nowadays, fire is insignificant in

this landscape, because of predominance of fire-unaffected forest ecosystems and effective

suppression of anthropogenic ignition causes (Thonicke and Cramer, 2006; Dietze et al.,

2018). Most radiocarbon ages derived from charcoal belong to the late Holocene (n = 13)

peaking at c. 800 a cal BP (Fig. 10D). Whereas most soil horizons and sediment layers show

a scattered distribution of macro charcoals (>200µm; Carcaillet, 2007), several palaeosol

horizons (fAh, fAi, fAa, fHv, fHa) from profiles directly located at the shoreline of Lakes

Fürstenseer See (e.g. FUER3/site ID 3, FUER6/site ID 4, FUER15/site ID 9; Fig. 4B) and

Hinnensee (e.g. HIN34, HIN52; Supplement 2) have very strong contents of both macro and

micro charcoals. Partly, the organic soil matrix is even dominated by charred substance (e.g.

FUER3). The radiocarbon data from charcoals of profiles FUER3 (2713-2379 a cal BP, Poz-

38930), FUER6 (961-798 a cal BP, Poz-37355) and FUER15 (908-729 a cal BP, Poz-47654)

point to a prehistoric (older Iron Age) to high Medieval age of the detected fire events. As

artifacts, such as ceramics or other objects, always lack, a context with local settlement

activities (housing) appears unlikely. Instead, fire could have reached the shorelines in the

course of slash-and-burn cultivation of adjoining forests. Generalised knowledge on fire

dynamics of the central European lowlands shows that humans have significantly affected the

fire regimes beyond the local scale, even in periods of low population densities (Dietze et al.,

2018). Further, even wet sites may contain substantial shares of rather old (Holocene)

pyrogenic carbon, amounting for a mean of 13.5% of soil carbon in central and northern

European peatlands (Leifeld et al., 2018).

Direct evidence for pyrolytic woodland conversion, i.e. charcoal production, and related

vegetation change, exists in the whole Serrahn area by the occurrence of vast quantities of

charcoal kilns (hearths) and of some tar kilns (Fig. 5B). They form a potential source of

charcoal found in surface soils and even in palaeosols of that area. Currently, about 1100

charcoal kilns are known with a conspicuous clustering in the southeastern part around

Waldsee village (Küster et al., 2015b). However, as a re-mapping campaign of charcoal kilns

around Lake Fürstenseer See has shown, increasing the number of known kilns from 30 to

230, this pattern is biased by different field mapping approaches and efforts (Nelle et al.,

2015). Semi-automated detection of charcoal kilns by using LiDAR-derived digital terrain

models (Schneider et al., 2015) failed for the Serrahn area due to too little size of these

structures with diameters of 3 to 6 m and heights of a few decimeters only. Although

radiometric or dendrochronological ages for the Serrahn kilns are still lacking, a tentative

dating into the period AD 1500 to 1900 seems very plausible following palynological and

historical evidence (Küster et al. 2015b; Nelle et al., 2015). Generally, the detection of

charcoal kilns both in lowland and upland forests of central Europe has recently shown (e.g.

Schmidt et al., 2016; Kočár et al., 2018; Raab et al., 2019; Schneider et al., 2020) that they

occur extensively. Numbers between thousands (e.g. Serrahn area; Nelle et al., 2015; this

study) and some hundreds of thousands (e.g. Polish uplands north of Cracow; Rutkiewicz et

al., 2019) have been recorded per study area. In addition to drastic changes of the very local

topsoil and relief, the enrichment of charred carbon could even positively influence the local

growth conditions in the long run (Hirsch et al., 2018; Bonhage et al, 2020).

6. Conclusions

Knowledge on the distribution, types, ages, and properties of palaeosols and their cover sediments plays an essential role in understanding how the lowlands in central Europe have changed over the millennia, being an indispensable requirement for evaluating long-term human impact including soil erosion and land-cover dynamics. Applying a multiproxy-approach by using data from pedology, micromorphology, geochronology, and palaeoecology, the following conclusions can be drawn:

- For the Serrahn study area, a total of 520 palaeosol-bearing soil profiles is available, comprising a buried soil area of 5.7 km^2. Palaeosols dominantly occur in areas with glaciofluvial sands but they are associated even with other geological facies such as terminal moraines, dunes, lake shores, and mires. Most sandy palaeosols belong to the soil types Cambisol, (partly-) eroded Arenosol and Gleysol. Dominant cover sediments are aeolian and colluvial sands as well as lacustrine sand and peat.

- The geochronological data derived from palaeosols (mostly radiocarbon data) and cover sediments (mostly OSL data) peak in the last 3000 years and 1000 years, respectively. This age distribution indicates intensified soil surface burying, i.e. enhanced geomorphical activity in the late Holocene.

- Implications on Lateglacial and Holocene geomorphodynamics could be concluded for several sedimentary environments (aeolian, colluvial, lacustrine, telmatic). A two-phase aeolian dynamic becomes evident, comprising a Lateglacial to early Holocene and a late Holocene period. Colluvial sedimentation, referring to local agriculture in the late Holocene, reached a maximum in the Medieval supplemented by further colluvial episodes in the Bronze Age, older Iron Age, Migration period, and Modern period. Palaeosols within lacustrine and peat sequences reveal lake and groundwater level fluctuations, respectively, particularly in the late Holocene.

1036   •   The palynological data obtained from palaeosols and their cover sediments show that

1037   first local agrarian land use occurred during the Neolithic and intensified during the

1038   Bronze Age. Subsequent prehistoric and historic settlement periods are represented by

1039   different land-use intensities. Anthracological data reveal a late Holocene dominance

1040   of pine complemented by oak and others, such as birch and beech.

1041

1056

1057 **References**

1058 Ad-hoc-AG Boden, 2005. Bodenkundliche Kartieranleitung. Schweizerbart, Hannover.

1059 AFSV – Arbeitsgemeinschaft Forstliche Standorts- und Vegetationskunde, 1995.

1060   Exkursionsführer zur 57. Jahrestagung der Arbeitsgemeinschaft Forstliche Standorts-

1061   und Vegetationskunde in Mecklenburg-Vorpommern 13.09.-16.09.1995. Schwerin.

1062   Alaily, F., Brande, A., 2002. Bodenentwicklung am Rande oligotropher Moore im Raum

1063   Berlin. Journal of Plant Nutrition and Soil Science 165, 305-312.

1064   Alexanderson, H., Murray, A., 2012. Problems and potential of OSL dating Weichselian and

1065   Holocene sediments in Sweden. Quaternary Science Reviews 44, 37-50.

1066   Alexanderson, H., Bernhardson, M., 2019. Late glacial and Holocene sand drift in northern

1067   Götaland and Värmland, Sweden: sediments and ages. GFF 141, 84-105.

1068   Argyilan, E.P., Forman S.L., Thompson T.A., 2010. Variability of Lake Michigan water level

1069   during the past 1000 years reconstructed through optical dating of a coastal strandplain.

1070   The Holocene 20, 723-731.

1071   Bayerl, G., Werner, A., Beetz, S., Plieninger, T., Rus, C.G., 2008. Landnutzungswandel. In:

1072   Hüttl, R.F., Bens, O., Plieninger, T. (Eds.), Zur Zukunft ländlicher Räume:

1073   Entwicklungen und Innovationen in peripheren Regionen Nordostdeutschlands.

1074   Interdisziplinäre Arbeitsgruppen Forschungsberichte. Akademieverlag, Berlin, pp. 41-

1075   56.

1076   Beuselinck, L., Govers, G., Poesen, J., Degraer, G., Froyen, L., 1998. Grain-size analysis by

1077   laser diffractometry: comparison with the sieve-pipette method. Catena 32, 193-208.

1078   BGR – Bundesanstalt für Geowissenschaften und Rohstoffe, 2011. BÜK200 –

1079   Bodenübersichtskarte 1:200.000, Blatt CC3142 Neubrandenburg. Hannover.

1080   Börner, A., 2015. Geologische Entwicklung des Gebietes um den Großen Fürstenseer See. In:

1081   Kaiser, K., Kobel, J., Küster, M., Schwabe, M. (Eds.), Neue Beiträge zum Naturraum

1082   und zur Landschaftsgeschichte im Teilgebiet Serrahn des Müritz-Nationalparks.

1083   Forschung und Monitoring 4, Geozon Science Media, Berlin, pp. 21-29.

1084   Börner, A., Schütze, K., 2005. Geologische Karte von Mecklenburg-Vorpommern 1:50.000,

1085   L2744 Neustrelitz. Landesamt für Umwelt, Naturschutz und Geologie, Güstrow.

1086   Böse, M., Brande, A., 2009. Landscape history and man-induced landscape changes in the

1087   young morainic area of the North European Plain – a case study from the Bäke Valley,

1088   Berlin. Geomorphology 122, 274-282.

1089   Böse, M., Ehlers, J., Lehmkuhl, F., 2018. Deutschlands Norden: vom Erdaltertum zur

1090   Gegenwart. Springer, Berlin.

1091   Bonhage, A., Hirsch, F., Schneider, A., Raab, A., Raab, T., Donovan, S., 2020. Long term

1092   anthropogenic enrichment of soil organic matter stocks in forest soils – detecting a

1093   legacy of historical charcoal production. Forest Ecology and Management 459, 117814.

1094   Bradshaw, R.H.W., Wolf, A., Møller, P.F., 2005. Long-term succession in a Danish temperate

1095   deciduous forest. Ecography 28, 157-164.

1096   Brande, A., 1996. Type region D-s, Berlin. In: Berglund, B.E., Birks, H.J.B., Ralska-

1097   Jasiewiczowa, M., Wright, H.E. (Eds.), Palaeoecological events during the last 15000

1098   years. Regional syntheses of palaeoecological studies of lakes and mires in Europe.

1099   Wiley, Chichester, pp. 518-523.

1100   Brauer, A., Hajdas, I., Blockley, S.P.E., Bronk Ramsey, C., Christl, M., Ivy-Ochs, S.,

1101   Moseley, G.E., Nowaczyk, N.N., Rasmussen, S.O., Roberts, H.M., Spötl, C., Staff,

1102   R.A., Svensson, A., 2014. The importance of independent chronology in integrating

1103   records of past climate change for the 60–8 ka INTIMATE time interval. Quaternary

1104   Science Reviews 106, 47-66.

1105   Brauer, A., Schwab, M.J., Brademann, B., Pinkerneil, S., Theuerkauf, M., 2019. Tiefer See

1106   – a key site for lake sediment research in NE Germany. DEUQUA Special Publications

1107   2, 89-93.

1108   Brock, F., Higham, T., Ditchfield, P., Ramsey, C.B., 2010. Current pretreatment methods for

1109   AMS radiocarbon dating at the Oxford Radiocarbon Accelerator Unit (ORAU).

1110   Radiocarbon 52, 103-112.

1111   Bronk Ramsey, C., 2009. Bayesian analysis of radiocarbon dates. Radiocarbon 51, 337-360.

1112 Bullock, P., Fedoroff, N., Jongerius, A., Stoops, G., Tursina, T. (Eds.), 1985. Handbook for

1113 soil thin section description. Waine Research Publications, Albrighton, Wolverhampton.

1114 Bussemer, S., Schlaak, N., Gärtner, P., 2009. Neue paläopedologische Befunde zu Habitus

1115 und Verbreitung des Finowbodens. Brandenburgische geowissenschaftliche Beiträge

1116 16, 79-86.

1117 Carcaillet, C., 2007. Charred particle analysis. In: Elias, S.A. (Ed.), Encyclopedia of

1118 Quaternary Science, vol. 2. Elsevier, Amsterdam, pp. 1582-1593.

1119 CLC – Corine Land Cover, 2012. Copernicus Land Portal. European Environment Agency

1120 (EEA), Copenhagen.

1121 Chapman, H., Adcock, J., Gater, J., 2009. An approach to mapping buried prehistoric

1122 palaeosols of the Atlantic seaboard in Northwest Europe using GPR, geoarchaeology

1123 and GIS and the implications for heritage management. Journal of Archaeological

1124 Science 36, 2308-2313.

1125 Chaopricha, N.T., Marín-Spiotta, E., 2014. Soil burial contributes to deep soil organic carbon

1126 storage. Soil Biology and Biochemistry 69, 251-264.

1127 Chendev, Y., Khokhlova, O., Ponomarenko, E., Ershova, E., Alexandrovskiy, A., Myakshina,

1128 T., 2018. Holocene environmental and anthropogenic changes of soils and vegetation in

1129 the Central Russian Upland: The case study in the "Belogorie" natural reserve.

1130 Geosciences 8, 473.

1131 Conrad, O., Bechtel, B., Bock, M., Dietrich, H., Fischer, E., Gerlitz, L., Wehberg, J.,

1132 Wichmann, V., Böhner, J., 2015. System for Automated Geoscientific Analyses

1133 (SAGA) v. 6.2.0. Geoscientific Model Development 8, 1991-2007.

1134 Costantini, E.A., Napoli, R., D'Egidio, G., 2007. Adding information about soils and

1135 paleosols to geological maps, through the application of the "pedostratigraphic level"

1136 concept. Quaternary International 175, 125-139.

1137   Couwenberg, J., de Klerk, P., Endtmann, E., Joosten, H., Michaelis, D., 2001.

1138   Hydrogenetische Moortypen in der Zeit – eine Zusammenschau. In: Succow, M.,

1139   Joosten, H. (Eds.), Landschaftsökologische Moorkunde. Schweizerbart, Stuttgart, pp.

1140   399-403.

1141   de Klerk, P., 2008. Patterns in vegetation and sedimentation during the Weichselian Late-

1142   glacial in north-eastern Germany. Journal of Biogeography 35, 1308-1322.

1143   Dieckmann, O., Kaiser, K., 1998. Pedologische und geomorphologische Befunde zur

1144   historischen Bodenerosion im Müritz-Nationalpark, Mecklenburg-Vorpommern. In:

1145   Asmus, I., Porada, H.T., Schleinert, D. (Eds.), Geographische und historische Beiträge

1146   zur Landeskunde Pommerns. Thomas Helms-Verlag, Schwerin, pp. 59-65.

1147   Dietze, E., Słowinski, M., Zawiska, I., Veh, G., Brauer, A., 2016. Multiple drivers of

1148   Holocene lake level changes at a lowland lake in northeastern Germany. Boreas 45,

1149   828-845.

1150   Dietze, E., Theuerkauf, M., Bloom, K., Brauer, A., Dörfler, W., Feeser, I., Feurdean, A.,

1151   Gedminiene, L., Giesecke, T., Jahns, S., Karpinska-Kołaczek, M., Kołaczek, P.,

1152   Lamentowicz, M., Latałowa, M., Marcisz, K., Obremska, M., Pedziszewska, A., Poska,

1153   A., Rehfeld, K., Stancikaite, M., Stivrins, N., Swieta-Musznicka, J., Szal, M., Vassiljev,

1154   J., Veski, S., Wacnik, A., Weisbrodt, D., Wiethold, J., Vanniere, B., Słowinski, M.,

1155   2018. Holocene fire activity during low-natural flammability periods reveals scale-

1156   dependent cultural human-fire relationships in Europe. Quaternary Science Reviews

1157   201, 44-56.

1158   Dobrotin, N., Bitinas, A., Michelevicius, D., Damušyte, A., Mazeika, J., 2013. Reconstruction

1159   of the Dead (Grey) Dune evolution along the Curonian Spit, Southeastern Baltic.

1160   Bulletin of the Geological Society of Finland 85, 53-64.

1161   Dotterweich, M., 2008. The history of soil erosion and fluvial deposits in small catchments of

1162   Central Europe: Deciphering the long-term interaction between humans and the

1163   environment – A review. Geomorphology 101, 192-208.

1164   Dreibrodt, S., Lubos, C., Terhorst, B., Damm, B., Bork, H.R., 2010. Historical soil erosion by

1165   water in Germany: scales and archives, chronology, research perspectives. Quaternary

1166   International 222, 80-95.

1167   Fægri, K., Iversen, J., 1989. Textbook of pollen analysis, 4th ed. Munksgaard, Copenhagen.

1168   FAO, 2006. Guidelines for Soil Description, fourth ed. Food and Agriculture Organization

1169   of the United Nations, Rome.

1170   Felix-Henningsen, P., Bleich, K., 2014. Böden und Bodenmerkmale unterschiedlichen Alters.

1171   Handbuch der Bodenkunde, Wiley-VCH Verlag, Weinheim, pp. 1-12.

1172   Giesecke, T., Wolters, S., Jahns, S., Brande, A., 2012. Exploring Holocene changes in

1173   palynological richness in northern Europe – Did Postglacial immigration matter? PLoS

1174   ONE 7, e51624.

1175   Gilbertson, D.D., Schwenninger, J.L., Kemp, R.A., Rhodes, E.J., 1999. Sand-drift and soil

1176   formation along an exposed North Atlantic coastline: 14,000 years of diverse

1177   geomorphological, climatic and human impacts. Journal of Archaeological Science 26,

1178   439-469.

1179   Graventein, H., 2013. Geomorphologische und sedimentologisch-bodenkundliche Befunde

1180   zur Paläohydrologie des Großen Fürstenseer Sees im Müritz-Nationalpark

1181   (Mecklenburg-Vorpommern). Diploma thesis, Marburg University.

1182   Hannon, G.E., Bradshaw, R.H., Nord, J., Gustafsson, M., 2008. The Bronze Age landscape of

1183   the Bjäre peninsula, southern Sweden, and its relationship to burial mounds. Journal of

1184   Archaeological Science 35, 623-632.

1185   Hardt, J., Böse, M., 2018. The timing of the Weichselian Pomeranian ice marginal position

1186   south of the Baltic Sea: A critical review of morphological and geochronological

1187   results. Quaternary International 478, 51-58.

1188   Heinrich, I., Balanzategui, D., Bens, O., Blasch, G., Blume, T., Böttcher, F., Borg, E.,

1189   Brademann, B., Brauer, A., Conrad, C., Dietze, E., Dräger, N., Fiener, P., Gerke, H.H.,

1190   Güntner, A., Heine, I., Helle, G., Herbrich, M., Heupel, K., Heußner, K.-U., Hohmann,

1191   C., Itzerott, S., Jurasinski, G., Kaiser, K., Kappler, C., Koebsch, F., Liebner, S.,

1192   Lischeid, G., Merz, B., Missling, K.D., Morgner, M., Pinkerneil, S., Plessen, B., Raab,

1193   T., Ruhtz, T., Sachs, T., Sommer, M., Spengler, D., Stender, V., Stüve, P., Wilken, F.,

1194   2018. Interdisciplinary geo-ecological research across time scales in the Northeast

1195   German Lowland Observatory (TERENO-NE). Vadose Zone Journal 17, 180116.

1196   Heiri, O., Lotter, A.F., Lemcke, G., 2001. Loss on ignition as a method for estimating

1197   organic and carbonate content in sediments: reproducibility and comparability of

1198   results. Journal of Paleolimnology 25, 101-110.

1199   Helbig, H., de Klerk, P., Kühn, P., Kwasniowski, J., 2002. Colluvial sequences on till plains

1200   in Vorpommern (NE Germany). Zeitschrift für Geomorphologie Supplement 128, 81-

1201   100.

1202   Henkner, J., Ahlrichs, J., Downey, S., Fuchs, M., James, B., Junge, A., Knopf, T., Scholten,

1203   T., Kühn, P., 2018. Archaeopedological analysis of colluvial deposits in favourable and

1204   unfavourable areas: reconstruction of land use dynamics in SW Germany. Royal Society

1205   open science 5, 171624.

1206   Hirsch, F., Schneider, A, Nicolay, A., Błaszkiewicz, M., Kordowski, J., Noryskiewicz, A.M.,

1207   Tyszkowski, S., Raab, A., Raab, T., 2015. Late Quaternary landscape development at

1208   the margin of the Pomeranian phase (MIS 2) near Lake Wygonin (Northern Poland).

1209   Catena 124, 28-44.

1210 Hirsch, F., Spröte, R., Fischer, T., Forman, S.L., Raab, T., Bens, O., Schneider, A., Hüttl,

1211   R.F., 2017. Late Quaternary aeolian dynamics, pedostratigraphy and soil formation in

1212   the North European Lowlands – new findings from the Baruther ice-marginal valley.

1213   Die Erde 148, 58-73.

1214 Hirsch, F., Raab, T., 2018. The Finow soil – a stratigraphic marker or just a pedologic

1215   horizon? Geophysical Research Abstracts 19, EGU2017-3997.

1216 Hirsch, F., Schneider, A., Bauriegel, A., Raab, A., Raab, T., 2018. Formation, classification

1217   and properties of soils at two relict charcoal hearth sites in Brandenburg, Germany.

1218   Frontiers in Environmental Science 6, 94.

1219 Hoffmann, T., Schlummer, M., Notebaert, B., Verstraeten, G., Korup, O., 2013. Carbon burial

1220   in soil sediments from Holocene agricultural erosion, Central Europe. Global

1221   Biogeochemical Cycles 27, 828-835.

1222 Hošek, J., Pokorný, P., Prach, J., Lisá, L., Grygar, T.M., Knésl, I., Trubač, J., 2017. Late

1223   Glacial erosion and pedogenesis dynamics: Evidence from high-resolution lacustrine

1224   archives and paleosols in south Bohemia (Czech Republic). Catena 150, 261-278.

1225 Hughes, A.L.C., Gyllencreutz, R., Lohne, Ø.S., Mangerud, J., Svendsen, J.I., 2016. The last

1226   Eurasian ice sheets – a chronological database and time-slice reconstruction, DATED-1.

1227   Boreas 45, 1-45.

1228 IUSS Working Group WRB, 2015. World reference base for soil resources 2014, update

1229   2015. World Soil Resources Report 106. FAO, Rome.

1230 Jahns, S., 2007. Palynological investigations into the Late Pleistocene and Holocene history

1231   of vegetation and settlement at the Löddigsee, Mecklenburg, Germany. Vegetation

1232   History and Archaeobotany 16, 157-169.

1233 Jahns, S., Christiansen, J., Kirleis, W., Sudhaus, D., 2013. On the Holocene vegetation history

1234   of Brandenburg and Berlin. In: Kadrow, S., Włodarczak, P. (Eds.), Environment and

1235   subsistence – forty years after Janusz Kruk's „Settlement studies…". Studien zur

1236   Archäologie in Ostmitteleuropa / Studia nad Pradziejami Europy Środkowej 11,

1237   Institute of Archaeology UR & Verlag Dr. Rudolf Habelt GmbH, Rzeszów & Bonn, pp.

1238   311-330.

1239 Jamrichová, E., Bobek, P., Šolcová, A., Tkáč, P., Hédl, R., Valachovič, M., 2019. Lowland

1240   pine forests in the northwestern Pannonian Basin: between natural vegetation and

1241   modern plantations. Regional Environmental Change 19, 2395-2409.

1242 Jankowski, M., 2012. Lateglacial soil paleocatena in inland-dune area of the Toruń Basin,

1243   Northern Poland. Quaternary International 265, 116-125.

1244 Jaroszewicz, B., Cholewinska, O., Gutowski, J.M., Samojlik, T., Zimny, M., Latałowa, M.,

1245   2019. Białowieża Forest – A relic of the high naturalness of European forests. Forests

1246   10, 849.

1247 Jeschke, L., 2014. Der Müritz-Nationalpark. In: Konold, W., Böcker, R., Hampicke, U.

1248   (Eds.), Handbuch Naturschutz und Landschaftspflege, Wiley-VCH, Weinheim, pp. 1-

1249   15.

1250 Johnson, D.L., 1998. Paleosols are buried soils. Quaternary International 51-52, 7.

1251 Jonczak, J., Florek, W., Kruczkowska, B., Gadziszewska, J., Niska, M., Uzarowicz, Ł., 2019.

1252   Late Vistulian and Holocene development of litho-morpho-pedogenic processes in the

1253   southern Baltic coastal zone: A case study from Dębina, northern Poland. Geoderma

1254   348, 21-36.

1255 Joosten, H., de Klerk, P., 2002. What's in a name? Some thoughts on pollen classification,

1256   identification, and nomenclature in Quaternary palynology. Review of Palaeobotany

1257   and Palynology 122, 29-45.

1258 Kaiser, K., Schoknecht, T., Prehn, B., Janke, W., Kloss, K., 2002. Geomorphologische,

1259   palynologische und archäologische Beiträge zur holozänen Landschaftsgeschichte im

1260   Müritzgebiet (Mecklenburg-Vorpommern). Eiszeitalter und Gegenwart 51, 15-32.

1261 Kaiser, K., Barthelmes, A., Czakó Pap, S., Hilgers, A., Janke, W., Kühn, P., Theuerkauf, M.,

1262   2006. A Lateglacial palaeosol cover in the Altdarss area, southern Baltic Sea coast

1263   (Northeast Germany): investigations on pedology, geochronology and botany.

1264   Netherlands Journal of Geosciences 85, 197-220.

1265 Kaiser, K., Hilgers, A., Schlaak, N., Jankowski, M., Kühn, P., Bussemer, S., Przegietka, K.,

1266   2009. Palaeopedological marker horizons in northern central Europe: characteristics of

1267   Lateglacial Usselo and Finow soils. Boreas 38, 591-609.

1268 Kaiser, K., Lorenz, S., Germer, S., Juschus, O., Küster, M., Libra, J., Bens, O., Hüttl, R.F.,

1269   2012. Late Quaternary evolution of rivers, lakes and peatlands in northeast Germany

1270   reflecting past climatic and human impact – an overview. E&G Quaternary Science

1271   Journal 61, 103-132.

1272 Kaiser, K., Küster, M., Fülling, A., Theuerkauf, M., Dietze, E., Graventein, H., Koch, P.J.,

1273   Bens, O., Brauer, A., 2014a. Littoral landforms and pedosedimentary sequences

1274   indicating late Holocene lake-level changes in northern central Europe – A case study

1275   from northeastern Germany. Geomorphology 216, 58-78.

1276 Kaiser, K., Koch, P.J., Mauersberger, R., Stüve, P., Dreibrodt, J., Bens, O., 2014b. Detection

1277   and attribution of lake-level dynamics in north-eastern central Europe in recent decades.

1278   Regional Environmental Change 14, 1587-1600.

1279 Kaiser, K., Oldorff, S., Breitbach, C., Kappler, C., Theuerkauf, M., Scharnweber, T., Schult,

1280   M., Küster, M., Engelhardt, C., Heinrich, I., Hupfer, M., Schwalbe, G., Kirschey, T.,

1281   Bens, O., 2018. A submerged pine forest from the early Holocene in the Mecklenburg

1282   Lake District, northern Germany. Boreas 47, 910-925.

1283 Kappler, C., Kaiser, K., Tanski, P., Klos, F., Fülling, A., Mrotzek, A., Sommer, M., Bens, O.,

1284   2018. Stratigraphy and age of colluvial deposits indicating Late Holocene soil erosion in

1285   northeastern Germany. Catena 170, 224-245.

1286 Kappler, C., Kaiser, K., Küster, M., Nicolay, A., Fülling, A., Bens, O., Raab, T., 2019. Late
1287   Pleistocene and Holocene terrestrial geomorphodynamics and soil formation in
1288   northeastern Germany: a review of geochronological data. Physical Geography 40, 405-
1289   432.

1290 Karasiewicz, T.M., 2019. The kettle-hole mire as archives of postglacial changes in biogenic
1291   sedimentation (Tuchola Forest, north-Central Poland). Catena 176, 26-44.

1292 Khamnueva-Wendt, S., Mitusov, A.V., Wendt, J., Bork, H.R., 2019. Classification of buried
1293   soils, cultural, and colluvial deposits in the Viking town Hedeby. Geoarchaeology, in
1294   press, doi.org/10.1002/gea.21777.

1295 Kittel, P., 2014. Slope deposits as an indicator of anthropopressure in the light of research in
1296   Central Poland. Quaternary International 324, 34-55.

1297 Klos, F., 2016. Kolluvien und Paläoböden im Einzugsgebiet des Tiefen Sees bei
1298   Hohengüstow (Uckermark) und des Tiefen Sees bei Klocksin (Mecklenburg) als
1299   Indikatoren der historischen Bodenerosion. Master thesis, Technische Universität
1300   Bergakademie Freiberg, Faculty of Geosciences, Geoengineering and Mining.

1301 Kočár, P., Petr, L., Kočárová, R., 2018. Vegetationswandel im Bergrevier Preßnitz. In:
1302   Derner, K. (Ed.), Mittelalterlicher Bergbau und Hüttenwesen in der Region Preßnitz im
1303   mittleren Erzgebirge. Veröffentlichungen des Landesamtes für Archäologie Sachsen 68
1304   – ArchaeoMontan 5, Landesamt für Archäologie Sachsen, Dresden, pp. 67-78.

1305 Kołodyńska-Gawrysiak, R., 2019. Holocene evolution of closed depressions and its relation to
1306   landscape dynamics in the loess areas of Poland. The Holocene 29, 543-564.

1307 Konstantinov, A., Loiko, S., Kurasova, A., Konstantinova, E., Novoselov, A., Istigechev, G.,
1308   Kulizhskiy, S., 2019. First findings of buried Late-Glacial paleosols within the dune
1309   fields of the Tomsk Priobye region (SE Western Siberia, Russia). Geosciences 9, 82.

1310   Kruczkowska, B., Błaszkiewicz, M., Jonczak, J., Uzarowicz, Ł., Moska, P., Brauer, A., Bonk,

1311   A., Słowiński, M., 2020. The Late Glacial pedogenesis interrupted by aeolian activity in

1312   Central Poland – Records from the Lake Gościąż catchment. Catena 185, 104286.

1313   Kühn, P., Lehndorff, E., Fuchs, M., 2017. Late Pleniglacial to Holocene pedogenesis and

1314   formation of colluvial deposits in central Europe (Gambach, Germany). Catena 154,

1315   118-135.

1316   Küster, M., 2014. Holozäne Landschaftsentwicklung der Mecklenburgischen Seenplatte:

1317   Relief- und Bodengenese, hydrologische Entwicklung sowie Siedlungs- und

1318   Landnutzungsgeschichte in Nordostdeutschland. PhD thesis, University of Greifswald.

1319   Küster, M., Preusser, F., 2009. Late Glacial and Holocene aeolian sands and soil formation

1320   from the Pomeranian outwash plain (Mecklenburg, NE-Germany). E&G Quaternary

1321   Science Journal 58, 156-163.

1322   Küster, M., Janke, W., Meyer, H., Lorenz, S., Lampe, R., Hübener, T., Klamt, A.-M., 2012.

1323   Zur jungquartären Landschaftsentwicklung der Mecklenburgischen Kleinseenplatte:

1324   Geomorphologische, bodenkundliche und limnogeologische Untersuchungen am

1325   Krummen See bei Blankenförde (Mecklenburg). Forschung und Monitoring 3. Geozon,

1326   Greifswald.

1327   Küster, M., Fülling, A., Kaiser, K., Ulrich, J., 2014. Aeolian sands and buried soils in the

1328   Mecklenburg Lake District, NE Germany: Holocene land use history and pedo-

1329   geomorphic response. Geomorphology 211, 64-76.

1330   Küster, M., Fülling, A., Ulrich, J., 2015a. Bw horizon in Holocene slope deposits

1331   (Kratzeburg, NE Germany) – dating and pedological characteristics. E&G Quaternary

1332   Science Journal 64, 111-117.

1333   Küster, M., Stöckmann, M., Fülling, A., Weber, R., 2015b. Kulturlandschaftselemente,

1334   Kolluvien und Flugsande als Archive der spätholozänen Landschaftsentwicklung im

1335   Bereich des Messtischblattes Thurow (Müritz-Nationalpark, Mecklenburg). In: Kaiser,

1336   K., Kobel, J., Küster, M., Schwabe, M. (Eds.), Neue Beiträge zum Naturraum und zur

1337   Landschaftsgeschichte im Teilgebiet Serrahn des Müritz-Nationalparks. Forschung und

1338   Monitoring 4, Geozon, Berlin, pp. 115-124.

1339 Landesforst Mecklenburg-Vorpommern, 2009. Anleitung für die forstliche

1340   Standortserkundung im nordostdeutschen Tiefland – SEA95. Malchin.

1341 Lange, E., Jeschke, L., Knapp, H.-D., 1986. Ralswiek und Rügen. Landschaftsentwicklung

1342   und Siedlungsgeschichte der Ostseeinsel. Teil I: Die Landschaftsgeschichte der Insel

1343   Rügen seit dem Spätglazial. Schriften zur Ur-und Frühgeschichte 38, Akademie-Verlag,

1344   Berlin.

1345 Layzell, A.L., Mandel, R.D., 2019. Using soil survey data as a predictive tool for locating

1346   deeply buried archaeological deposits in stream valleys of the Midwest, United States.

1347   Geoarchaeology 34, 80-99.

1348 Leifeld, J., Alewell, C., Bader, C., Krüger, J.P., Mueller, C.W., Sommer, M., Steffens, M.,

1349   Szidat, S., 2018. Pyrogenic carbon contributes substantially to carbon storage in intact

1350   and degraded northern peatlands. Land Degradation & Development 29, 2082-2091.

1351 LFoA M-V, 1999. Bohrpunkt-, Arbeitsroh-, und Arbeitsreinkarten der Standortkartierung

1352   1997/1998 in den Forstrevieren im TG Serrahn, Maßstab 1:5.000. Landesforst

1353   Mecklenburg-Vorpommern, Betriebsteil Forstplanung-Versuchswesen-

1354   Informationssysteme, Schwerin.

1355 LiV – Landesamt für innere Verwaltung Mecklenburg-Vorpommern, 2015. DTK50 –

1356   Digitale Topografische Karte 1:50.000, Blatt 2744 Neustrelitz. Amt für Geoinformation,

1357   Vermessung- und Katasterwesen, Schwerin.

1358 Lorenz, S., 2007. Die spätpleistozäne und holozäne Gewässernetzentwicklung im Bereich der

1359   Pommerschen Haupteisrandlage Mecklenburgs. PhD thesis, University of Greifswald.

1360 Lorenz, S., Küster, M., Fülling, A., Gehlhar, U., 2015. Erste Ergebnisse zu bodenkundlich-

1361   geomorphologischen Untersuchungen zur spätholozänen Erosionsgeschichte auf der

Insel Vilm (Greifswalder Bodden, Mecklenburg-Vorpommern). In: Gehlhar, U., Knapp, H.D. (Eds.), Erste Ergebnisse der Naturwaldforschung im Naturwaldreservat Insel Vilm. BfN-Skripten 390, Bundesamt für Naturschutz, Bonn, pp. 45-51.

Lorenz, S., Rother, H., Kenzler, M., Kaphengst, S., 2019. Late Glacial to Holocene dune development at southern Krakower See. DEUQUA Special Publications 2, 83-88.

Lüthgens, C., Böse, M., Preusser, F., 2011. Age of the Pomeranian ice marginal position in northeastern Germany determined by Optically Stimulated Luminescence (OSL) dating of glaciofluvial sediments. Boreas 40, 598-615.

LUNG, 2005. Geologische Karte von Mecklenburg-Vorpommern 1:50.000 digital, L2744 Neustrelitz. Landesamt für Umwelt, Naturschutz und Geologie Mecklenburg-Vorpommern, Güstrow.

Lungershausen, U., Larsen, A., Bork, H.R., Duttmann, R., 2018. Anthropogenic influence on rates of aeolian dune activity within the northern European Sand Belt and socio-economic feedbacks over the last ~2500 years. The Holocene 28, 84-103.

Mangerud, J., Jakobsson, M., Alexanderson, H., Astakhov, V., Clarke, G.K.C, Henriksen, M., Hjort, C., Krinner, G., Lunkka, J.-P., Möller, P., Murray, A., Nikolskaya, O., Saarnisto, M., Svendsen, J.I., 2004. Ice-dammed lakes and rerouting of the drainage of northern Eurasia during the Last Glaciation. Quaternary Science Reviews 23, 1313-1332.

Marin-Spiotta, E., Chaopricha, N.T., Plante, A.F., Diefendorf, A.F., Mueller, C.W., Grandy, A.S., Mason, J.A., 2014. Long-term stabilization of deep soil carbon by fire and burial during early Holocene climate change. Nature Geoscience 7, 428-432.

Mauz, B., Felix-Henningsen, P., 2005. Palaeosols in Saharan and Sahelian dunes of Chad: archives of Holocene North African climate changes. The Holocene 15, 453-458.

Mendyk, Ł., Markiewicz, M., Bednarek, R., Świtoniak, M., Gamrat, W. W., Krześlak, I., Sykuła, M., Gersztyn, L., Kupniewska, A., 2016. Environmental changes of a shallow

1387   kettle lake catchment in a young glacial landscape (Sumowskie Lake catchment), North-

1388   Central Poland. Quaternary International 418, 116-131.

1389   Missiaen, T., Verhegge, J., Heirman, K., Crombé, P., 2015. Potential of cone penetrating

1390   testing for mapping deeply buried palaeolandscapes in the context of archaeological

1391   surveys in polder areas. Journal of Archaeological Science 55, 174-187.

1392   Monella, D., Sommer, K., Fricker, G., Völker, U., 2000. Vergleichende Untersuchungen zur

1393   Teilchengrößenanalyse. Chemie Ingenieur Technik 72, 273-276.

1394   Moore, P.D., Webb, J.A., Collinson, M.E., 1991. Pollen analysis. Blackwell Science, Oxford.

1395   Müller, F., Bergmann, M., Dannowski, R., Dippner, J.W., Gnauck, A., Haase, P., Jochimsen,

1396   M.C., Kasprzak, P., Kröncke, I., Kümmerlin, R., Küster, M., Lischeid, G., Meesenburg,

1397   H., Merz, C., Millat, G., Müller, J., Padisák, J., Schimming, C.G., Schubert, H., Schult,

1398   M., Selmeczy, G., Shatwell, T., Stoll, S., Schwabe, M., Soltwedel, T., Straile, D.,

1399   Theuerkauf, M., 2016. Assessing resilience in long-term ecological data sets. Ecological

1400   Indicators 65, 10-43.

1401   Müller, H.M., 1962. Pollenanalytische Untersuchungen im Bereich des Messtischblattes

1402   Thurow/Südostmecklenburg. PhD thesis, University of Halle/Saale.

1403   Müller, V., 2014. Landschaftsgeschichtliches Potenzial von Boden-Sediment-Sequenzen am

1404   Hinnensee, Müritz-Nationalpark. Diploma thesis, Technische Universität Dresden,

1405   Institute of Geography.

1406   Muhs, D.R., Mason, J.A., Jacobs, P.M., Singer, M.J., Verosub, K.L., Kemp, R.A., Bettis III,

1407   E.A., McFadden, L., Kohfeld, K.E., 2013. Paleosols and wind-blown sediments. In:

1408   Elias, S.A. (Ed.), Encyclopedia of Quaternary Science, 2nd edition. Elsevier, London,

1409   pp. 2075-2137.

1410   Mundel, G., Trettin, R., Hiller, A., 1983. Zur Moorentwicklung und Landschaftsgeschichte

1411   des Havelländischen Luches. Archiv für Naturschutz und Landschaftsforschung 23,

1412   225-264.

1413   Nelle, O., Jansen, D., Evers, K., Weber, R., Schwabe, M., 2015. Relikte der Köhlerei –

1414   Potenzial für die Landschaftsgeschichte im Teilgebiet Serrahn des Müritz-

1415   Nationalparks. In: Kaiser, K., Kobel, J., Küster, M., Schwabe, M. (Eds.), Neue Beiträge

1416   zum Naturraum und zur Landschaftsgeschichte im Teilgebiet Serrahn des Müritz-

1417   Nationalparks. Forschung und Monitoring 4, Geozon, Berlin, pp. 137-147.

1418   Nettleton, W.D., Olson, C.G., Wysocki, D.A., 2000. Paleosol classification: problems and

1419   solutions. Catena 41, 61-92.

1420   Olsen, L., 1998. Pleistocene paleosols in Norway: implications for past climate and glacial

1421   erosion. Catena 34, 75-103.

1422   Petzelberger, B.E., Behre, K.E., Geyh, M.A., 1999. Beginn der Hochmoorentwicklung und

1423   Ausbreitung der Hochmoore in Nordwestdeutschland: erste Ergebnisse eines neuen

1424   Projektes. Telma 29, 21-38.

1425   Pierik, H.J., van Lanen, R.J., Gouw-Bouman, M.T., Groenewoudt, B.J., Wallinga, J., Hoek,

1426   W.Z., 2018. Controls on late-Holocene drift-sand dynamics: The dominant role of

1427   human pressure in the Netherlands. The Holocene 28, 1361-1381.

1428   Pitkäranta, R., 2009. Pre-late Weichselian podzol soil, permafrost features and

1429   lithostratigraphy at Penttilänkangas, western Finland. Bulletin of the Geological Society

1430   of Finland 81, 53-74.

1431   Preusser, F., Degering, D., Fuchs, M., Hilgers, A., Kadereit, A., Klasen, N., Krbetschek, M.,

1432   Richter, D., Spencer, J., 2008. Luminescence dating: basics, methods and applications.

1433   E&G Quaternary Science Journal 57, 95-149.

1434   Quinton, J.N., Govers, G., van Oost, K., Bardgett, R.D., 2010. The impact of agricultural soil

1435   erosion on biogeochemical cycling. Nature Geoscience 3, 311-314.

1436   Raab, A., Bonhage, A., Schneider, A., Raab, T., Rösler, H., Heußner, K.U., Hirsch, F., 2019.

1437   Spatial distribution of relict charcoal hearths in the former royal forest district Tauer

1438   (SE Brandenburg, Germany). Quaternary International 511, 153-165.

Reimer, P.J., Bard, E., Bayliss, A., Beck, J.W., Blackwell, P.G., Ramsey, C.B., Buck, C.E.,

Cheng, H., Edwards, R.L., Friedrich, M., Grootes, P.M., Guilderson, T.P., Haflidason,

H., Hajdas, I., Hatte, C., Heaton, T.J., Hoffmann, D.L., Hogg, A.G., Hughen, K.A.,

Kaiser, K.F., Kromer, B., Manning, S.W., Niu, M., Reimer, R.W., Richards, D.A.,

Scott, E.M., Southon, J.R., Staff, R.A, Turney, C.S.M., van der Plicht, J., 2013. Intcal13

and marine13 radiocarbon age calibration curves 0–50,000 years cal Bp. Radiocarbon

55, 1869-1887.

Robin, V., Talon, B., Nelle, O., 2013. Pedoanthracological contribution to forest naturalness

assessment. Quaternary International 289, 5-15.

Robin, V., Nelle, O., 2014. Contribution to the reconstruction of central European fire history,

based on the soil charcoal analysis of study sites in northern and central Germany.

Vegetation History and Archaeobotany 23, 51-65.

Rowinsky, V., Kobel, J., 2011. Erfassung, Bewertung und Wiedervernässung von Mooren im

Müritz-Nationalpark. Telma Beiheft 4, 49-72.

Rutkiewicz, P., Malik, I., Wistuba, M., Osika, A., 2019. High concentration of charcoal hearth

remains as legacy of historical ferrous metallurgy in southern Poland. Quaternary

International 512, 133-143.

Schaetzl, R.J., Anderson, S., 2005. Soils: Genesis and Geomorphology. Cambridge University

Press, Cambridge.

Schich, W., 2003. Der Ausbau des Landes Stargard unter der Herrschaft der Markgrafen von

Brandenburg – die mittelalterlichen Grundlagen der Kulturlandschaft im östlichen Teil

von Mecklenburg-Strelitz. In: Stark, K. (Ed.), Vom Anfang und Ende Mecklenburg-

Strelitzer Geschichte. Steffen, Friedland, pp. 11-44.

Schirmer, W., 1999. Definitions concerning coversand, fossil soil and paleosol. In: Schirmer,

W. (Ed.), Dunes and fossil soils. GeoArchaeoRhein 3, pp. 187-190.

1465   Schlaak, N., 2015. Ein Paläoboden als Leithorizont. In: Stackebrandt, W., Franke, D. (Eds.),

1466   Geologie von Brandenburg. Schweizerbart, Stuttgart, pp. 676-679.

1467   Schlichting, E., Blume, H.-P., Stahr, K., 1995. Bodenkundliches Praktikum. Blackwell

1468   Wissenschaft, Berlin.

1469   Schmidt, M., Mölder, A., Schönfelder, E., Engel, F., Fortmann-Valtink, W., 2016. Charcoal

1470   kiln sites, associated landscape attributes and historic forest conditions: DTM-based

1471   investigations in Hesse (Germany). Forest Ecosystems 3, 8.

1472   Schneider, A., Takla, M., Nicolay, A., Raab, A., Raab, T., 2015. A template-matching

1473   approach combining morphometric variables for automated mapping of charcoal kiln

1474   sites. Archaeological Prospection 22, 45-62.

1475   Schneider, A., Hirsch, F., Wechler, K.-P., Raab, A., Raab, T., 2017. Reconstruction of a

1476   palaeosurface and archaeological site location in an anthropogenic drift sand area.

1477   Archaeological Prospection 24, 297-310.

1478   Schneider, A., Bonhage, A., Raab, A., Hirsch, F., Raab, T., 2020. Large-scale mapping of

1479   anthropogenic relief features – legacies of past forest use in two historical charcoal

1480   production areas in Germany. Geoarchaeology, in press, DOI: 10.1002/gea.21782.

1481   Schneider, T., 2017. Paläoböden im Teilgebiet Serrahn des Müritz-Nationalparks:

1482   Stratigraphie, Genese und landschaftsgeschichtliche Aussage. Master thesis, University

1483   of Potsdam, Institute of Earth- and Environmental Science.

1484   Schwabe, M., Küster, M., Fülling, A., Heinrich, S., 2015. Waldbestandsentwicklung und

1485   Standortskartierung um Serrahn, Müritz-Nationalpark. In: Kaiser, K., Kobel, J., Küster,

1486   M., Schwabe, M. (Eds.), Neue Beiträge zum Naturraum und zur Landschaftsgeschichte

1487   im Teilgebiet Serrahn des Müritz-Nationalparks. Forschung und Monitoring 4, Geozon

1488   Science Media, Berlin, pp. 179-190.

1489   Schweingruber, F.H., 1990. Anatomy of European Woods. Haupt, Bern.

1490   Sevink, J., Koster, E.A., Van Geel, B., Wallinga, J., 2013. Drift sands, lakes, and soils: the

1491   multiphase Holocene history of the Laarder Wasmeren area near Hilversum, the

1492   Netherlands. Netherlands Journal of Geosciences 92, 243-266.

1493   Sevink, J., van Geel, B., Jansen, B., Wallinga, J., 2018. Early Holocene forest fires, drift

1494   sands, and Usselo-type paleosols in the Laarder Wasmeren area near Hilversum, the

1495   Netherlands: Implications for the history of sand landscapes and the potential role of

1496   Mesolithic land use. Catena 165, 286-298.

1497   Silverman, B.W., 1986. Density Estimation for Statistics and Data Analysis. Chapman and

1498   Hall, New York.

1499   Słowinski, M., Błaszkiewicz, M., Brauer, A.,Noryskiewicz, B., Ott, F., Tyszkowski, S., 2015.

1500   The role of melting dead ice on landscape transformation in the early Holocene in

1501   Tuchola Pinewoods, North Poland. Quaternary International 388, 64-75.

1502   Smolska, E., 2011. Relation between radiocarbon, archaeological dating and sediment

1503   properties on the example of colluvial deposits (NE Poland). Geochronometria 38, 325-

1504   333.

1505   Sommer, M., Gerke, H.H., Deumlich, D., 2008. Modelling soil landscape genesis – a 'time

1506   split' approach for hummocky agricultural landscapes. Geoderma 145, 480-493.

1507   Spörlein, P., Dilling, J., Joneck, M., 2004. Pilotstudie zur Gleichwertigkeit oder

1508   Vergleichbarkeit der Korngrößenbestimmung von Bodenproben nach E DIN ISO

1509   11277: 06.94 (Pipettmethode) und mit dem Sedigraphen. Journal of Plant Nutrition and

1510   Soil Science 167, 649-656.

1511   StaO, 1962. Ergebnisse der Standortserkundung im Staatlichen Forstwirtschaftsbetrieb

1512   Neustrelitz, Erläuterungen zu den Standortskarten. Institut für Forsteinrichtung und

1513   Standortserkundung, Abt. Standortserkundung, Arbeitsgruppe Schwerin. Schwerin.

1514   Starkel, L., 2005. Anthropogenic soil erosion since the Neolithic in Poland. Zeitschrift für

1515   Geomorphologie Supplement 139, 189-201.

1516 Starkel, L., Michczyńska, D., Krąpiec, M., Margielewski, W., Nalepka, D., Pazdur, A., 2013.

1517 Progress in the Holocene chrono-climatostratigraphy of Polish territory.

1518 Geochronometria 40, 1-21.

1519 Stivrins, N., Liiv, M., Heinsalu, A., Gałka, M., Veski, S., 2017. The final meltdown of dead-

1520 ice at the Holocene Thermal Maximum (8500–7400 cal. yr BP) in western Latvia,

1521 eastern Baltic. The Holocene 27, 1146-1157.

1522 Stoops, G., 2003. Guidelines for analysis and description of soil and regolith thin sections.

1523 Soil Science Society of America, Madison.

1524 Stüve, P. (2015): Die jüngere hydrometeorologische Entwicklung im Serrahner Gebiet und

1525 Umgebung. In: Kaiser, K., Kobel, J., Küster, M., Schwabe, M. (Eds.), Neue Beiträge

1526 zum Naturraum und zur Landschaftsgeschichte im Teilgebiet Serrahn des Müritz-

1527 Nationalparks. Forschung und Monitoring 4, Geozon Science Media, Berlin, pp. 203-

1528 231.

1529 Tempel, H., 2003. Die Waldentwicklung in den Serrahner Bergen bis zur Einrichtung des

1530 Wildparks Serrahn 1849. Natur und Naturschutz in Mecklenburg-Vorpommern 38, 26-

1531 33.

1532 Theuerkauf, M., 2015. Vegetationsgeschichtliche Untersuchungen im Serrahner Gebiet –

1533 Möglichkeiten der Nutzung alter Daten für neue Analysen. In: Kaiser, K., Kobel, J.,

1534 Küster, M., Schwabe, M. (Eds.), Neue Beiträge zum Naturraum und zur

1535 Landschaftsgeschichte im Teilgebiet Serrahn des Müritz-Nationalparks. Forschung und

1536 Monitoring 4, Geozon Science Media, Berlin, pp. 233-239.

1537 Theuerkauf, M., Joosten, H., 2012. Younger Dryas cold stage vegetation patterns of central

1538 Europe – climate, soil and relief controls. Boreas 41, 391-407.

1539 Thonicke, K., Cramer, W., 2006. Long-term trends in vegetation dynamics and forest fires in

1540 Brandenburg (Germany) under a changing climate. Natural Hazards 38, 283-300.

1541 Tolksdorf, J.F., Kaiser, K., 2012. Holocene aeolian dynamics in the European sand-belt as

1542   indicated by geochronological data. Boreas 41, 408-421.

1543 Tolksdorf, J.F., Turner, F., Kaiser, K., Eckmeier, E., Bittmann, F., Veil, S., 2014. Potential of

1544   palaeosols, sediments and archaeological features to reconstruct Late Glacial fire

1545   regimes in northern Central Europe – case study on Grabow site and overview.

1546   Zeitschrift für Geomorphologie 58, Supplement 1, 211-232.

1547 van der Kroef, I., Koszinski, S., Grinat, M., van der Meij, M., Hierold, W., Südekum, W.,

1548   Sommer, M., 2019. Digital mapping of buried soil horizons using 2D and pseudo-3D

1549   geoelectrical measurements in a ground moraine landscape. European Journal of Soil

1550   Science 71, 10-26.

1551 van der Meij, W.M., Reimann, T., Vornehm, V.K., Temme, A.J.A.M., Wallinga, J., van Beek,

1552   R., Sommer, M., 2019. Reconstructing rates and patterns of colluvial soil redistribution

1553   in agrarian (hummocky) landscapes. Earth Surface Processes and Landforms 44, 2408-

1554   2422.

1555 van Mourik, J.M., Seijmonsbergen, A.C., Slotboom, R.T., Wallinga, J., 2012. Impact of

1556   human land use on soils and landforms in cultural landscapes on aeolian sandy

1557   substrates (Maashorst, SE-Netherlands). Quaternary International 265, 74-89.

1558 van Mourik, J.M., van der Meer, J. (Eds.), 2019. Reading the Soil Archives: Unraveling the

1559   Geoecological Code of Palaeosols and Sediment Cores. Developments in Quaternary

1560   Sciences 18, Elsevier, Amsterdam, pp. 1-298.

1561 Verhegge, J., Missiaen, T., Crombé, P., 2016. Exploring integrated geophysics and

1562   geotechnics as a paleolandscape reconstruction tool: Archaeological prospection of

1563   (prehistoric) sites buried deeply below the Scheldt Polders (NW Belgium).

1564   Archaeological Prospection 23, 125-145.

1565   Vogel, S., Märker, M., Esposito, D., Seiler, F., 2016. The ancient rural settlement structure in the hinterland of Pompeii inferred from spatial analysis and predictive modeling of villae rusticae. Geoarchaeology 31, 121-139.

1568   Wang, Z., van Oost, K., Lang, A., Quine, T., Clymans, W., Merckx, R., Notebaert, B., Govers, G., 2014. The fate of buried organic carbon in colluvial soils: a long-term perspective. Biogeosciences 11, 873-883.

1571   Woodward, C., Shulmeister, J., Larsen, J., Jacobsen, G. E., Zawadzki, A., 2014. The hydrological legacy of deforestation on global wetlands. Science 346, 844-847.

1573   Zeeden, C., Hambach, U., Obreht, I., Hao, Q., Abels, H.A., Veres, D., Lehmkuhl, F., Gavrilov, M.B., Marković, S.B., 2018. Patterns and timing of loess-paleosol transitions in Eurasia: Constraints for paleoclimate studies. Global and Planetary Change 162, 1-7.

1576   Zerbe, S., Brande, A., 2003. Woodland degradation and regeneration in Central Europe during the last 1,000 years – a case study in NE Germany. Phytocoenologia 33, 683-700.

1578

Figures

1580   Fig. 1: Location and properties of the Serrahn study area, northeastern Germany. A: Location in northern central Europe. The last glaciation (Weichselian) is indicated, showing the glacial maximum at 20 ka (Mangerud et al., 2004). B: Serrahn area as one of the two parts of Müritz National Park. C: Topographical map of Serrahn area (green: forest, light green: grassland, light blue: lake, beige: arable land, purple: settlement; LiV, 2015). D: Digital elevation model of Serrahn (LiV, 2015). E: Geological map of Serrahn (after Börner and Schütze, 2005, modified). F: Pedological map of Serrahn (BGR, 2011). G: Landcover map of Serrahn (CLC, 2012).

1588

1589   Fig. 2: Photographs of typical landscapes in the Serrahn area. A: Oblique aerial view showing the transition from terminal moraine to outwash plain at Lake Hinnensee with beech forests

1591   in the foreground and plantations of Scots pine in the background (Photo: P. Stüve). B:

1592   Oblique aerial view of Lake Fürstenseer See surrounded by pine plantations (Photo: P.

1593   Wernicke). C: Rolling hills ('Serrahner Berge') west of Serrahn village with 'Mückengrund'

1594   kettle-hole covered by near-natural beech forest of the UNESCO World Natural Heritage

1595   Serrahn site (Photo: K. Bartels). The length and depth of the kettle-hole are c. 400 m and c.

1596   25 m, respectively. D: Small hummocky dune located in the outwash plain around Waldsee

1597   village covered by planted pines (Photo: M. Küster). The length of the oval ground plan and

1598   the height of the dune are c. 10 m and c. 1.5 m, respectively. E: Oblique aerial view of Lake

1599   Großer Serrahnsee surrounded by a mire with the UNESCO World Natural Heritage Serrahn

1600   site in the background (Photo: P. Wernicke). F: South-eastern shoreline of Lake Fürstenseer

1601   See with sandy terrace plain (Photo: U. Meßner).

1602

1603   Fig. 3: Geologic-topographic cross-section through the Serrahn area showing the thick

1604   package of Quaternary sediments attaining a local thickness of 230 m (Börner and Schütze,

1605   2005).

1606

1607   Fig. 4: Soil profiles available in the Serrahn area. A: Spatial distribution of all soil profiles

1608   recorded (n = 5214). B: Soil profiles with buried palaeosols recorded (n = 520) with a subset

1609   having geochronological data (n = 26). The red numbers indicate the site IDs.

1610

1611   Fig. 5: Soil profile characteristics and land use traces in the Serrahn area. A: Distribution of

1612   soil profiles showing thin sand covering ($\leq$ 20 cm), erosion and deposition (aggradation). B:

1613   Sites with kilns (charcoal, tar) and relic plough horizons (fAp) indicating former wood use

1614   and arable land use, respectively.

1615

1616   Fig. 6: Photographs with pedologic and geochronological information of selected soil profiles

1617   with palaeosols recorded in the Serrahn area (site ID in parentheses). The sediment types

1618   covering the palaeosols are given below the photo. For location of the profiles see Figure 4B.

1619

1620   Fig. 7: Geostatistical modeling of palaeosol areas in the Serrahn area. The somewhat angular

1621   shapes of the palaeosol areas result from the mathematic method used for partition, i.e.

1622   construction of Voronoi-Thiessen polygons based on the detection of local palaeosol

1623   occurrences.

1624

1625   Fig. 8: Micromorphology of palaeosol horizons of profile S-1/site ID 20 (IIfBv horizon; A-D)

1626   and KFS8/site ID 13 (transition from IIfAeh to Hr horizon; E-H). For location of the profiles

1627   see Figure 4B. A: (ppl) Sand sized material with brown fine mass between the sand grains

1628   and partly covering them. B: Like A (xpl) – note the low birefringence of the fine material. C:

1629   (ppl) Weathered sand grains and ferruginous punctuation of the fine mass. D: Like C (oil). E:

1630   (ppl) Uppermost horizon consisting of peat (plant tissue residues and decomposed material).

1631   F: (ppl) Bioturbation in the peat layer and charcoal pieces. G: (ppl) Intermediate horizon

1632   consisting of sand grains. Note the faunal infilling that is rich in organic material. H: (ppl)

1633   Lowermost horizon representing a fAeh horizon.

1634

1635   Fig. 9: Pedosedimentary sequences from kettle-holes in the Serrahn area with lithological,

1636   pedological, geochronological, palynological, and sedimentological data. A: Profile

1637   KFS8/site ID 13 east of Lake Fürstenseer See. B: Profile Mü-1/site ID 17 west of Serrahn

1638   village. For location of the profiles see Figure 4B.

1639

1640   Fig. 10: Geochronological data from palaeosols and sediments of the Serrahn area.

1641   Radiocarbon ages are given in red, luminescence ages are given in blue. Bio-/pollenzones

1642 (after Firbas in Giesecke et al., 2012) are given in Roman numbers and separated by dashed

1643 lines. A1, A2: Relative probability and kernel density estimate of radiocarbon and

1644 luminescence ages, respectively, from all geochronological data available. B1, B2: Relative

1645 probability and kernel density estimate of radiocarbon and luminescence ages from buried

1646 humic and peaty surface soil horizons (fAh, fAa, fHv, fHa, fHr). C: Kernel density estimate

1647 of luminescence ages from colluvial soil horizons (M, fM). D: Relative probability estimate

1648 from radiocarbon ages on charcoal and partly charred wood indicating past fire dynamics.

1649

1650 Fig. 11: Conceptual models showing the formation of pedosedimentary sequences in the

1651 Serrahn area. Terminology of the horizons given is simplified. A: Aeolian setting in the

1652 terminal moraine area west of Serrahn. B: Colluvial setting in the terminal moraine area west

1653 of Serrahn. C: Lacustrine setting of terrace sites at Lake Fürstenseer See. D: Mire (telmatic)

1654 setting at the surroundings of Lake Fürstenseer See.

1655

1656 Fig. 12: Erosional pattern in the Serrahn area indicated by the preservation stage of the

1657 periglacial surface (after Dieckmann and Kaiser, 1998, modified) and by calculating the

1658 intensity of soil relocation applying the ArcGIS tool 'Point density'.

1659

1660 **Tables**

1661 Tab. 1: Distribution of soil profiles with palaeosols, thin sand coverings and plough horizons

1662 in the Serrahn area depending from geological units.

1663

1664 Tab. 2: Statistics of soil analytical data from the Serrahn area grouped into topsoil/subsoil and

1665 buried horizons as well as sediments.

1666

1667 Tab. 3: Radiocarbon data of the soil profiles investigated in the Serrahn area. Data calibration

1668 was performed with OxCal version 4.2 (Bronk Ramsey, 2009; Reimer et al., 2013) with a

1669 range of two sigma deviation for analysis.

1670

1671 Tab. 4: Optically stimulated luminescence dating (OSL) results and radioisotope

1672 concentrations of the soil profiles investigated in the Serrahn area.

1673

1674 **Supplements**

1675 Supplement 1: Archaeological record of the Serrahn area and surroundings (data: State

1676 Archaeological Survey of Mecklenburg-Vorpommern, unpublished material). The calculation

1677 of the archaeological sites shown within the map frame yielded the following numbers:

1678 Neolithic, n = 1; Bronze Age, n = 52; Pre-Roman Iron Age, n = 5; Roman Age, n = 2; Slavic

1679 Medieval, n = 13; German Medieval, n = 10.

1680

1681 Supplement 2: Pedological and sedimentological data from the soil profiles sampled in the

1682 Serrahn area. Soil horizons are given both according to the German (Ad-hoc-AG Boden,

1683 2005) and international pedological standard (FAO, 2006).

1684

1685 Supplement 3: Approximate translation of German soil horizons (Ad-hoc-AG Boden, 2005)

1686 into the international pedological classification (FAO, 2006).

1687

1688 Supplement 4: Description of relief characteristics deduced from the DEM used as predictor

1689 variables for the determination of palaeosol sites.

1690

1691 Supplement 5: Box-and-whisker plots of relief characteristics of palaeosols in the Serrahn

1692 area (n = 506). For ranking of their relative statistical importance see Supplement 6.

1693

1694   Supplement 6: Ranking of relative statistical importance of relief characteristics for palaeosol

1695   sites deduced from the absolute deviation of the median.

1696

1697   Supplement 7: Simplified pollen diagram Mü-1 (from Küster, 2014). For location see Fig.

1698   4B.

1699

1700   Supplement 8: Simplified pollen diagram KFS8. For location see Fig. 4B.

1701

1702   Supplement 9: Simplified pollen diagram FUER14. For location see Fig. 4B.

1703

1704   Supplement 10: Simplified pollen and macrofossil/compartment diagram FUER15.

1705   Macrofossils/compartments are given in total numbers (for countable objects) or estimated

1706   proportions of the total volume for charcoal, sand, tissues and wood (adapted from Kaiser et

1707   al., 2014a). For location see Fig. 4B.

1708

1709   Supplement 11: Simplified pollen diagrams FUER3 and FUER6 comprising single pollen

1710   samples of these profiles. The pollen sum includes all tree pollen types, *Corylus*, and pollen

1711   types attributed to upland herbs. The low pollen sums result from poor pollen preservation

1712   and concentration in most of the samples. The samples of FUER3 consist nearly entirely of

1713   charcoal particles, so that explicit counting of charcoal particles, as performed in FUER6,

1714   was unfeasible (adapted from Kaiser et al., 2014a). For locations see Fig. 4B.

1715

1716   Supplement 12: Charcoal analysis (soil anthracology) of soil profiles east and west of Serrahn

1717   village.

1718
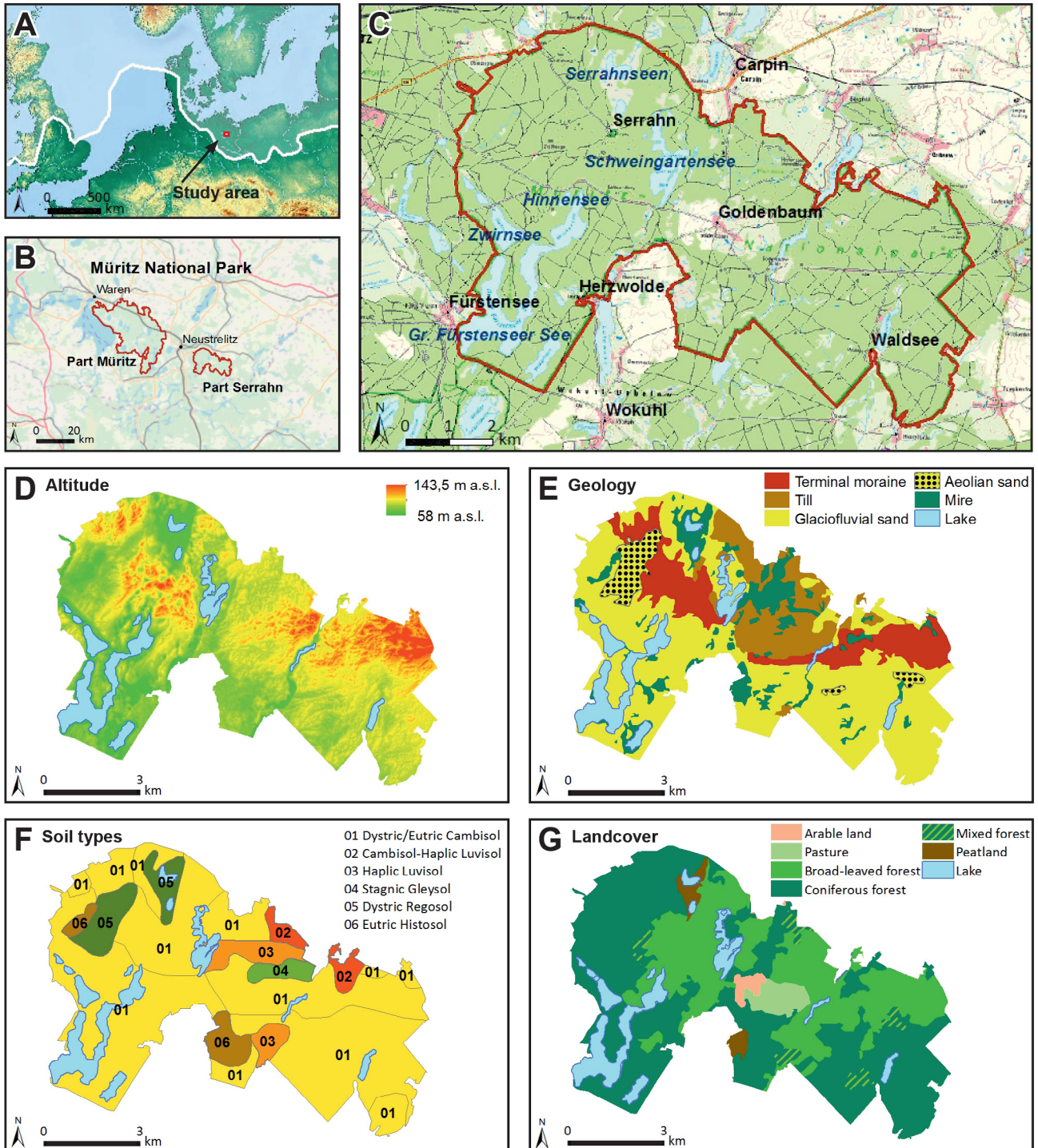
Fig. 1: Location and properties of the Serrahn study area, northeastern Germany. A: Location in northern central Europe. The last glaciation (Weichselian) is indicated, showing the glacial maximum at 20 ka (Mangerud et al., 2004). B: Serrahn area as one of the two parts of Müritz National Park. C: Topographical map of Serrahn area (green: forest, light green: grassland, light blue: lake, beige: arable land, purple: settlement; LiV, 2015). D: Digital elevation model of Serrahn (LiV, 2015). E: Geological map of Serrahn (after Börner and Schütze, 2005, modified). F: Pedological map of Serrahn (BGR, 2011). G: Landcover map of Serrahn (CLC, 2012).

Fig. 2: Photographs of typical landscapes in the Serrahn area. A: Oblique aerial view showing the transition from terminal moraine to outwash plai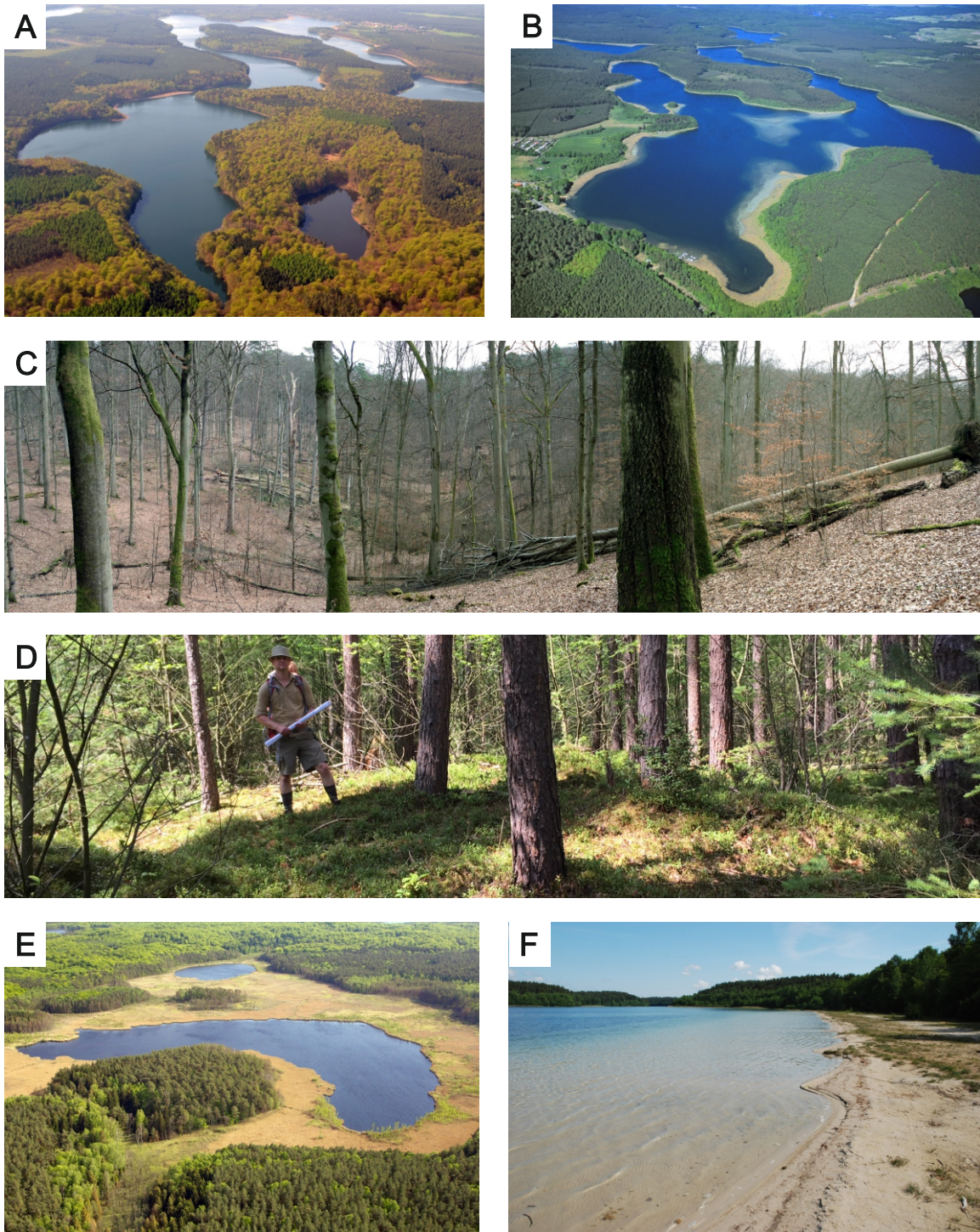n at Lake Hinnensee with beech forests in the foreground and plantations of Scots pine in the background (Photo: P. Stüve). B: Oblique aerial view of Lake Fürstenseer See surrounded by pine plantations (Photo: P. Wernicke). C: Rolling hills (`Serrahner Berge') west of Serrahn village with `Mückengrund' kettle-hole covered by near-natural beech forest of the UNESCO World Natural Heritage Serrahn site (Photo: K. Bartels). The length and depth of the kettle-hole are c. 400 m and c. 25 m, respectively. D: Small hummocky dune located in the outwash plain around Waldsee village covered by planted pines (Photo: M. Küster). The length of the oval ground plan and the height of the dune are c. 10 m and c. 1.5 m, respectively. E: Oblique aerial view of Lake Großer Serrahnsee surrounded by a mire with the UNESCO World Natural Heritage Serrahn site in the background (Photo: P. Wernicke). F: South-eastern shoreline of Lake Fürstenseer See with sandy terrace plain (Photo: U. Meßner).

West   N a t i o n a l   P a r k   A r e a   **East**

Neustrelitz   *Serrahner Berge*   *Grünow*

W

H

W

S / W

S

E / S

E / S

Miocene
(younger)

Miocene
(older)

E

T

Oligocene

Miocene

Oligocene

Eocene

5 km

m a.s.l./b.s.l.   m a.s.l./b.s.l.

Water	**H** Holocene
Peat	**W** Weichselian
Aeolian sand	**S** Saalian
Glacio(fluvio)lacustrine silt and sand	**E** Elsterian
Glaciofluvial sand and gravel	**T** Tertiary
Till	
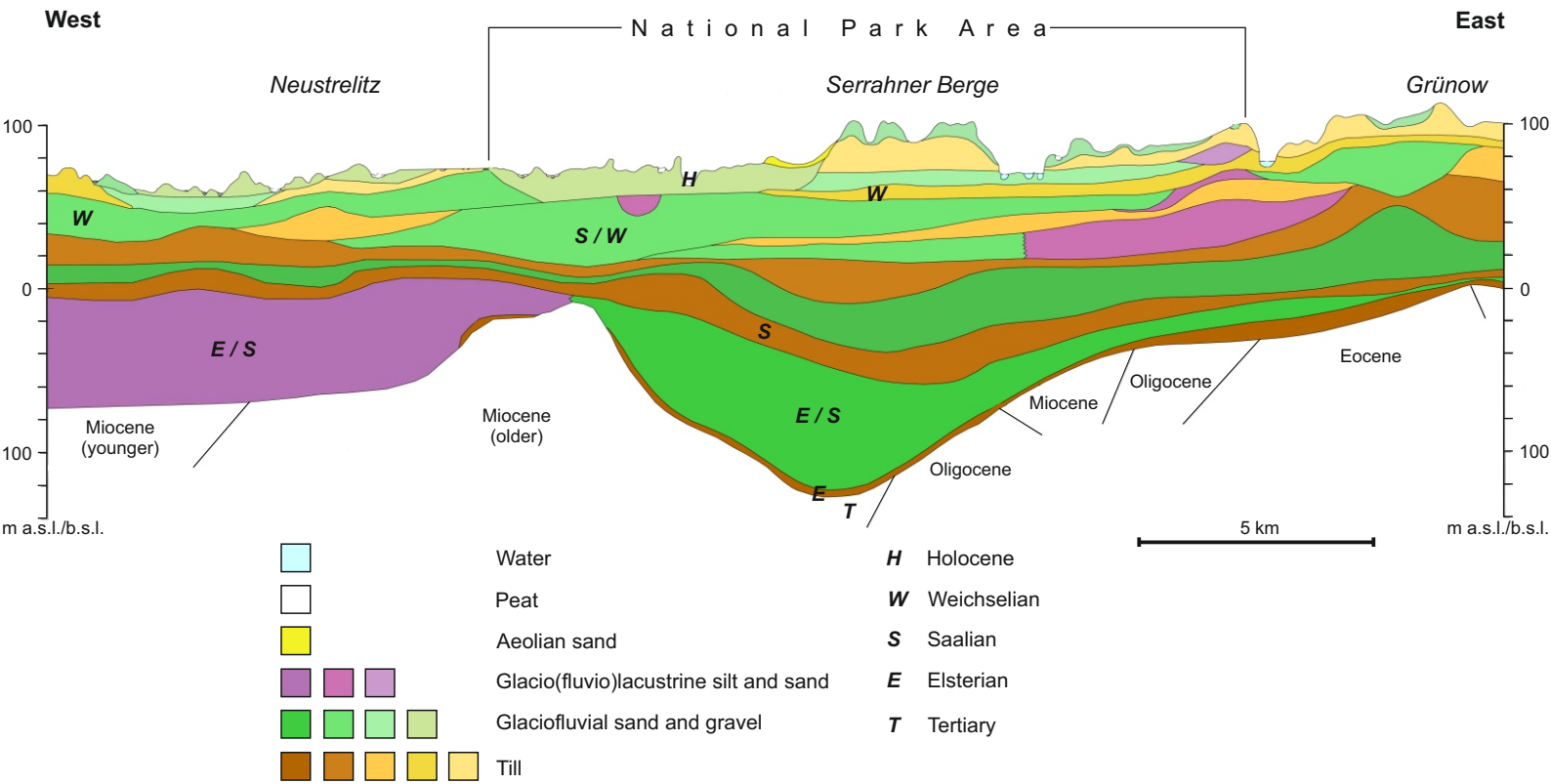
Fig. 3: Geologic-topographic cross-section through the Serrahn area showing the thick package of Quaternary sediments attaining a local thickness of 230 m (Börner and Schütze, 2005).
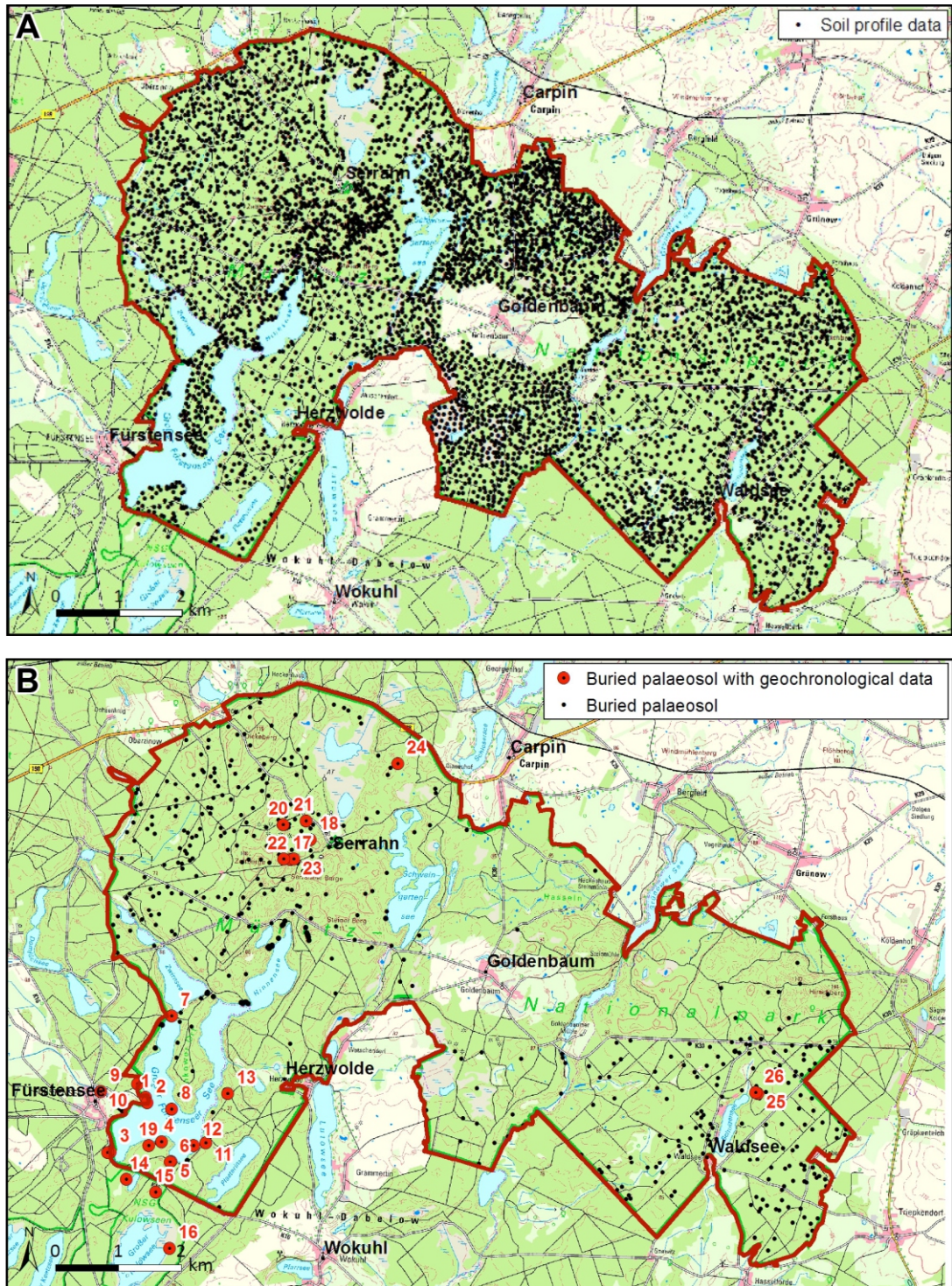
Fig. 4: Soil profiles available in the Serrahn area. A: Spatial distribution of all soil profiles recorded (n = 5214). B: Soil profiles with buried palaeosols recorded (n = 520) with a subset having geochronological data (n = 26). The red numbers indicate the site IDs.
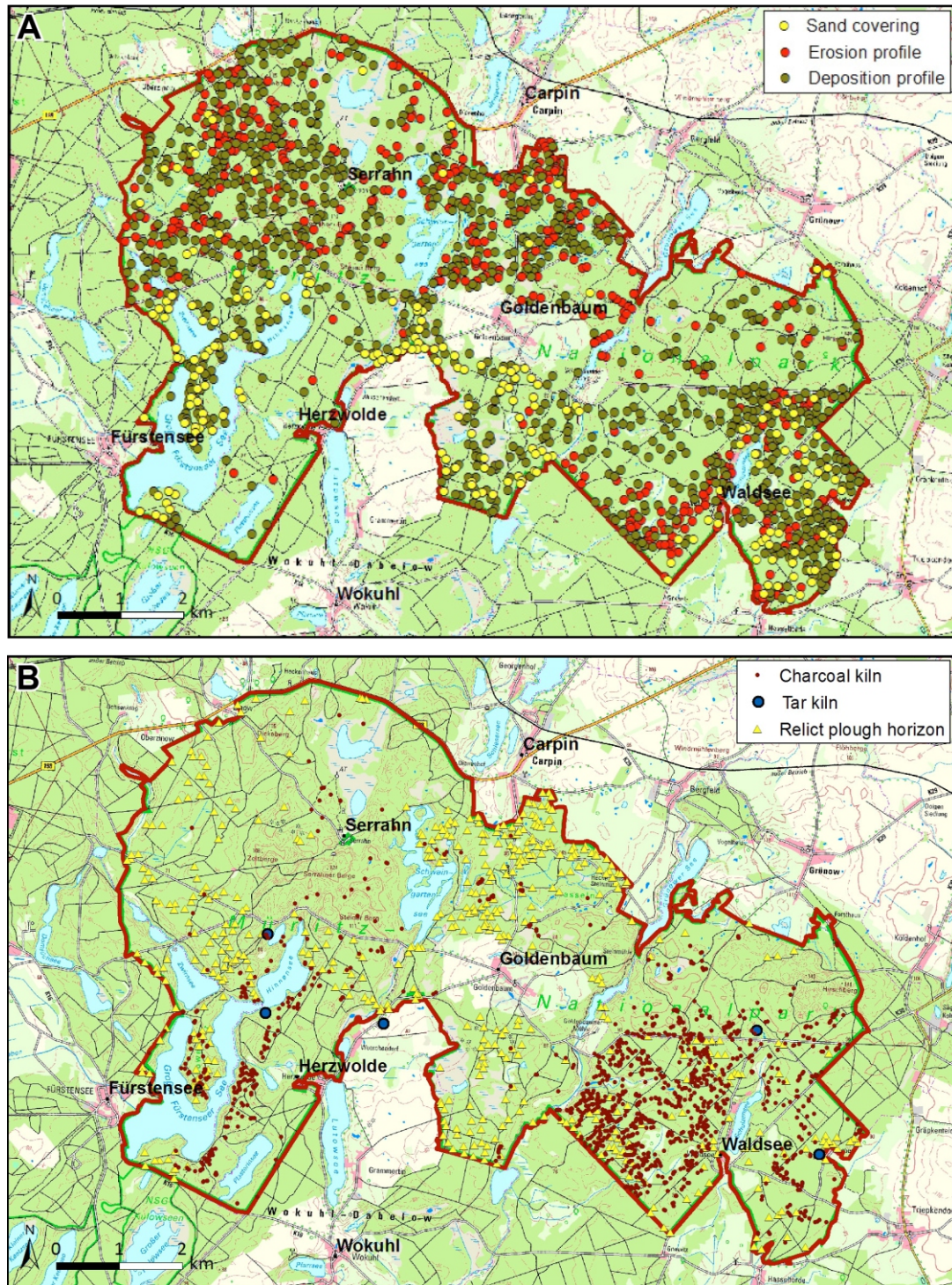
Fig. 5: Soil profile characteristics and land use traces in the Serrahn area. A: Distribution of soil profiles showing thin sand covering (≤ 20 cm), erosion and deposition (aggradation). B: Sites with kilns (charcoal, tar) and relic plough horizons (fAp) indicating former wood use and arable land use, respectively.
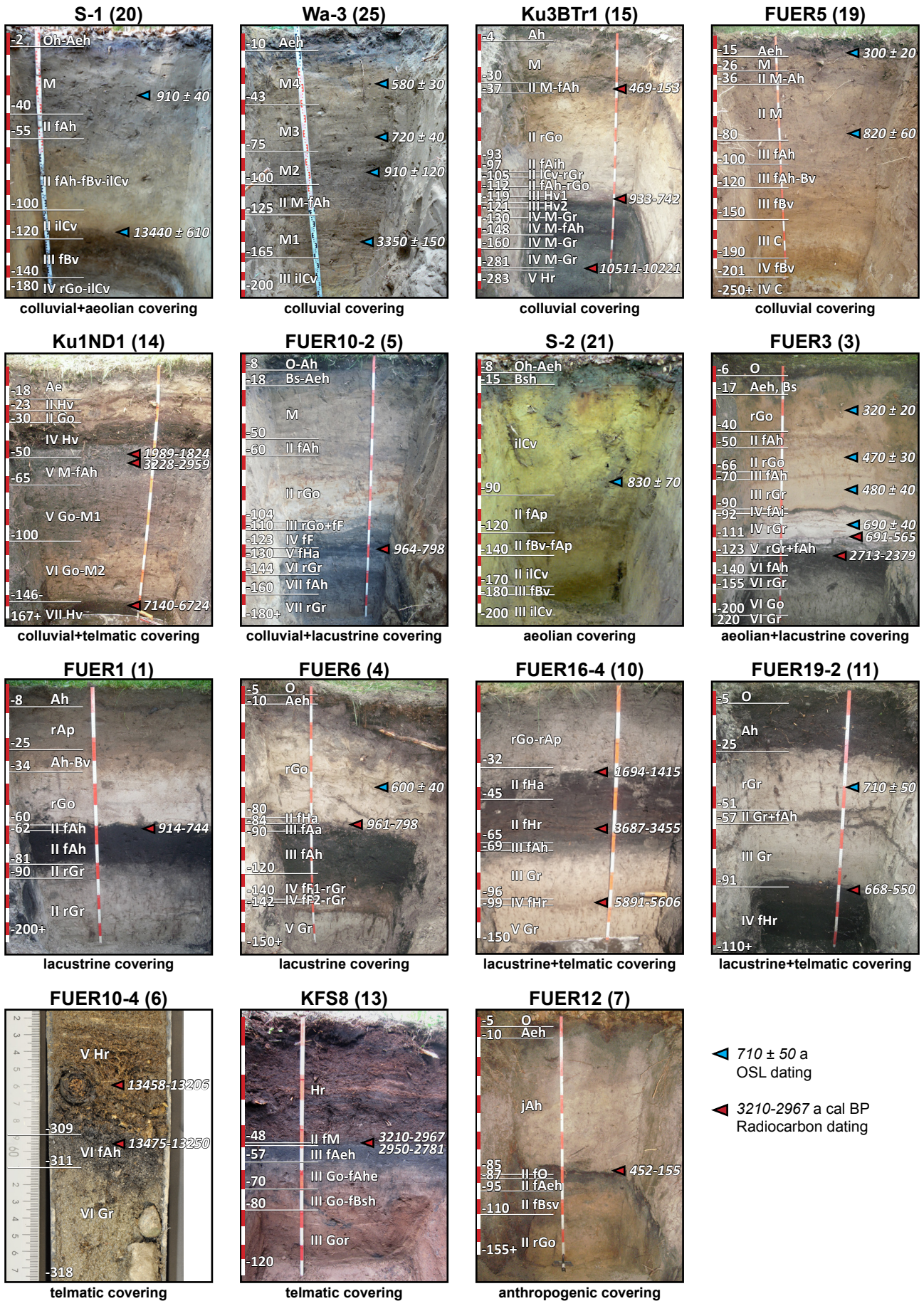
Fig. 6: Photographs with pedologic and geochronological information of selected soil profiles with palaeosols recorded in the Serrahn area (site ID in parentheses). The sediment types covering the palaeosols are given below the photo. For location of the profiles see Figure 4B.
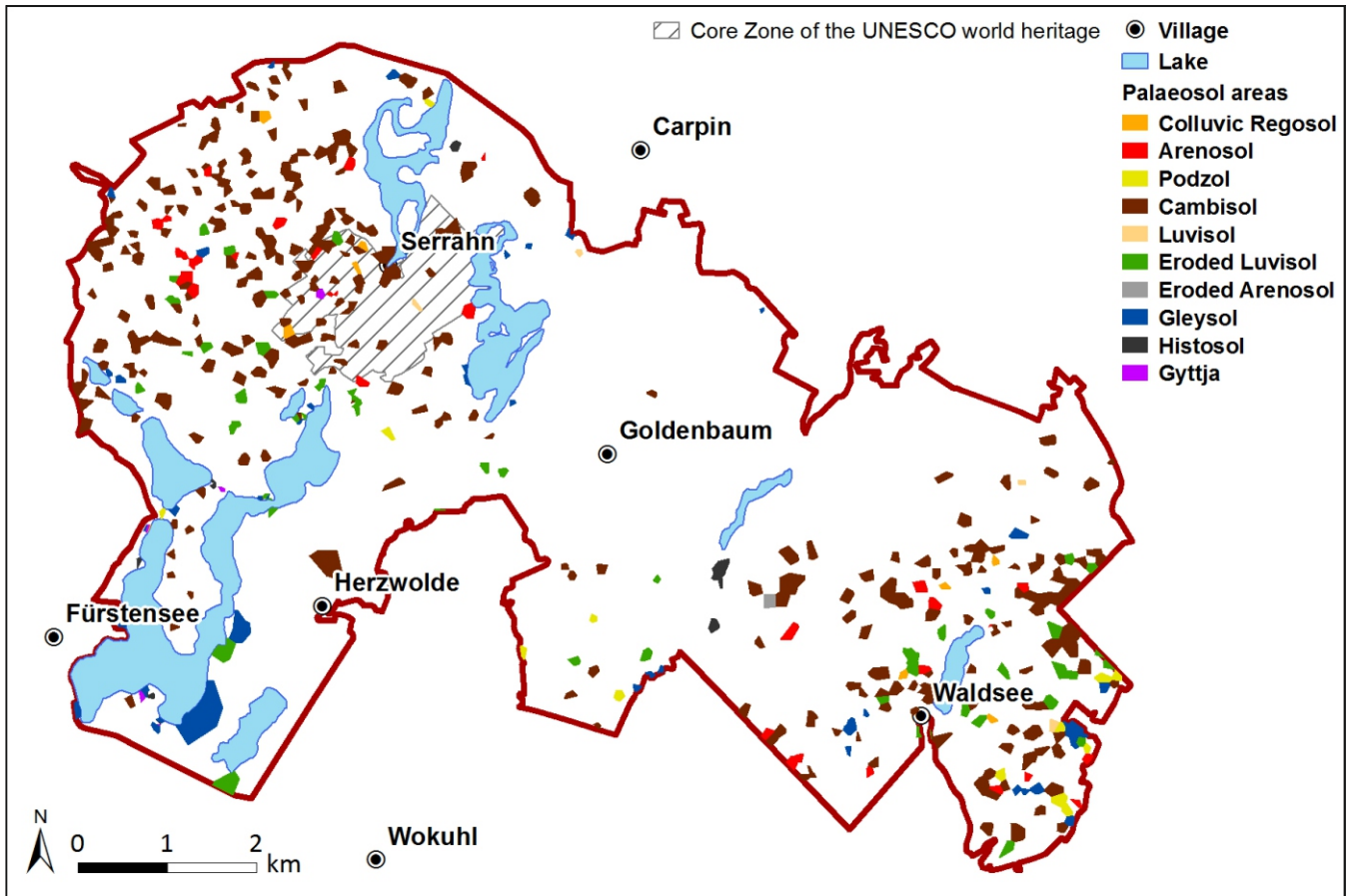
Fig. 7: Geostatistical modeling of palaeosol areas in the Serrahn area. The somewhat angular shapes of the palaeosol areas result from the mathematic method used for partition, i.e. construction of Voronoi-Thiessen polygons based on the detection of local palaeosol occurrences.
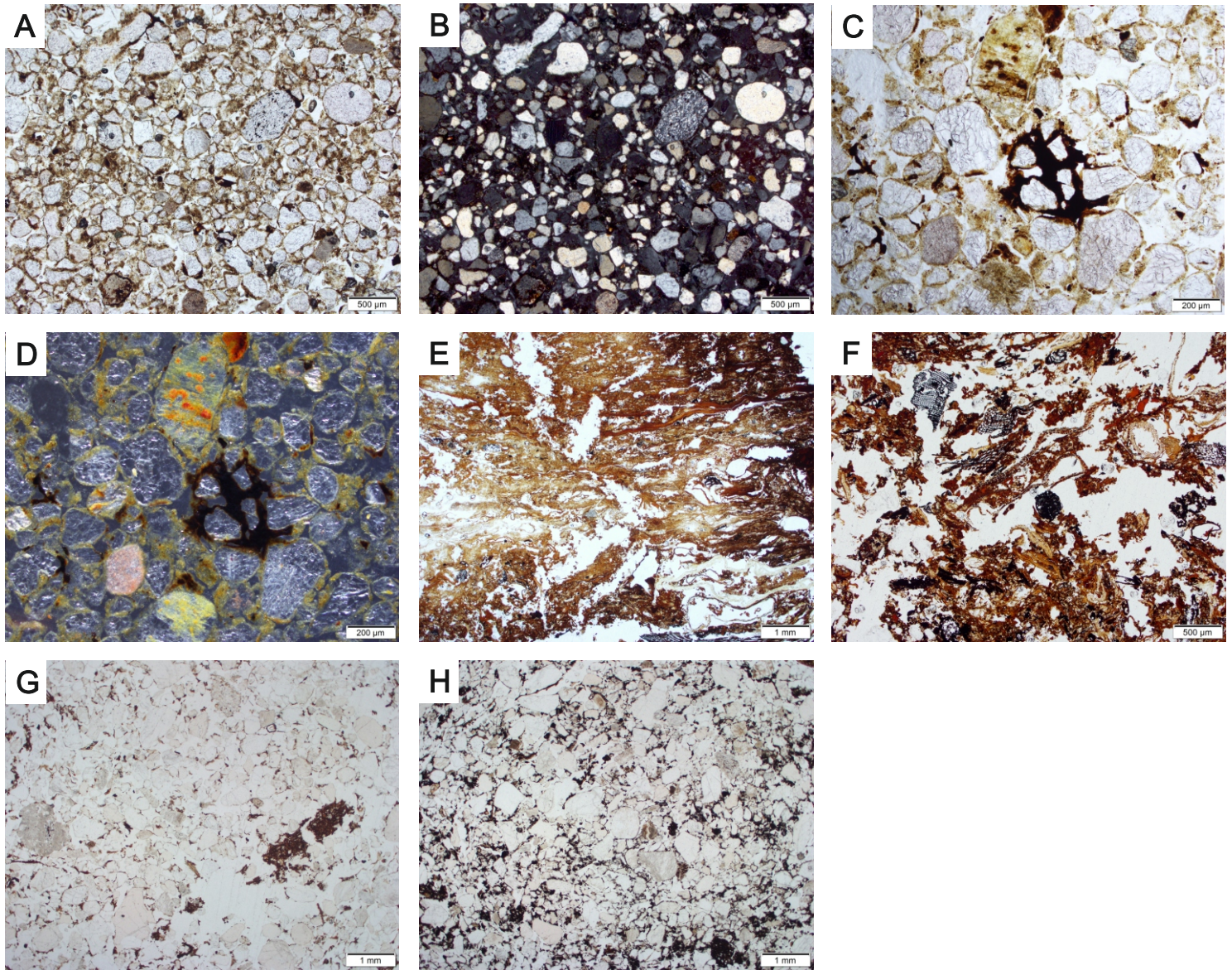
Fig. 8: Micromorphology of palaeosol horizons of profile S-1/site ID 20 (IIfBv horizon; A-D) and KFS8/site ID 13 (transition from IIfAeh to Hr horizon; E-H). For location of the profiles see Figure 4B. A: (ppl) Sand sized material with brown fine mass between the sand grains and partly covering them. B: Like A (xpl) - note the low birefringence of the fine material. C: (ppl) Weathered sand grains and ferruginous punctuation of the fine mass. D: Like C (oil). E: (ppl) Uppermost horizon consisting of peat (plant tissue residues and decomposed material). F: (ppl) Bioturbation in the peat layer and charcoal pieces. G: (ppl) Intermediate horizon consisting of sand grains. Note the faunal infilling that is rich in organic material. H: (ppl) Lowermost horizon representing a fAeh horizon.

Fig. 9: Pedosedimentary sequences from kettle-holes in the Serrahn area with lithological, pedological, geochronological, palynological, and sedimentological data. A: Profile KFS8/site ID 13 east of Lake Fürstenseer See. B: Profile Mü-1/site ID 17 west of Serrahn village. For location of the profiles see Figure 4B.
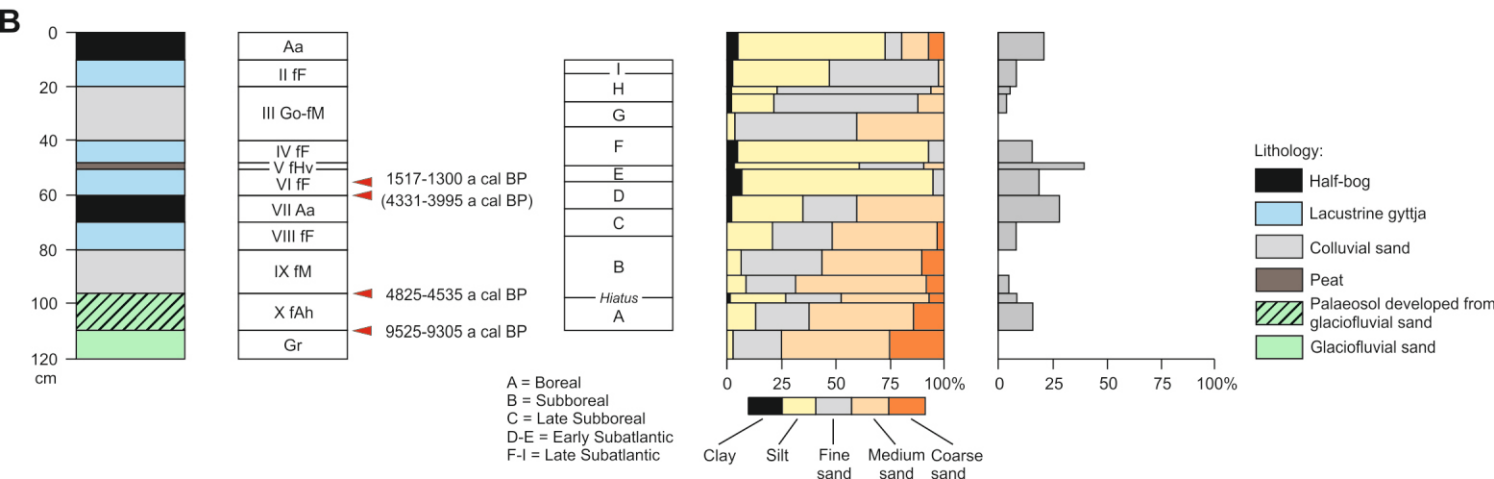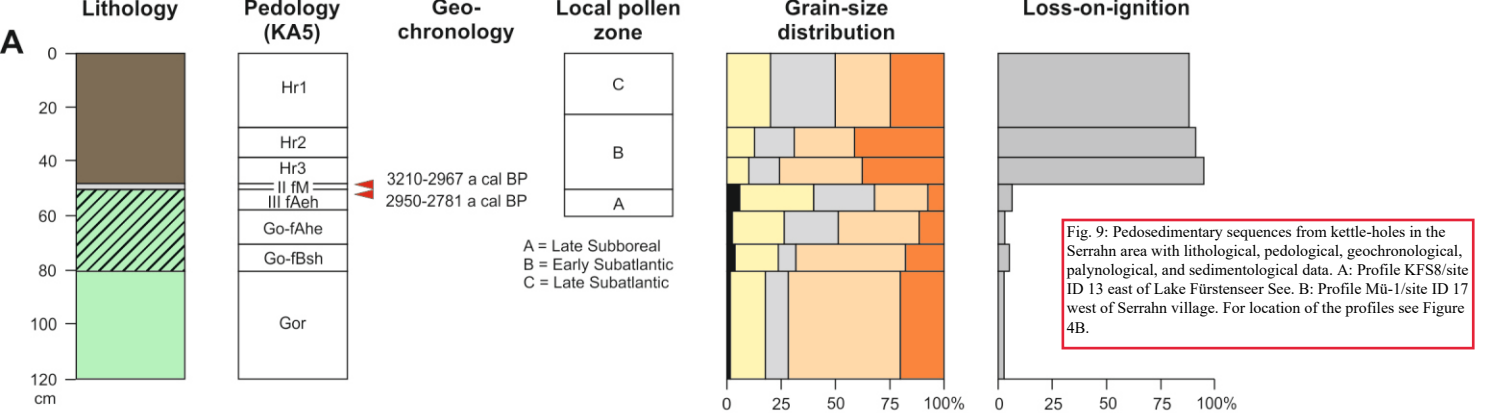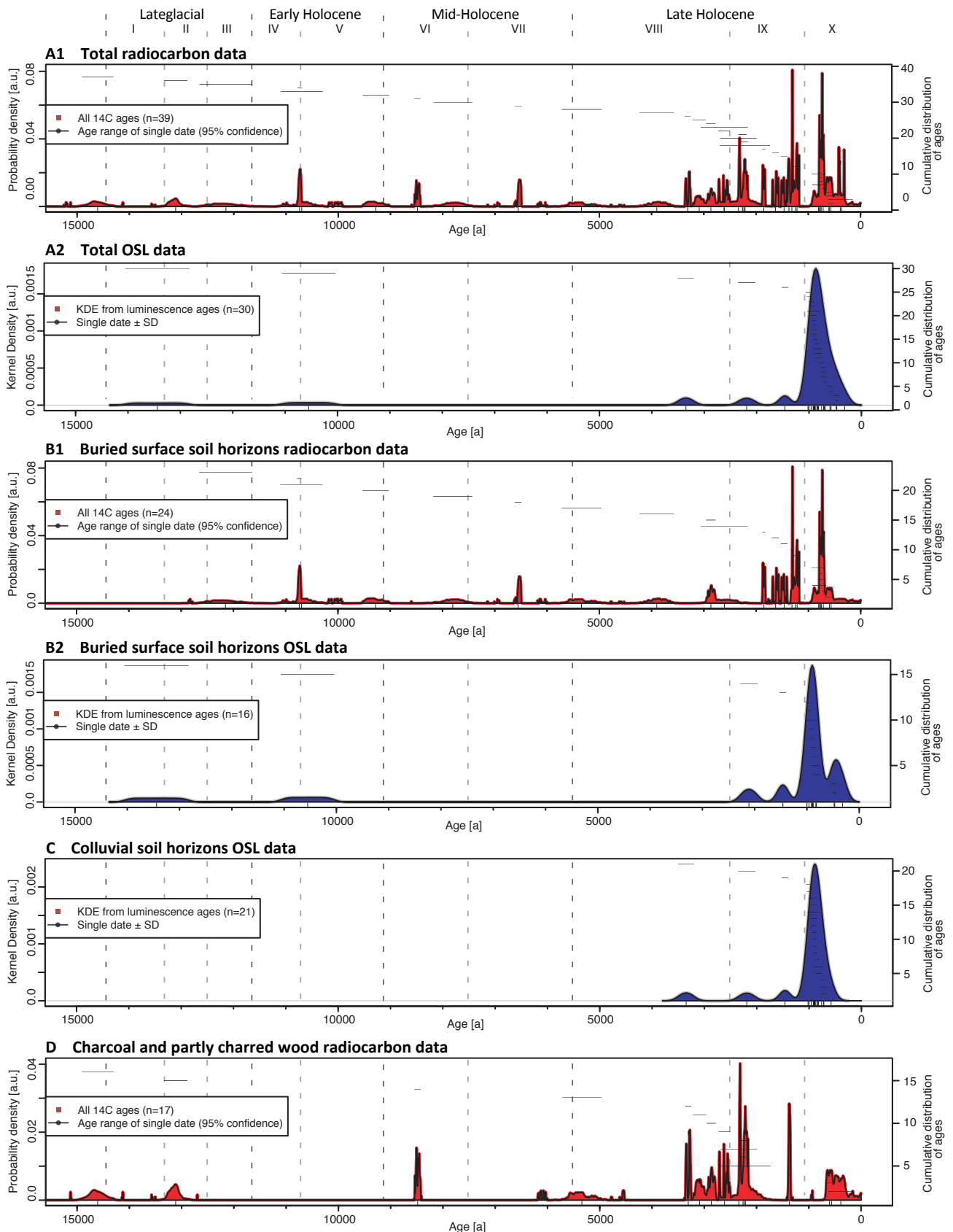
Fig. 10: Geochronological data from palaeosols and sediments of the Serrahn area. Radiocarbon ages are given in red, luminescence ages are given in blue. Bio-/pollenzones (after Firbas in Giesecke et al., 2012) are given in Roman numbers and separated by dashed lines. A1, A2: Relative probability and kernel density estimate of radiocarbon and luminescence ages, respectively, from all geochronological data available. B1, B2: Relative probability and kernel density estimate of radiocarbon and luminescence ages from buried humic and peaty surface soil horizons (fAh, fAa, fHv, fHa, fHr). C: Kernel density estimate of luminescence ages from colluvial soil horizons (M, fM). D: Relative probability estimate from radiocarbon ages on charcoal and partly charred wood indicating past fire dynamics.
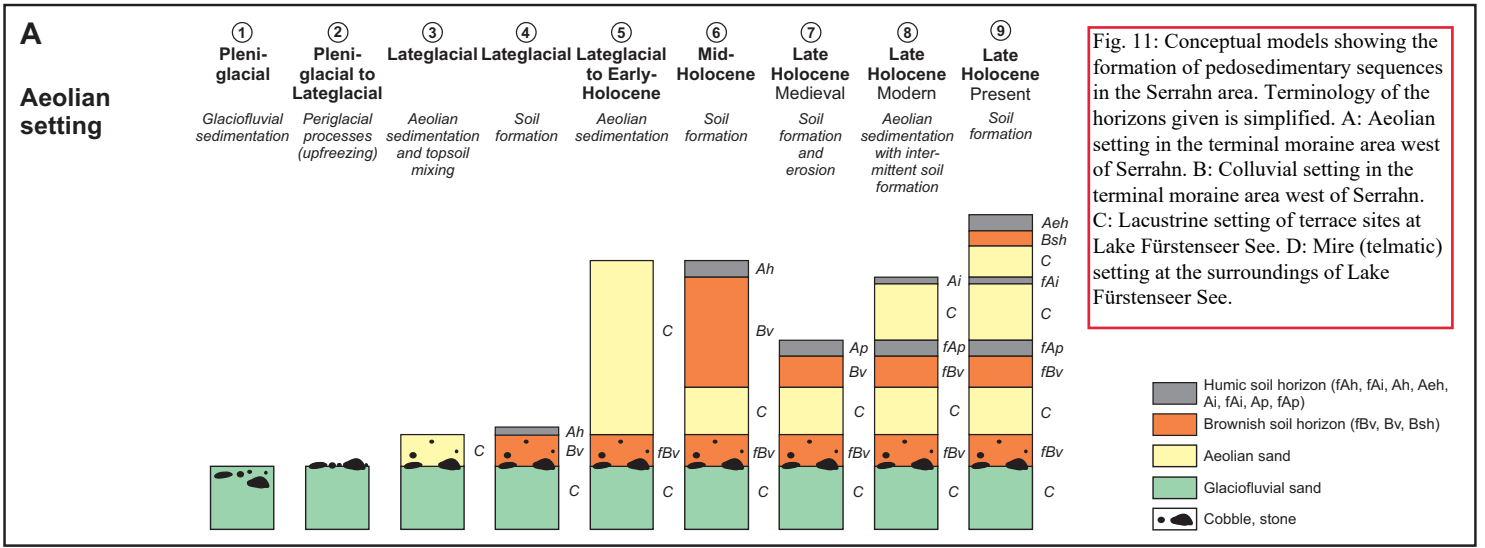
Fig. 11: Conceptual models showing the formation of pedosedimentary sequences in the Serrahn area. Terminology of the horizons given is simplified. A: Aeolian setting in the terminal moraine area west of Serrahn. B: Colluvial setting in the terminal moraine area west of Serrahn. C: Lacustrine setting of terrace sites at Lake Fürstenseer See. D: Mire (telmatic) setting at the surroundings of Lake Fürstenseer See.
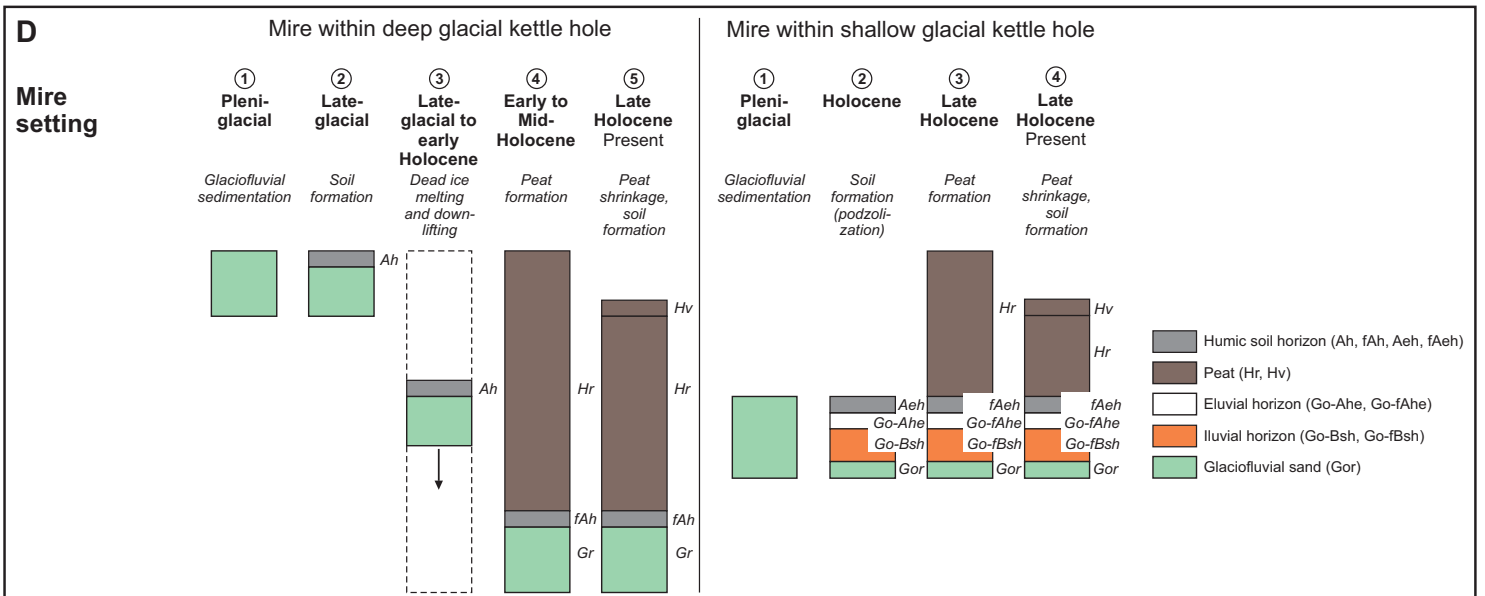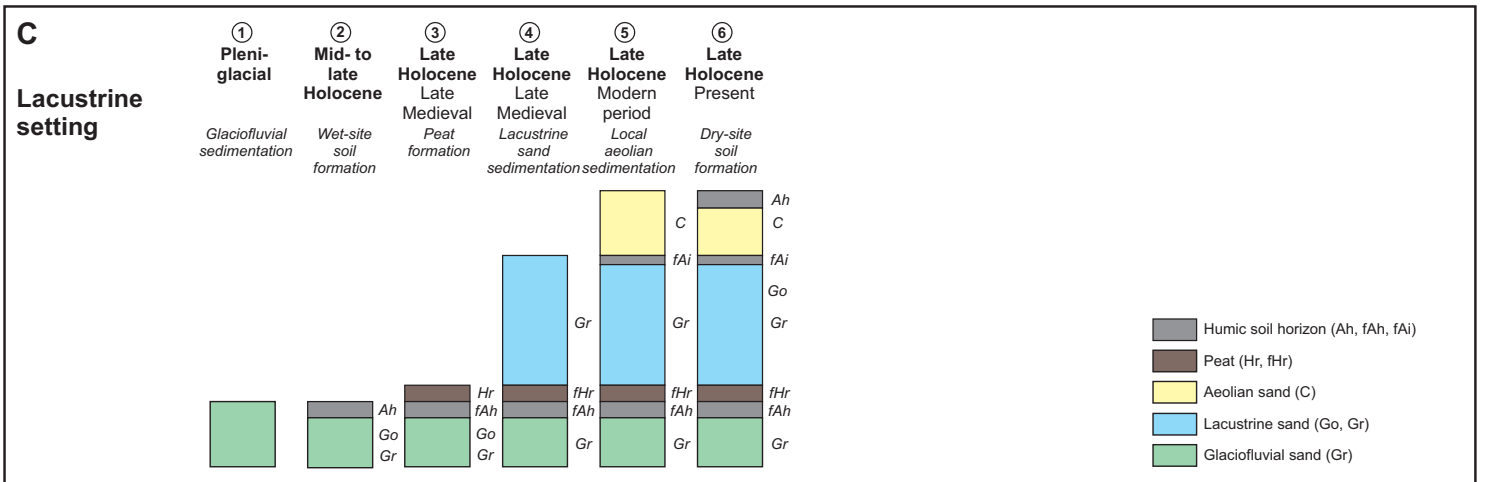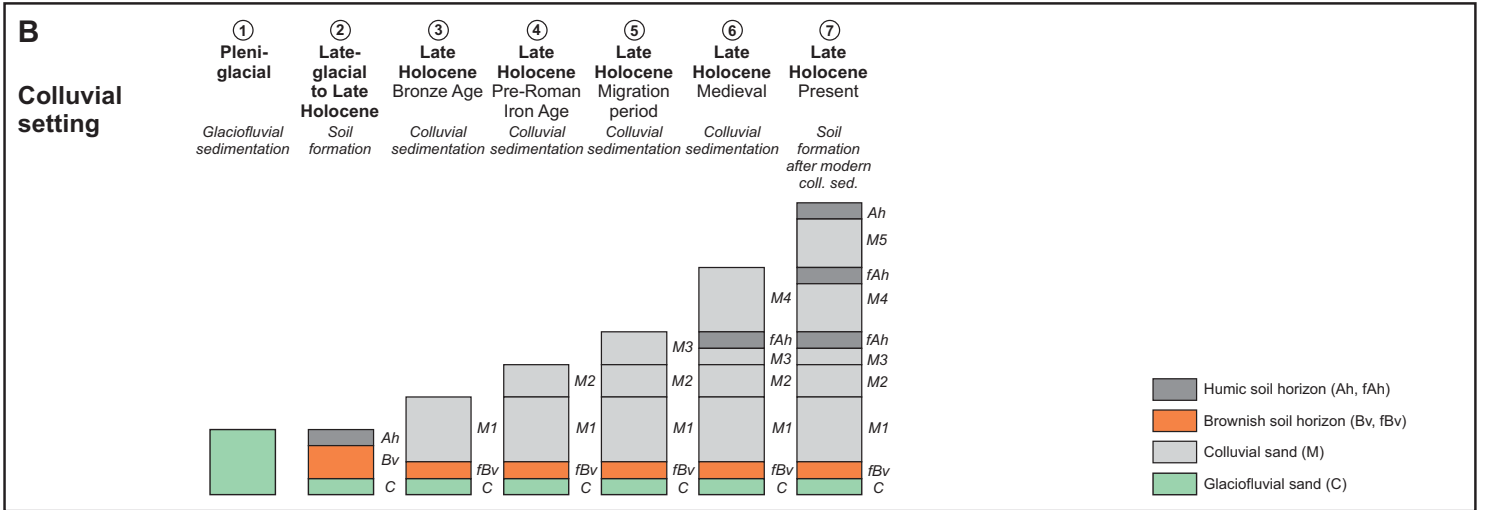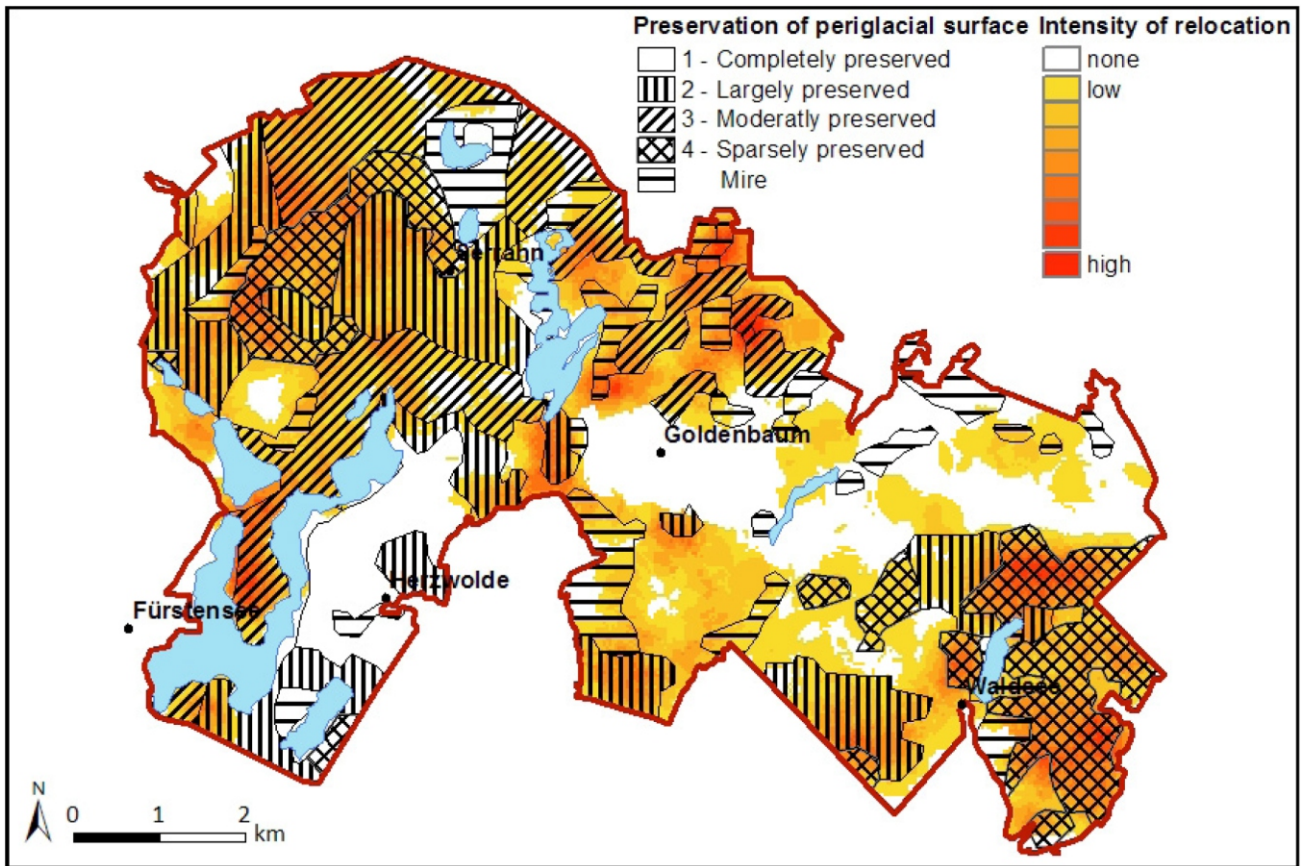
Fig. 12: Erosional pattern in the Serrahn area indicated by the preservation stage of the periglacial surface (after Dieckmann and Kaiser, 1998, modified) and by calculating the intensity of soil relocation applying the ArcGIS tool `Point density'.

Tab. 1: Distribution of soil profiles with palaeosols, thin sand coverings and plough horizons in the Serrahn area depending from geological units.

Geological unit	Soil profile without palaeosol		Soil profile with palaeosol		Thin sand covering (≤ 20 cm)		Relict plough horizon	
	n	(%)	n	(%)	n	(%)	n	(%)
Terminal moraine	836	17.8	76	14.6	7	3.3	17	3.1
Till	719	15.3	14	2.7	7	3.3	91	16.8
Glaciofluvial sand	2340	49.9	322	61.9	179	85.6	356	65.6
Aeolian sand	178	3.8	57	11.0	4	1.9	13	2.4
Mire	603	12.8	20	3.8	12	5.7	61	11.2
Lake shoreline	18	0.4	31	6.0	0	0	5	0.9
Total	4694	100	520	100	209	100	543	100

Tab. 2: Statistics of soil analytical data from the Serrahn area grouped into topsoil/subsoil and buried horizons as well as sediments.

Soil horizons, sediments	Horizon thickness Mean [cm]	SD [cm]	n	Layer thickness Mean [cm]	SD [cm]	n	Clay <0.002 mm Mean [%]	SD [%]	Silt <0.063 mm Mean [n]	SD [%]	Fine sand <0.2 mm Mean [%]	SD [%]	Medium sand <0.63 mm Mean [%]	SD [%]	Coarse sand <2 mm Mean [%]	SD [%]	n	Loss-on-ignition Mean [%]	SD [%]	n	CaCO$_3$ Mean [%]	SD [n]	n	pH [CaCl$_2$ / KCl] Mean [%]	SD [%]	n
Top- and subsoil horizons																										
Ah, rAp, Aeh, M-Ah, Bv-Ah, Bv-Ap, Bv+Ah, Oh-Ah, Oh-Aeh, Go-rAp	11.4	9.5	30	-	-	-	2.9	2.6	8.5	5.0	31.8	15.4	46.5	11.1	10.3	7.9	35	4.4	3.5	36	0.0	0.0	36	3.5	0.3	28
Aa, rAap	11.8	5.7	4	-	-	-	1.1	2.1	29.8	26.0	24.4	15.6	35.2	14.6	9.6	4.3	4	17.7	1.8	4	0.0	0.0	3	n.a.	n.a.	1
Bv, Ah-Bv	36.0	17.0	8	-	-	-	4.9	2.2	6.3	1.7	37.0	13.5	43.4	8.8	8.4	5.3	10	0.5	0.3	10	0.0	0.0	10	4.1	0.2	10
Bsh	4.3	2.5	3	-	-	-	3.1	1.1	3.1	3.3	46.2	14.2	43.0	4.2	4.5	5.5	2	1.6	0.2	2	0.0	0.0	2	3.6	0.1	2
M, Go-M, Bsh-M, M-Go	47.8	39.3	16	-	-	-	2.6	2.2	6.2	4.7	40.9	15.1	42.2	13.1	8.1	7.0	28	2.2	1.6	28	0.0	0.0	28	4.4	0.4	24
ICv, C, Cv-Bv, Cv-Bb, Bb-Cv, ilC	41.7	28.3	29	-	-	-	2.0	1.6	3.5	2.5	35.2	17.6	48.3	10.6	10.9	8.4	34	0.2	0.2	34	0.5	2.0	34	4.9	1	33
Go, Gr, rGo, rGr, Gor	38.3	32.0	34	-	-	-	0.2	0.3	3.2	3.0	29.4	20.4	54.0	15.2	13.2	12.1	40	0.9	0.8	40	0.0	0.0	38	5.2	0.7	19
Buried horizons																										
fAh, fAi, fAe, fAh-fBv-ilCv, fBv-fAp, M-fAh, fAe	15.7	11.6	36	-	-	-	1.2	1.8	5.5	4.1	36.8	17.5	45.2	11.5	11.2	12.1	42	4.5	4.6	42	0.0	0.0	42	4.6	0.7	25
fAa	14.5	12.0	2	-	-	-	0.8	0.9	21.5	12.8	30.6	18.5	37.3	13.9	9.9	14.7	3	24.0	2.7	3	0.0	0.0	3	n.a.	n.a.	0
fHr, fHv, fHa	13.3	8.1	17	-	-	-	1.2	1.1	28.0	18.3	25.3	16.0	35.2	20.5	9.2	10.3	6	60.9	18.8	17	0.0	0.0	16	3.1	0.4	2
fBv, fAh-Bv, fBhv	37.4	25.1	7	-	-	-	3.7	1.9	7.3	4.7	45.8	15.3	35.9	10.5	7.2	7.9	7	3.2	1.9	7	0.0	0.0	7	4.9	0.4	7
fBsh	n.a.	n.a.	1	-	-	-	0.3	0.1	2.5	0.2	48.3	0.1	45.1	2.5	3.5	0.2	2	2.6	1.3	2	0.0	0.0	2	3.9	0.1	2
fF	14.9	16.1	11	-	-	-	1.9	2.1	48.7	35.6	20.5	14.8	20.7	22.5	6.5	9.0	11	8.9	5.0	11	15.8	32.4	11	n.a.	n.a.	0
Sediments																										
Glaciofluvial sand	-	-	-	83.3	55.7	24	2.4	2.3	5.2	3.7	34.7	15.1	47.0	9.9	10.6	8.5	92	1.5	2.2	91	0.2	1.3	90	4.5	0.9	79
Colluvial sand	-	-	-	69.8	58.1	14	2.3	2.3	6.6	4.7	41.1	14.0	42.3	10.6	7.8	7.0	53	4.0	4.2	53	0.0	0.0	54	4.2	0.7	48
Aeolian sand	-	-	-	105.5	43.2	4	2.4	1.6	4.0	4.6	54.5	14.3	36.1	10.7	2.9	2.5	14	1.6	1.2	14	0.0	0.0	14	4.5	0.6	13
Lacustrine sand	-	-	-	57.2	29.8	19	0.1	0.2	6.9	7.5	20.3	15.7	55.8	15.4	16.9	12.9	16	4.9	6.3	16	0.0	0.0	15	n.a.	n.a.	0
Lacustrine gyttja	-	-	-	20.3	22.5	6	1.9	2.1	45.6	38.3	20.8	15.8	18.8	23.2	5.7	9.3	8	8.6	4.7	11	17.8	32.0	11	n.a.	n.a.	0
Peat	-	-	-	17.3	12.8	16	1.2	1.1	28.0	18.3	25.3	16.0	33.9	20.5	9.2	10.3	6	62.7	19.7	18	0.0	0.0	17	3.1	0.4	2
Anthropogenic sand	-	-	-	n.a.	n.a.	1	1.0	0.1	0.9	0.4	48.7	2.0	41.1	2.1	8.4	3.5	2	0.6	0.4	2	0.0	0.0	2	4.8	0.1	2

Tab. 3: Radiocarbon data of the soil profiles investigated in the Serrahn area. Data calibration was performed with OxCal version 4.2 (Bronk Ramsey, 2009; Reimer et al., 2013) with a range of two sigma deviation for analysis.

Sample ID	Site ID	Northing	Easting	Depth [cm]	Material dated	Soil horizon [KA5, simplified]	Sedimentary facies	Lab ID	Age [a BP]	Age calibrated [2sigma, a cal BP]	Reference
FUER1	1	53°18'26.8"	13°09'30.4"	60-62	humic sand	fAa	glaciofluvial	Poz-37353	905 ± 30	914-744	Kaiser et al., 2014a
FUER2	2	53°18'23.5"	13°09'32.9"	58-59	peat	fHa	telmatic	Poz-37390	1340 ± 30	1306-1185	Kaiser et al., 2014a
FUER3a	3	53°17'57.9"	13°09'02.9"	109	charcoal	rGr	lacustrine	Poz-37354	705 ± 30	691-565	Kaiser et al., 2014a
FUER3b	3	53°17'57.9"	13°09'02.9"	123-124	humic sand	fAh	glaciofluvial	Poz-38930	2465 ± 35	2713-2379	Kaiser et al., 2014a
FUER6	4	53°18'03.4"	13°09'43.4"	80-84	peat	fHa	telmatic	Poz-37355	990 ± 30	961-798	Kaiser et al., 2014a
FUER10-2	5	53°17'52.9"	13°09'53.9"	123-124	peat	fHa	telmatic	Poz-46604	995 ± 30	964-798	Kaiser et al., 2014a
FUER10-4 KM3a	6	53°17'53.8"	13°09'53.1"	24-26	charcoal	Hr	telmatic	Poz-46606	1620 ± 30	1569-1412	this study
FUER10-4 KM3b	6	53°17'53.8"	13°09'53.1"	111-112	partly charred wood	Hr	telmatic	Poz-46607	6860 ± 35	7785-7616	this study
FUER10-4 KM3c	6	53°17'53.8"	13°09'53.1"	245-247	wood (birch bark)	Hr	telmatic	Poz-46608	10540 ± 60	12690-12237	this study
FUER10-4 KM3d	6	53°17'53.8"	13°09'53.1"	306	wood (pine cone)	Hr	telmatic	Poz-46610	11490 ± 60	13458-13206	this study
FUER10-4 KM3e	6	53°17'53.8"	13°09'53.1"	308	charcoal	fAh	glaciofluvial	Poz-46611	11520 ± 60	13475-13250	this study
FUER12	7	53°19'14.6"	13°09'88.1"	80-82	soil litter	fO	glaciofluvial	Poz-38927	280 ± 30	452-155	Kaiser et al., 2014a
FUER14a	8	53°18'34.0"	13°09'79.8"	41-42	plant macro-remains	fHv	telmatic	Poz-38928	7570 ± 50	8456-8212	Kaiser et al., 2014a
FUER14b	8	53°18'34.0"	13°09'79.8"	49-50	peat	fHv	telmatic	Poz-38929	8510 ± 60	9580-9417	Kaiser et al., 2014a
FUER15a	9	53°18'48.3"	13°08'87.8"	140-141	peat	fHv	telmatic	Poz-47654	880 ± 30	908-729	Kaiser et al., 2014a
FUER15b	9	53°18'48.3"	13°08'87.8"	154-155	peat	fHv	telmatic	Poz-47655	1405 ± 30	1355-1283	Kaiser et al., 2014a
FUER16-4a	10	53°18'55.7"	13°09'40.1"	32-34	peat	fHa	telmatic	Erl-16596	1656 ± 44	1694-1415	Kaiser et al., 2014a
FUER16-4b	10	53°18'55.7"	13°09'40.1"	57-58	peat	fHr	telmatic	Erl-16597	3331 ± 46	3687-3455	Kaiser et al., 2014a
FUER16-4c	10	53°18'55.7"	13°09'40.1"	96-99	peat	fHr	telmatic	Erl-16598	4987 ± 47	5891-5606	Kaiser et al., 2014a
FUER19-2	11	53°18'07.0"	13°10'38.3"	91-92	peat	fHr	telmatic	Erl-16599	637 ± 41	668-550	Kaiser et al., 2014a
GFS11-A0	12	53°18'2.5"	13°10'11.6"	104	charcoal	F	lacustrine	Poz-61452	11270 ± 100	13334-12893	Dietze et al., 2016
KFS8a	13	53°18'27.6"	13°10'42.9"	48.5	partly charred wood	Gr	colluvial	Poz-98722	2940 ± 40	3210-2967	this study
KFS8b	13	53°18'27.6"	13°10'42.9"	50	charcoal	fAeh	glaciofluvial	Poz-98723	2765 ± 35	2950-2781	this study
Ku1ND1b	14	53°17'42.2"	13°09'16.6"	48-50	peat	fHv	telmatic	Erl-16602	1954 ± 39	1989-1824	this study
Ku1ND1c	14	53°17'42.2"	13°09'16.6"	50-55	charcoal	M-fAh	colluvial	Erl-16603	2944 ± 46	3228-2959	this study
Ku1ND1d	14	53°17'42.2"	13°09'16.6"	146-148	peat	fHv	telmatic	Erl-16604	6019 ± 55	7140-6724	this study
Ku3BTr1a	15	53°17'38.0"	13°09'41.8"	30-37	charcoal	M-fAh	colluvial	Erl-16605	284 ± 41	469-153	this study
Ku3BTr1b	15	53°17'38.0"	13°09'41.8"	112-119	peat	fHv	telmatic	Erl-16606	939 ± 49	933-742	this study
Ku3BTr1c	15	53°17'38.0"	13°09'41.8"	281-283	peat	fHv	telmatic	Erl-16607	9166 ± 68	10511-10221	this study
Ku4.1	16	53°17'09.2"	13°09'55.1"	30-31	peat	fHr	telmatic	Erl-16600	1785 ± 41	1822-1605	this study
Mü-1a	17	53°20'30.5"	13°11'24.4"	49	plant remains	fHv	telmatic	Beta-291880	1480 ± 40	1517-1300	Küster, 2014
Mü-1b	17	*53°20'30.5"*	*13°11'24.4"*	*59*	*charcoal*	*fAa*	*Telmatic (?)*	*Beta-291881*	*3790 ± 40*	*4331-3995*	*Küster, 2014*
Mü-1c	17	53°20'30.5"	13°11'24.4"	95	charcoal	fAh	glaciofluvial	Beta-291882	4140 ± 40	4825-4535	Küster, 2014
Mü-1d	17	53°20'30.5"	13°11'24.4"	109	charcoal	fAh	glaciofluvial	Beta-291883	8410 ± 50	9525-9305	Küster, 2014
S-3a	18	53°20'40.8"	13°11'46.8"	55	charcoal	ylC	anthropogen (pit fill)	Erl-14731	334 ± 34	480-308	Küster, 2014
S-3b	18	53°20'40.8"	13°11'46.8"	80	charcoal	ylC	anthropogen (pit fill)	Erl-14732	2267 ± 37	2350-2156	Küster, 2014
S-3c	18	53°20'40.8"	13°11'46.8"	130	charcoal	ylC	anthropogen (pit fill)	Erl-14733	2385 ± 31	2677-2344	Küster, 2014
S-3d	18	53°20'40.8"	13°11'46.8"	140	charcoal	ylC	anthropogen (pit fill)	Erl-14734	2279 ± 35	2353-2158	Küster, 2014
S-3e	18	53°20'40.8"	13°11'46.8"	150	charcoal	ylC	anthropogen (pit fill)	Erl-14735	2190 ± 37	2326-2115	Küster, 2014
S-3f	18	53°20'40.8"	13°11'46.8"	155	charcoal	ylC	anthropogen (pit fill)	Erl-14736	2118 ± 38	2300-1992	Küster, 2014

Sample ID	Site ID	Northing	Easting	Depth [cm]	Material dated	Soil horizon [KA5, simplified]	Lab. No.	U[a] [ppm]	Th[a] [ppm]	K[a] [%]	Cosmic dose rate[b] [Gy/ka]	Water cont. measured[c] [%]	Water cont. estimated[c] [%]	Dose rate [Gy/ka]	Equivalent dose (D$_e$)[d] [Gy]	Age model	OSL age [ka]	OSL age [a]	Reference
FUER2	2	53°18'23.5"	13°09'32.9"	40	Lacustrine sand	rGo	HUB-0324	0.79 ± 0.08	2.49 ± 0.12	1.07 ± 0.03	0.21 ± 0.01	9.1	10 ± 5	1.46 ± 0.09	3.05 ± 0.29	MAM	2.09 ± 0.24	2090 ± 24	Kaiser et al., 2014a
FUER3-1	3	53°17'57.9"	13°09'02.9"	27	aeolian sand	rGo	HUB-0187	0.58 ± 0.05	1.88 ± 0.17	1.01 ± 0.02	0.21 ± 0.01	5.7	6 ± 4	1.39 ± 0.07	0.44 ± 0.01	CAM	0.32 ± 0.02	320 ± 20	Kaiser et al., 2014a
FUER3-2	3	53°17'57.9"	13°09'02.9"	55	aeolian sand	rGo	HUB-0188	0.62 ± 0.09	1.96 ± 0.19	1.02 ± 0.02	0.20 ± 0.01	10.0	10 ± 5	1.34 ± 0.08	0.63 ± 0.01	CAM	0.47 ± 0.03	470 ± 30	Kaiser et al., 2014a
FUER3-3	3	53°17'57.9"	13°09'02.9"	76	aeolian sand	rGr	HUB-0189	0.62 ± 0.07	1.70 ± 0.11	1.00 ± 0.02	0.20 ± 0.01	9.3	10 ± 5	1.31 ± 0.08	0.63 ± 0.03	CAM	0.48 ± 0.04	480 ± 40	Kaiser et al., 2014a
FUER3-4	3	53°17'57.9"	13°09'02.9"	100	lacustrine sand	rGr	HUB-0325	0.62 ± 0.05	1.74 ± 0.07	1.20 ± 0.03	0.20 ± 0.01	9.5	10 ± 5	1.49 ± 0.09	1.02 ± 0.02	CAM	0.69 ± 0.04	690 ± 40	Kaiser et al., 2014a
FUER5-1	19	53°18'1.8"	13°09'34.6"	12	colluvial sand	M	HUB-0190	0.85 ± 0.07	3.06 ± 0.11	1.17 ± 0.03	0.21 ± 0.01	8.2	8 ± 4	1.64 ± 0.08	0.49 ± 0.03	MAM	0.30 ± 0.02	300 ± 20	Kaiser et al., 2014a
FUER5-2	19	53°18'1.8"	13°09'34.6"	75	colluvial sand	M	HUB-0191	1.20 ± 0.12	3.67 ± 0.22	1.19 ± 0.03	0.20 ± 0.01	10.5	11 ± 5	1.70 ± 0.11	1.40 ± 0.06	CAM	0.82 ± 0.06	820 ± 60	Kaiser et al., 2014a
FUER6	4	53°18'03.4"	13°09'43.4"	60	lacustrine sand	rGo	HUB-0326	0.61 ± 0.06	1.83 ± 0.09	1.05 ± 0.04	0.20 ± 0.01	3.0	10 ± 5	1.36 ± 0.08	0.81 ± 0.03	CAM	0.60 ± 0.04	600 ± 40	Kaiser et al., 2014a
FUER19-2	11	53°18'07.0"	13°10'38.3"	40	lacustrine sand	rGr	HUB-0327	0.55 ± 0.06	1.72 ± 0.14	0.80 ± 0.02	0.21 ± 0.01	11.4	10 ± 5	1.12 ± 0.07	0.80 ± 0.02	CAM	0.71 ± 0.05	710 ± 50	Kaiser et al., 2014a
S-1a	20	53°20'48.2"	13°11'23.1"	30	colluvial sand	M	HUB-0044	0.80 ± 0.02	2.43 ± 0.06	0.94 ± 0.03	0.21 ± 0.01	5.3	5 ± 3	1.42 ± 0.06	1.29 ± 0.02	CAM	0.91 ± 0.04	910 ± 40	Küster, 2014
S-1b	20	53°20'48.2"	13°11'23.1"	115	aeolian sand	ilC	HUB-0045	0.95 ± 0.05	5.39 ± 0.13	0.97 ± 0.03	0.19 ± 0.01	5.3	5 ± 3	1.67 ± 0.07	22.42 ± 0.51	CAM	13.44 ± 0.61	13440 ± 610	Küster, 2014
S-2a	21	53°20'48.2"	13°11'23.1"	80	aeolian sand	ilC	HUB-0046	0.41 ± 0.01	1.38 ± 0.06	0.83 ± 0.02	0.20 ± 0.01	2.1	3 ± 2	1.18 ± 0.04	0.98 ± 0.07	MAM	0.83 ± 0.07	830 ± 70	Küster, 2014
S-3a	18	53°20'40.8"	13°11'46.8"	85	colluvial sand	ylC	HUB-0047	0.55 ± 0.01	1.87 ± 0.06	0.89 ± 0.03	0.20 ± 0.01	2.8	3 ± 2	1.30 ± 0.04	19.42 ± 0.48	CAM	14.94 ± 0.62	14940 ± 620	Küster, 2014
S-4a	22	53°20'30.5"	13°11'30.4"	55	colluvial sand	M	HUB-0053	0.79 ± 0.02	2.97 ± 0.05	1.14 ± 0.03	0.20 ± 0.01	4.3	4 ± 2	1.66 ± 0.05	1.46 ± 0.03	CAM	0.88 ± 0.03	880 ± 30	Küster, 2014
S-4b	22	53°20'30.5"	13°11'30.4"	80	colluvial sand	M	HUB-0054	0.80 ± 0.03	2.59 ± 0.14	1.09 ± 0.03	0.20 ± 0.01	4.6	4 ± 2	1.58 ± 0.05	2.31 ± 0.05	CAM	1.46 ± 0.06	1460 ± 60	Küster, 2014
S-5a	23	53°20'30.6"	13°11'33.2"	20	colluvial sand	M	HUB-0048	0.79 ± 0.03	3.01 ± 0.03	0.97 ± 0.03	0.21 ± 0.01	4.7	4 ± 2	1.50 ± 0.05	1.24 ± 0.13	MAM	0.83 ± 0.09	830 ± 90	Küster, 2014
S-5b	23	53°20'30.6"	13°11'33.2"	55	colluvial sand	M	HUB-0049	0.70 ± 0.02	2.56 ± 0.07	0.97 ± 0.03	0.20 ± 0.01	3.0	4 ± 2	1.45 ± 0.05	1.31 ± 0.07	MAM	0.91 ± 0.06	910 ± 60	Küster, 2014
S-5c	23	53°20'30.6"	13°11'33.2"	105	colluvial sand	M	HUB-0050	0.74 ± 0.02	2.57 ± 0.01	0.98 ± 0.03	0.20 ± 0.01	4.2	4 ± 2	1.46 ± 0.05	1.24 ± 0.04	MAM	0.85 ± 0.04	850 ± 40	Küster, 2014
S-5d	23	53°20'30.6"	13°11'33.2"	155	colluvial sand	M	HUB-0051	0.73 ± 0.01	2.57 ± 0.02	0.93 ± 0.03	0.19 ± 0.01	5.6	6 ± 3	1.37 ± 0.06	1.32 ± 0.02	CAM	0.96 ± 0.04	960 ± 40	Küster, 2014
S-5e	23	53°20'30.6"	13°11'33.2"	180	colluvial sand	M	HUB-0052	0.89 ± 0.08	3.17 ± 0.05	0.96 ± 0.03	0.19 ± 0.01	7.5	7 ± 3	1.46 ± 0.06	3.19 ± 0.20	MAM	2.19 ± 0.16	2190 ± 160	Küster, 2014
S-6a	24	53°21'21.1"	13°13'00.4"	30	colluvial sand	M	HUB-0055	1.02 ± 0.03	3.59 ± 0.11	1.02 ± 0.03	0.21 ± 0.01	12.2	10 ± 3	1.53 ± 0.06	1.16 ± 0.06	MAM	0.76 ± 0.05	760 ± 50	Küster, 2014
S-6b	24	53°21'21.1"	13°13'00.4"	40	colluvial sand	M	HUB-0056	0.77 ± 0.05	2.79 ± 0.09	0.97 ± 0.03	0.20 ± 0.01	7.0	10 ± 3	1.39 ± 0.06	1.24 ± 0.02	CAM	0.90 ± 0.04	900 ± 40	Küster, 2014
S-6c	24	53°21'21.1"	13°13'00.4"	65	colluvial sand	M	HUB-0057	0.76 ± 0.02	2.76 ± 0.12	0.97 ± 0.03	0.20 ± 0.01	6.8	10 ± 3	1.38 ± 0.06	1.27 ± 0.02	CAM	0.92 ± 0.04	920 ± 40	Küster, 2014
S-6d	24	53°21'21.1"	13°13'00.4"	80	colluvial sand	M	HUB-0058	1.24 ± 0.03	3.85 ± 0.10	1.06 ± 0.03	0.20 ± 0.01	13.6	14 ± 3	1.55 ± 0.06	1.39 ± 0.02	CAM	0.90 ± 0.04	900 ± 40	Küster, 2014
S-6e	24	53°21'21.1"	13°13'00.4"	100	colluvial sand	M	HUB-0059	0.69 ± 0.03	2.48 ± 0.15	0.98 ± 0.03	0.20 ± 0.01	8.8	10 ± 3	1.35 ± 0.06	1.38 ± 0.02	CAM	1.02 ± 0.04	1020 ± 40	Küster, 2014
S-6f	24	53°21'21.1"	13°13'00.4"	110	colluvial sand	M	HUB-0060	1.06 ± 0.02	3.33 ± 0.05	0.99 ± 0.03	0.19 ± 0.01	9.8	10 ± 3	1.49 ± 0.06	1.49 ± 0.02	CAM	1.00 ± 0.04	1000 ± 40	Küster, 2014
S-6g	24	53°21'21.1"	13°13'00.4"	197	aeolian sand	fAh-Bv-ilCv	HUB-0061	2.32 ± 0.06	13.96 ± 0.22	0.97 ± 0.04	0.18 ± 0.01	13.2	10 ± 3	2.31 ± 0.09	24.38 ± 0.64	CAM	10.55 ± 0.51	10550 ± 510	Küster, 2014
Wa-2a	25	53°18'36.1"	13°18'15.7"	60	colluvial sand	M	HUB-0112	1.23 ± 0.02	3.93 ± 0.16	1.12 ± 0.02	0.20 ± 0.01	6.3	6 ± 3	1.76 ± 0.07	1.26 ± 0.06	CAM	0.72 ± 0.04	720 ± 40	Küster, 2014
Wa-2b	25	53°18'36.1"	13°18'15.7"	80	colluvial sand	M	HUB-0113	1.52 ± 0.02	4.18 ± 0.16	1.08 ± 0.02	0.20 ± 0.01	7.9	8 ± 3	1.76 ± 0.07	1.57 ± 0.04	CAM	0.89 ± 0.04	890 ± 40	Küster, 2014
Wa-3c	26	53°18'36.5"	13°18'14.6"	30	colluvial sand	M	HUB-0114	0.77 ± 0.03	2.49 ± 0.10	0.92 ± 0.02	0.21 ± 0.01	6.2	6 ± 3	1.39 ± 0.05	0.81 ± 0.03	CAM	0.58 ± 0.03	580 ± 30	Küster, 2014
Wa-3d	26	53°18'36.5"	13°18'14.6"	65	colluvial sand	M	HUB-0115	0.76 ± 0.02	2.48 ± 0.09	0.97 ± 0.02	0.20 ± 0.01	5.6	6 ± 3	1.42 ± 0.05	1.02 ± 0.04	CAM	0.72 ± 0.04	720 ± 40	Küster, 2014
Wa-3e	26	53°18'36.5"	13°18'14.6"	90	colluvial sand	M	HUB-0116	0.87 ± 0.02	2.72 ± 0.13	0.95 ± 0.02	0.20 ± 0.01	6.0	6 ± 3	1.44 ± 0.05	1.31 ± 0.16	MAM	0.91 ± 0.12	910 ± 120	Küster, 2014
Wa-3f	26	53°18'36.5"	13°18'14.6"	150	colluvial sand	M	HUB-0117	0.95 ± 0.02	3.11 ± 0.15	0.98 ± 0.02	0.19 ± 0.01	7.4	7 ± 3	1.49 ± 0.06	4.98 ± 0.11	CAM	3.35 ± 0.15	3350 ± 150	Küster, 2014

[a] U-238 and Th-232 contents were determined via gamma spectrometry using the equivalent U and Th contents of following natural daughter products: U-238: Th-234 (63.3 keV), Ra-226 (186.1 keV), Pb-214 (295.2 keV, 351.9 keV), Bi-214 (609.3 keV, 1120.3 keV, 1764.5 keV), Pb-210 (46.5 keV). Th-232: Ac-228 (338.3 keV, 911.2 keV, 969.0 keV), Pb-212 (238.6 keV), Bi-212 (727.3 keV), Tl-208 (583.2 keV). K-40: 1461.0 keV.
For dose rate calculation the weighted mean of all peaks was used (U-238 and Th-232).

[b] Cosmic dose rates were estimated regarding geographic position, altitude and sampling depth.

[c] Water content of sediment samples in % of dry mass (24 h oven drying at 105 °C). The estimated water contents were used for dose rate calculation.

[d] Equivalent doses were calculated using the Central Age Model (CAM) and the Minimum Age Model (MAM, sigma b = 0.1) respectively (Galbraith et al. 1999).

Number of aliquots measured per sample: 48 aliquots (FUER2, FUER3-4, FUER5-1, FUER19-2); 30 aliquots (Wa-3f); 24 aliquots (all other samples).

Supplement 1: Archaeological record of the Serrahn area and surroundings (data: State Archaeological Survey of Mecklenburg-Vorpommern, unpublished material). The calculation of the archaeological sites shown within the map frame yielded the following numbers: Neolithic, n = 1; Bronze Age, n = 52; Pre-Roman Iron Age, n = 5; Roman Age, n = 2; Slavic Medieval, n = 13; German Medieval, n = 10.

Legend:

- ◉ Village
- ◆ (dark red) Bronze Age, Urn grave
- ◆ (cyan) Roman Age, Urn grave
- ● (dark blue) Neolithic, Settlement
- ● (orange) Pre Roman Iron Age, Settlement
- ● (yellow) Slavic Medieval, Settlement
- ● (red) Bronze Age, Settlement
- ◆ (orange) Pre Roman Iron Age, Urn grave
- ● (grey) German Medieval, Settlement
- ■ (red) Bronze Age, Burial mound
- ● (light blue) Roman Age, Settlement
- ▲ German Medieval, Tower hill fortification
- ▼ German Medieval, Earth work

Supplement 2: Pedological and sedimentological data from the soil profiles sampled in the Serrahn area. Soil horizons are given both according to the German (Ad-hoc-AG Boden, 2005) and international pedological standard (FAO, 2006)

Profile	Site ID	Coordinates Northing	Easting	Landform	Sample	Sampling depth	Sediment classification	Soil horizon	Soil horizon	Grain-size composition, total			Grain-size composition, sand fraction			Textural class	LOI	CaCO₃	pH	Reference, remark
										Clay <0.002 mm	Silt <0.063 mm	Sand <2 mm	Fine >0.2 mm	Medium >0.63 mm	Coarse <2 mm					
						[cm]		[KA5]	[FAO]	[%]	[%]	[%]	[%]	[%]	[%]	[KA5]	[%]	[%]	[CaCl₂ / KCl]	

[1]Ad-hoc-AG Boden, 2005. Bodenkundliche Kartieranleitung (KA5), 5th edition. Schweizerbart, Hannover.
[2]FAO, 2006. Guidelines for Soil Description, 4th edition. FAO, Rome.
[3]Based on laser diffraction for profiles FUER1, 2, 3, 6, 14 and for all profiles with IDs Mü...; "S..." and "Wa..."; based on a wet sieving test for profiles FUER10-2, 15, 16-4, 17-5, 16-1, 19-2, 22-7, 26-1; based on combined pipette sieving and sedimentation (KÖHN) test for all samples with ID "HIN..." and profiles Zinow, Serrahn, Heilige Hallen, Lüttenhagen, and Steinmühle.
[4]In case of lacking clay values the silt value represents the clay-silt-sum.
[5]For profiles Zinow-AFSV-ÖWK, Serrahn-AFSV-BZE, Steinmühle-AFSV, Heilige Hallen-AFSV, Waldsee-AFSV and Lüttenhagen-ÖWK the values for total carbon (Ct) are given.

Supplement 3: Approximate translation of German soil horizons (Ad-hoc-AG Boden, 2005) into the international pedological classification (FAO, 2006).

Topsoil and subsoil horizons

German classification / KA5 (Ad-hoc-AG Boden, 2005[1])	International classification / FAO (FAO, 2006[2])	Remark
Hr	Hi	-
Hv	He	-
Ha	Ha	-
O	O	-
O+Ah	AhO	-
Oh+Aeh	AhO	-
Oh-Ah	AhO	-
Oh-Aeh	AhO	-
Aa	Ah	strongly humic (half-bog) horizon
rAap	Ap	relict ploughing
Ah	Ah	-
Ai	Ah	thin / initial humic horizon
Aeh	Ah	-
M-Ah	Ah	colluvial horizon
Bv-Ah	AhBw	-
Bv+Ah	Ah/Bw	-
Go-Aeh	AhCl	-
Go-Ahe	ECl	-
Ap	Ap	-
rAp	Ap	relict ploughing
rGo-rAp	ApCl	relict ploughing, relict gleyic conditions
Go-rAp	ApCl	relict ploughing
Bv-Ap	ApBw	-
Ah-Bv	BwAh	-
Bv	Bw	-
Bv+Cv-Bv	Bw/BwC	-
Bsh	Bsh	-
Cv-Bv	BwC	-
Cv-Bbt	BtC	-
Go-Bsh	BshCl	-
Bbt-Cv	CBt	-
Bv-Cv	CBw	-
Bbt-ilCv	CBt	-
M	C	colluvial horizon
Go-M	Cl	colluvial horizon
Bsh-M	CBsh	colluvial horizon
M-Go	Cl	colluvial horizon
Gr-M	Cr	colluvial horizon
lCv	C	-
C	C	-
ilC	C	-
rGo-ilCv	C	relict gleyic conditions
ylC	Cu	-
Cc	Ck	-
Go	Cl	-
Gr	Cr	-
rGo	Cl	relict gleyic conditions
rGr	Cr	relict gleyic conditions
Gor	Cr	-

Buried horizons

German classification / KA5 (Ad-hoc-AG Boden, 2005[1])	International classification / FAO (FAO, 2006[2])	Remark
fHr	Hib	-
fHv	Heb	-
fHa	Hab	-
fH	Hb	-
rGo+fHa	Hab/Cl	-
fO	Ob	-
fAa	Ahb	strongly humic (half-bog) horizon
fAh	Ahb	-
fAi	Ahb	thin / initial humic horizon
M-fAh	Ahb	colluvial horizon
fAeh	Ahb	-
fAp	Apb	-
fBv-fAp	ApBwb	-
Go-fAhe	EbCl	-
Gr+fAh	Cr/Ahb	-
rGr+fAh	Cr/Ahb	relict gleyic conditions
fAh-fBv-ilCv	CBwAhb	-
fBsh-fAh	AhBshb	-
fAh-fBv	BwAhb	-
fAe	Eb	-
fBv	Bwb	-
fBhv	Bhwb	-
fBsh	Bshb	-
Go-fBsh	BshbCl	-
fM	C	colluvial horizon
Gr-fM	Cr	colluvial horizon
fF	Lb	-
fF-rGr	Lb	relict gleyic conditions

[1]Ad-hoc-AG Boden, 2005. Bodenkundliche Kartieranleitung. Schweizerbart, Hannover.
[2]FAO, 2006. Guidelines for Soil Description, fourth ed. Food and Agriculture Organization of the United Nations, Rome.

Further information
Discontinuities (geological stratification) are indicated in KA5 as prefixes by Roman numerals (I, II, III…) and in FAO by Arabic numerals (1, 2, 3…).
Buried soil horizons are indicated in KA5 as suffixes by "f" and in FAO by "b".

Supplement 4: Description of relief characteristics deduced from the DEM used as predictor variables for the determination of palaeosol sites.

Relief characteristics	Description/method/reference
Elevation	Elevation above sea level
Slope	Slope gradient The amount of inclination of the land surface to the horizontal (SAGA terrain analysis module; Zevenbergen and Thorne, 1987).
Plan curvature	Horizontal curvature of the land surface. It can be also described as the curvature of the hypothetical contour line that passes through a specific cell. The plan curvature is positive for concave contours and negative for convex contours and can be associated with the accumulation and dispersion of surface water flow (SAGA terrain analysis module; Zevenbergen and Thorne, 1987).
Profile curvature	Vertical curvature of the land surface in the direction of the steepest slope and perpendicular to the plan curvature (SAGA terrain analysis module; Zevenbergen and Thorne, 1987).
Relative slope position	Relative slope position of a cell between valley floor (0) and ridge top (1) (SAGA terrain analysis module; Böhner and Selige, 2006).
Vertical distance to channel network	Vertical distance between the elevation of a cell and the elevation of the closest channel. It utilizes a channel network density of 5% (SAGA terrain analysis module; Olaya and Conrad, 2009).
LS factor	Relation between erosive slope length and slope gradient to predict the potential vulnerability of a site to soil erosion (SAGA terrain analysis module; Olaya and Conrad, 2009).
Flow accumulation	Number of upslope cells flowing into each downslope cell. Cells with a high flow accumulation are areas of concentrated flow and may be used to identify stream channels (SAGA terrain analysis module; Freeman, 1991).
Convergence index	Parameterizes how surface water in a cell converges or respectively diverges (SAGA terrain analysis module; Köthe and Lehmeier, 1996).
Topographic wetness index	Anticipated soil moisture of an area in terms of its surrounding topography (SAGA terrain analysis module; Olaya and Conrad, 2009).

Böhner, J., Selige, T., 2006. Spatial prediction of soil attributes using terrain analysis and climate regionalisation. In: Böhner, J., McCloy, K.R., Strobl, J. (Eds.), SAGA – Analysis and Modelling Applications. Göttinger Geographische Abhandlungen 115, Goltze, Goettingen, pp. 13-28.

Freeman, G.T., 1991. Calculating catchment area with divergent flow based on a rectangular grid. Computers & Geosciences 17, 413-422.

Köthe, R., Lehmeier, F., 1996. SARA – System zur Automatischen Relief-Analyse. User Manual, 2. Edition. Dept. of Geography, University of Göttingen, unpublished.
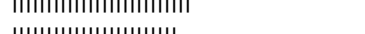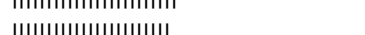
Olaya, V., Conrad, O., 2009. Geomorphometry in SAGA. In: Hengl, T., Reuter, H.I. (Eds.), Geomorphometry: Concepts, software, applications. Developments in Soil Science 33, Elsevier, Amsterdam, pp. 293-308.

Zevenbergen, L.W., Thorne, C.R., 1987. Quantitative analysis of land surface topography. Earth Surface Processes and Landforms 12, 47-56.

Supplement 5: Box-and-whisker plots of relief characteristics of palaeosols in the Serrahn area (n = 506). For ranking of their relative statistical importance see Supplement 6.
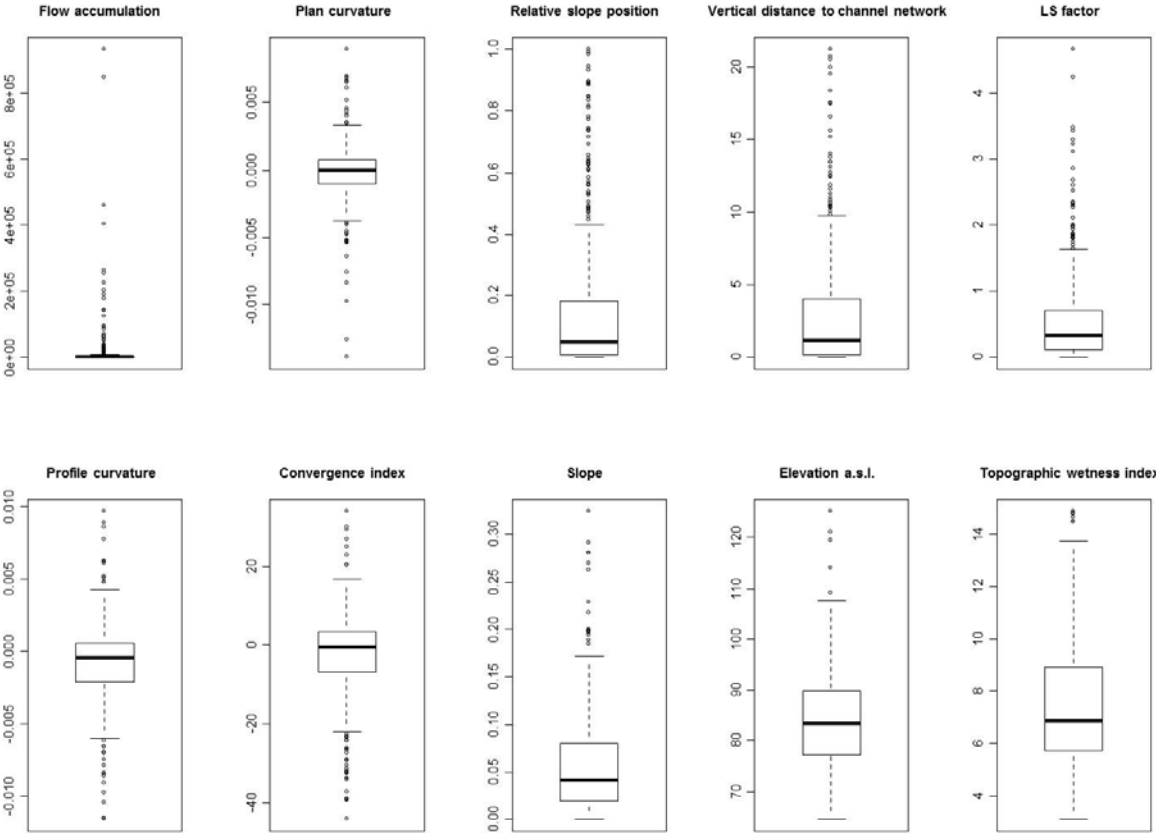
Supplement 6: Ranking of relative statistical importance of relief characteristics for palaeosol sites deduced from the absolute deviation of the median.

Rank	Relief characteristics	Relative statistical importance [%]	
1	Flow accumulation	100	||||||||||||||||||||||||||||||||||||||||||||||||||
2	Plan curvature	65.7	|||||||||||||||||||||||||||||||
3	Relative slope position	60.5	||||||||||||||||||||||||||||
4	Vertical distance to channel network	54.1	||||||||||||||||||||||||
5	LS factor	52.1	|||||||||||||||||||||||
6	Profile curvature	47.4	|||||||||||||||||||||
7	Convergence index	46.2	|||||||||||||||||||||
8	Slope	21.4	||||||||||
9	Elevation	11.2	||||||
10	Topographic wetness index	0.7		

Supplement 7: Simplified pollen diagram Mü-1 (from Küster, 2014). For location see Fig. 4B.


Pollen diagram Mü-1 (Mückengrund)
Analysis: Manuela Schult
S = Settlement phases 1-3
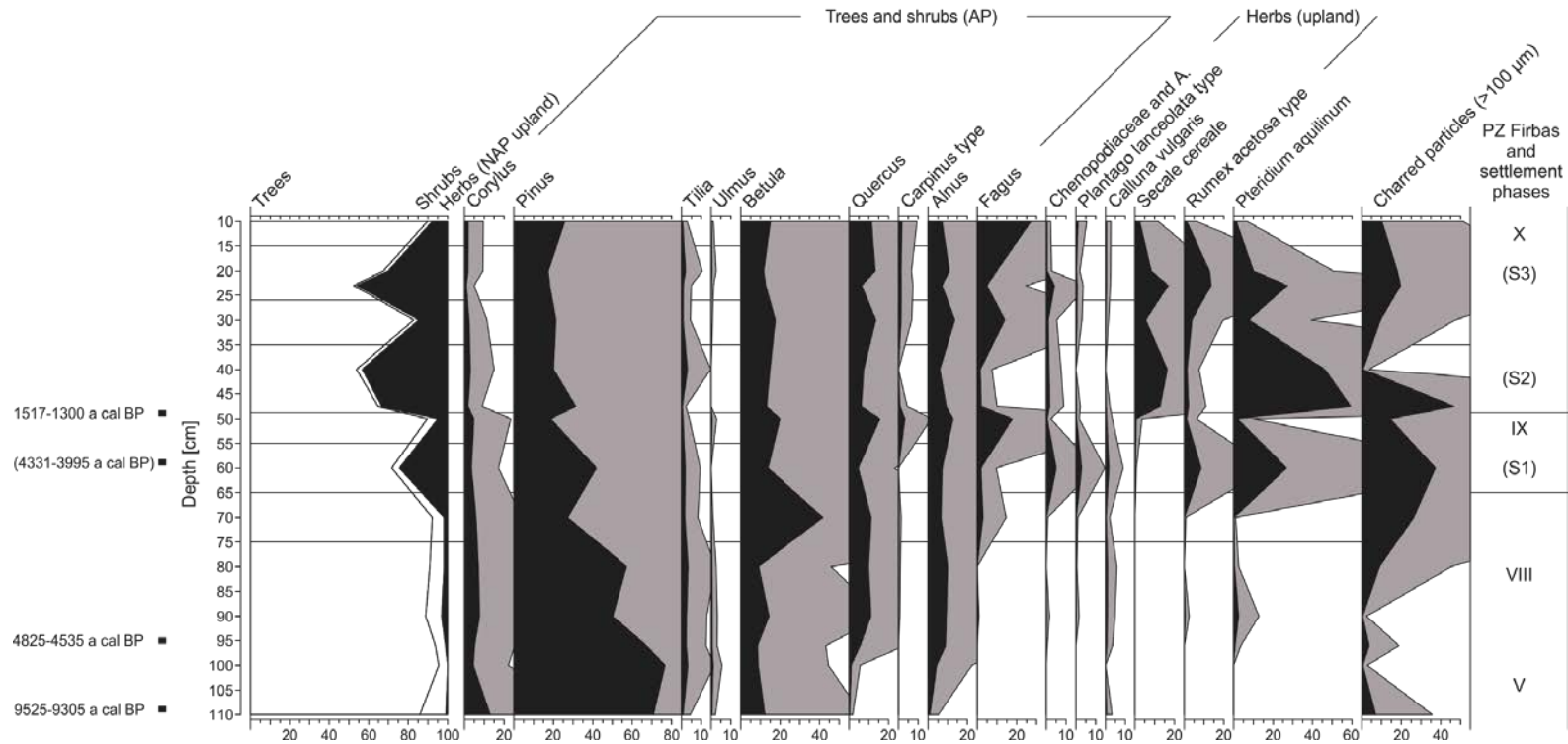
Supplement 8: Simplified pollen diagram KFS8. For location see Fig. 4B.

Pollen diagram KFS8
Analysis: Martin Theuerkauf
values based on an upland Pollensum
classification of pollen and spores mainly follows Moore et al. 1991,
except types indicated with (B) - Beug 2004 and (P) - Punt et al. 1976 ff.
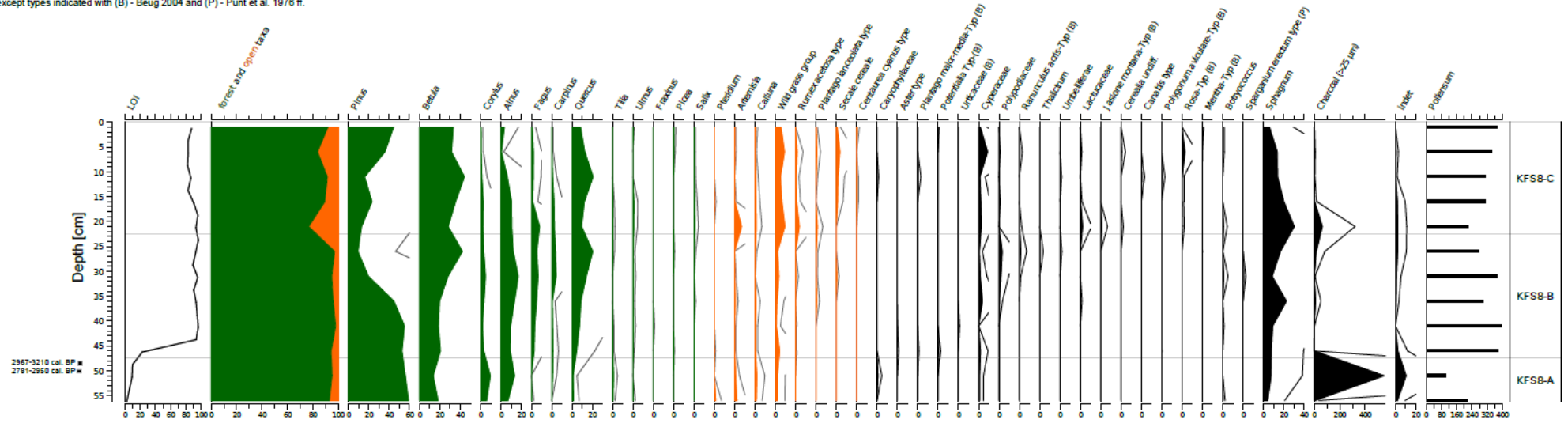
Supplement 9: Simplified pollen diagram FUER14. For location see Fig. 4B.
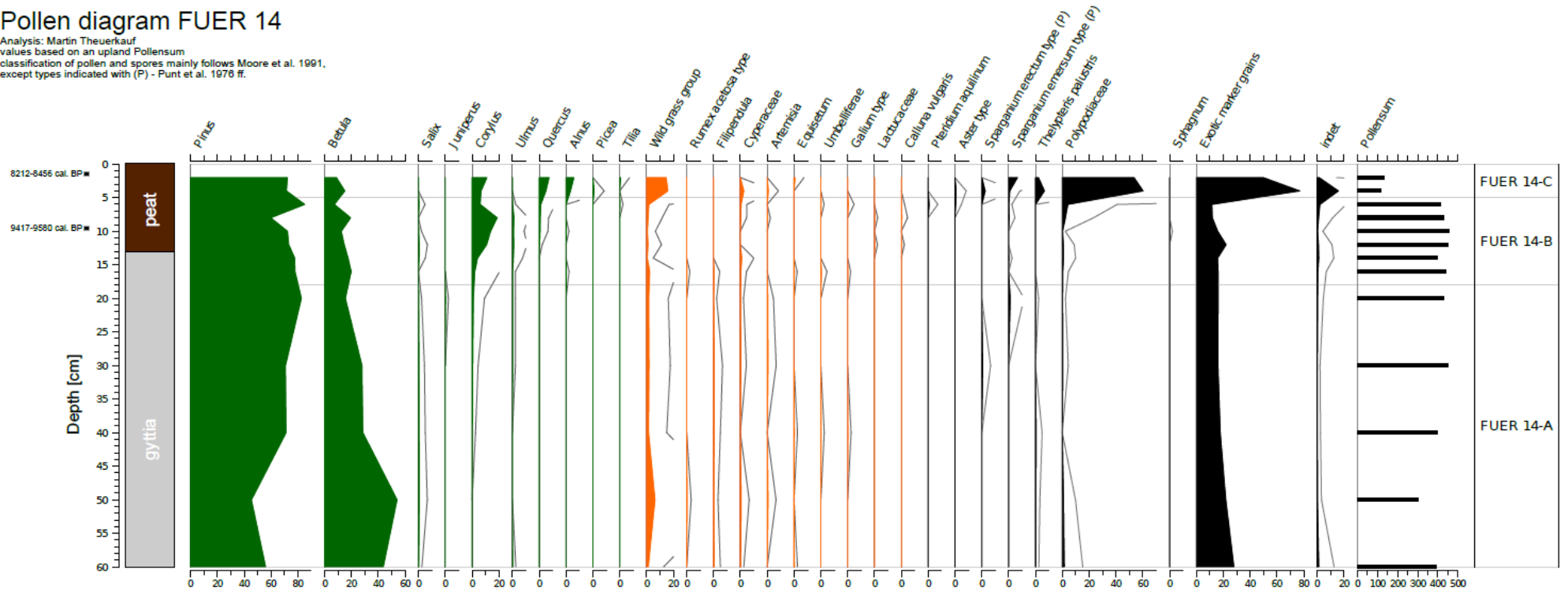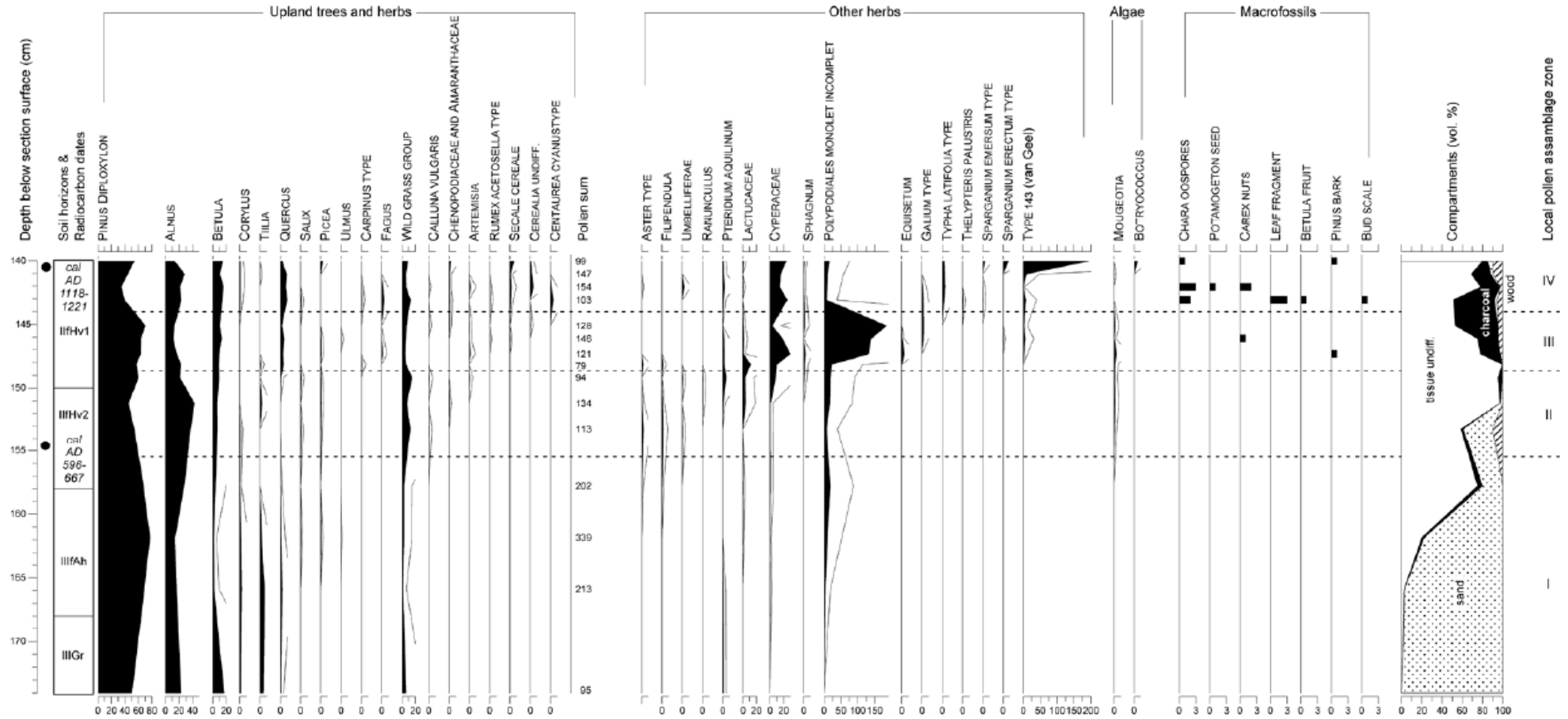

Pollen diagram FUER 14

Analysis: Martin Theuerkauf
values based on an upland Pollensum
classification of pollen and spores mainly follows Moore et al. 1991,
except types indicated with (P) - Punt et al. 1976 ff.

Supplement 10: Simplified pollen and macrofossil/compartment diagram FUER15. Macrofossils/compartments are given in total numbers (for countable objects) or estimated proportions of the total volume for charcoal, sand, tissues and wood (adapted from Kaiser et al., 2014a). For location see Fig. 4B.

Supplement 11: Simplified pollen diagrams FUER3 and FUER6 comprising single pollen samples of these profiles. The pollen sum includes all tree pollen types, Corylus, and pollen types attributed to upland herbs. The low pollen sums result from poor pollen preservation and concentration in most of the samples. The samples of FUER3 consist nearly entirely of charcoal particles, so that explicit counting of charcoal particles, as performed in FUER6, was unfeasible (adapted from Kaiser et al., 2014a). For locations see Fig. 4B.
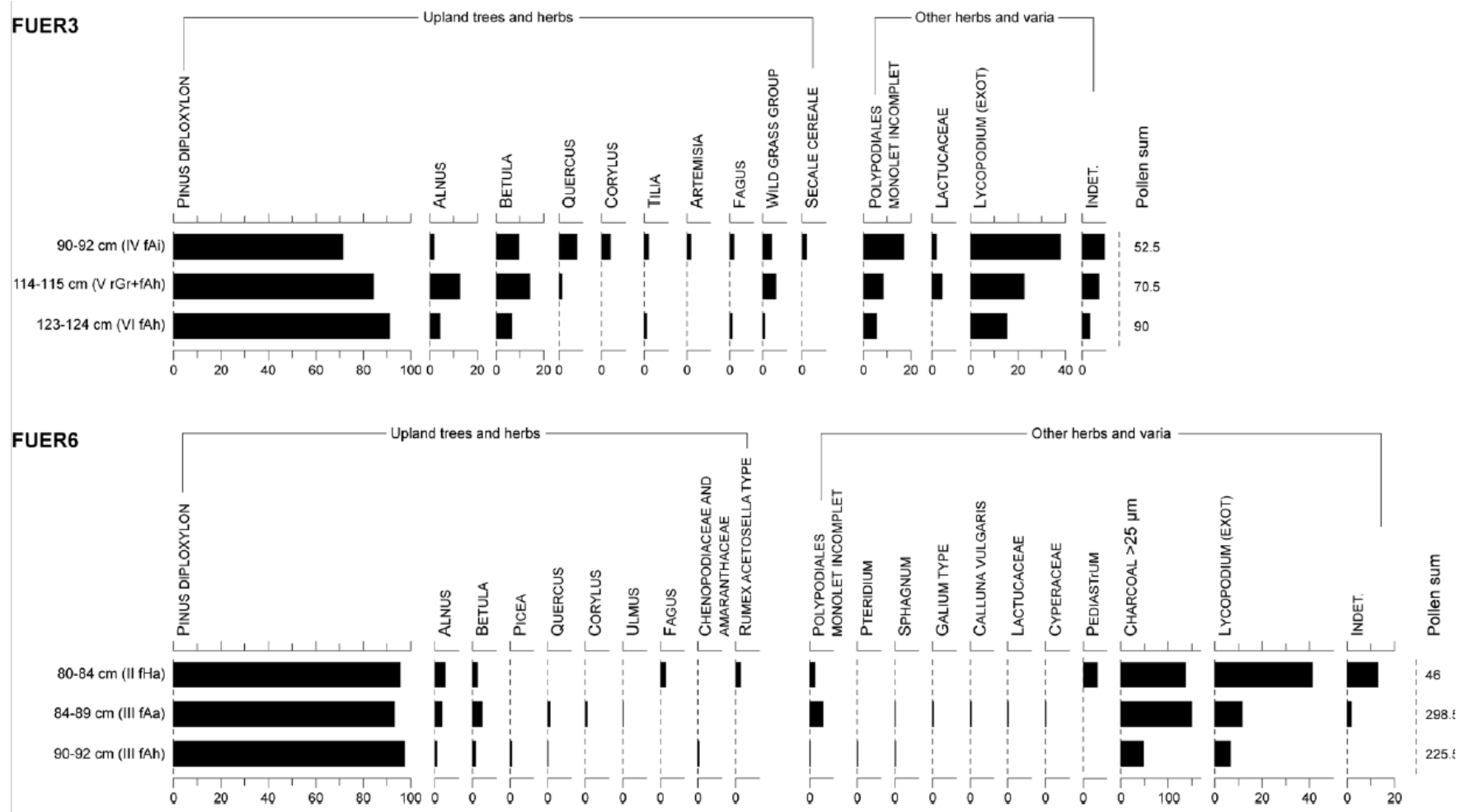
Supplement 12: Charcoal analysis (soil anthracology) of soil profiles east and west of Serrahn village.

Profile	Site ID	Depth [cm]	Soil horizon [KA5, simplified]	Dating[1] [Culture, geol. era]	Mean diameter[2] [cm]	Pinus [n]	Quercus [n]	Betula [n]	Populus/Salix [n]	Fagus [n]	Alnus [n]	Fraxinus [n]	cf. Prunus [n]	Decidous wood indet. [n]	Charred non-wood [n]	Sum [n]
S-1	20	10-50	M	(Slavic) Medieval	4	34	-	1	-	-	-	-	-	1	3	39
S-1	20	50-100	fAh-fBv-ilCv	?	5	29	11	-	2	-	-	-	-	-	1	43
S-1	20	140-160	rGo-ilCv	Late Pleistocene	8	20	2	-	-	-	-	-	-	-	17	39
S-3	18	0-20	Aeh, Bsh-M, M	Modern Age	1	13	11	5	1	-	1	-	1	-	3	35
S-3	18	30-70	ylC	Modern Age	4	23	1	2	-	-	-	-	-	1	6	33
S-3	18	56-100	ylC	Pre-Roman Iron Age	5	29	6	1	1	-	-	-	-	-	4	41
S-3	18	130-160	ylC	Pre-Roman Iron Age	10	16	16	2	-	-	-	-	-	2	7	43
S-3	18	50-90	ylC	?	2	20	1	1	-	-	-	-	-	-	12	34
S-5	23	6-25	Bsh, M	(Slavic) Medieval	2	52	5	-	-	-	-	-	-	-	3	60
S-5	23	25-95	M	(Slavic) Medieval	1	15	22	1	-	-	-	-	-	-	1	39
S-5	23	95-165	M	(Slavic) Medieval	9	6	38	2	4	-	-	-	-	-	-	50
S-5	23	165-175	fAh	?	10	3	49	-	-	3	-	-	-	-	-	55
S-5	23	175-195	M	Pre-Roman Iron Age	11	-	38	-	-	1	-	-	-	-	2	41
S-6	24	5-36	M	(Slavic) Medieval	2	21	6	3	-	2	-	-	-	-	9	41
S-6	24	45-85	M	(Slavic) Medieval	6	20	15	3	-	-	-	1	-	-	6	45
S-6	24	85-95	fAh	(Slavic) Medieval	3	31	4	3	-	-	-	-	-	-	2	40
S-6	24	95-104	M	(Slavic) Medieval	2	24	4	5	2	-	-	-	-	-	4	39
S-6	24	104-120	M	(Slavic) Medieval	7	15	14	10	-	1	-	-	-	-	4	44
Sum	-	-	-		-	371	243	39	10	7	1	1	1	4	84	761
Share[3] [%]	-	-	-		-	54.8	35.9	5.8	1.5	1.0	0.1	0.1	0.1	0.6	-	-

[1]Dating is based on geochronological data from the profiles.

[2]Reconstruction is based on the method described in: Nelle, O., 2002. Zur holozänen Vegetations- und Waldnutzungsgeschichte des Vorderen Bayerischen Waldes anhand von Pollen- und Holzkohleanalysen. Hoppea - Denkrschriften der Regensburgischen Botanischen Gesellschaft 63, 161-361.

[3]Refers to the share of wood charcoal (sum = 677 particles) excluding charred particles being no wood.